UNIVERSITEIT VAN PRETORIA
UNIVERSITY OF PRETORIA
YUNIBESITHI YA PRETORIA

ENERGY AND COST OPTIMAL SCHEDULING OF BELT CONVEYOR SYSTEMS

by

Tebello Ntsiki Don Mathaba

Submitted in partial fulfillment of the requirements for the degree

Philosophiae Doctor (Electronic Engineering)

in the

Department of Electrical, Electronic and Computer Engineering

Faculty of Engineering, Built Environment and Information Technology

UNIVERSITY OF PRETORIA

November 2016

SUMMARY

ENERGY AND COST OPTIMAL SCHEDULING OF BELT CONVEYOR SYSTEMS

by

Tebello Ntsiki Don Mathaba

Promoter(s):	Prof. Xiaohua Xia
Department:	Electrical, Electronic and Computer Engineering
University:	University of Pretoria
Degree:	Philosophiae Doctor (Electronic Engineering)
Keywords:	Belt conveyor system , demand-side management, optimal scheduling, electricity pricing, price forecasting, energy efficiency, energy model, chance-constraints, model predictive control, variable speed drive, regenerative drives, troughed conveyor, root mean square, maximum absolute percentage error, rank correlation

This work deals with the energy management of belt conveyor systems (BCS) under various demand-side management (DSM) programmes. The primary objective of this work is to model the energy consumption and energy related cost of operating troughed belt conveyor systems under different electricity pricing tariffs. This research is motivated by the increasing need for energy efficiency and energy cost reduction in the operation of BCS. This is as a result of technological improvements in BCS technology leading to increasingly longer belts being commissioned and as a result of rapidly rising electricity costs.

An energy model derived from established industry standards is proposed for long conveyors. The newly proposed model uses a first-order partial differential equation (PDE) in order to capture the state of material on the belt. This new model describes the conveyor's power requirement using an equation with two parameters. A system identification set-up involving a recursive parameter estimating algorithm is simulated for measurements with varying degrees of noise. The results show

that the proposed model estimates conveyor power and material delivered by long conveyors more accurately than the existing steady-state models.

Downhill conveyors (DHCs) are important potential energy sources that can be tapped to improve the overall energy efficiency of BCSs. A generic optimisation model that is able to optimally schedule three configurations of BCS with DHC is proposed. The economic assessment of implementing dynamic braking and regenerative drives technology on downhill conveyors is undertaken with the help of the model. The assessment shows that combining regenerative drives and optimal operation of BCS with DHC generates energy savings that give attractive payback period of less than 5 years.

A chance-constrained model predictive control (cc-MPC) algorithm is proposed for scheduling belt conveyor systems with uncertain material demand on the output storage. The chance-constraints are based on the modelling of material demand by a sum of known mean demand and, zero-mean and normally distributed random component. The cc-MPC algorithm is shown to produce schedules that give a smaller number and smaller magnitude of storage limit violations compared to normal MPC and chance-constrained optimal control algorithms. An equation that gives the amount of effective storage required to meet storage constraints for a given value of standard deviation is established.

The optimal scheduling of BCS under the real-time pricing (RTP) tariff is considered. This study develops a methodology for establishing the economic value of price forecasting schemes for loads capable of load-shifting. This methodology is used to show that the economic benefit obtained from a forecast is highly dependent on the volatility of the electricity prices being predicted and not their mean value. The methodology is also used to illustrate why the commonly used indices mean absolute percentage error (MAPE) and root mean square error (RMSE) are poor indicators of economic benefit. The proposed index using Kendall's rank correlation between the actual and predicted prices is shown to be a good indicator of economic benefit, performing far better than RSME and MAPE.

DEDICATION

I dedicate this thesis to my wife, Mookho; your persistent support and encouragement carried me through. I want to thank you for all those days when this imposing mountain seemed insurmountable. To say you made it easier, would be an understatement.

ACKNOWLEDGEMENTS

I would like to thank my supervisor for his guidance and support. Your mentorship has open a whole new world of energy for me. Thank you to all of my former colleagues at CNES for your help. I have come to realize this was as much a psychological as it was an academic challenge. Therefore, let me speak frankly without any loss of meaning in translation:

Ke qala pele ka ho leboha uena 'M'e, ena tholoana e jaliloe ke uena. U mpontšitse boleng ba bophelo; ho iphumanela likarabo ka ho iketsetsa lipatlisiso, ho tseba hore "tlou hae hloloe ke moroalo", boitelo lelapeng ba hau, mamello le ho phehella. U itse nka fihlella tsohle hobane ke na le bokhoni. Ke susumelitsoe ke mantsoe ana, ke batlile ho iponela, ho a beha tekong. Ntate, u itse "sentle ke ho boea le lithebe le marungoana", ke tseo. Bo-more; 'P', 'Mampoli, S'katla, le nthutile boikarabello. Le mpontšitse hore ke lokela ho labalabela ho etsa hantle ka ho phethahala.

Bo-mphato sekolong se seholo sa sechaba, kea leboha. Tlotla ea hoba mosebetsi 'moho le lona e ntšutumellelitse ho batla ho fihlela tse kholo. Ke qhololitsoe ke boiphihlelo ba lona. Max, ke bone ka uena hore tsena tsohle li ka etsahala. U ntataisitse, oa se mphe tlhapi empa oa nthuta ho e tšoasa. Zak ke lakatsa ho fihlela kholo eo ke e boneng ho uena. S'forino, ke ne ke sa kholoe tsietsi ea hau, ke iponetse ka aka mahlo. Ke tsoile 'mokola, ke re "heiii ha ke sa likena!... ke namola!" haha!. Ke khothetse ha ke u hopola.

Potjo le banna ba techware, le ntutlile la ntšisinya ho fihlella 'mokong, haho thuto eka fetang eno. Le khaolo ea bohlokoa bo phahameng bukeng eaka. Mahlatsi le ba hau, kea leboha. Phala ebile boitebatso bo hlokahalang letong lena. Motaung oa Sefikeng, moifo oa banna ba hae o koano Tšoane le bohle beo ke sitoang ho ba qolla lebitsong la khahello ea leqephe, ha ke nyenyefatse tlatsetso ea lona.

M'ratuoa, ke sitoa ho leboha ka mokhoa o lekaneng. U e phetse le 'na, he u khothalitse Mofokeng. U thabile le 'na ha ho le monate, U ferekane le 'na ha ho nyolosetsa, u mamelletse bosieo baka ke le haufi le uena, u lutse u khothetse ka linako tsohle. Nkeke ka khona ho buselletsa tlatsetso ea hau, empa ke tla leka. U etšoere ka bohaleng ele ka 'nete.

Qetellong, sena se phethahalitsoe ka thuso ea bohle ba ahileng semelo saka, ba nkentseng seo ke leng sona. Hobane ke ile ka tlameha ho tseba na ke mang. Ke morutoana oa bophelo, ke labalabela ho phethahala, ke rata ho tlisa phetoho le phethahatso ea tebello.

Ke Tebello Ntsiki Don Mathaba.

Ke leboha ho menahane.

PUBLICATIONS

- T. Mathaba and X. Xia, "Optimal and energy efficient operation of conveyor-belt systems with downhill conveyors," *Energy Efficiency*, Jul. 2016.

- T. Mathaba and X. Xia, "A parametric energy model for energy management of long belt conveyors," *Energies*, vol. 8, no. 12, pp. 13590–13608, 2015.

- T. Mathaba, X. Xia, and J. Zhang, "Analysing the economic benefit of electricity price forecast in industrial load scheduling," *Electric Power Systems Research*, vol. 116, pp. 158–165, Nov. 2014.

- T. Mathaba, X. Xia, and J. Zhang, "Optimal scheduling of conveyor belt systems under critical peak pricing," in *International Power and Energy Conference (IPEC) 2012*, Ho Chi Minh City, Vietnam: IEEE, 12-14 Dec. 2012, pp. 315–320.

LIST OF ABBREVIATIONS

AFE	Active front-end
ANFIS	Adaptive neuro-fuzzy inference system
BC	Belt conveyor
BCS	Belt conveyor system
BE	Implicit backward Euler method
CC	Capital costs
CEMA	Conveyor equipment manufacturing association
COD	Coefficient of determination
CPP	Critical peak pricing
CPP-ED	Extreme-day Critical peak pricing
CPP-F	Fixed-period Critical peak pricing
CPP-V	Variable-period Critical peak pricing
DHC	Downhill conveyor
DR	Demand response
DSM	Demand-side management
FDM	Finite difference methods
FEBI	Forecast economic benefit index
FiT	Feed-in tariff
FIFO	First-in First-out
FP	Flat price
GA	Genetic algorithm
IBP	Incentive based programme
IGBT	Insulated-gate bipolar transistor
IPP	Independent power producer
LCC	Life-cycle cost
LSSVM	Least-square support vector machine
MAE	Mean absolute error
MAPE	Mean absolute percentage error
MDEC	Mean daily energy cost
MP	Mean electricity price

LIST OF ABBREVIATIONS (continued)

MPC	Model predictive control
r-MPC	restrained model predictive control
cc-MPC	Chance-constrained model predictive control
OC	Optimal control
OOC	On-off control
OPC	Operating cash-flow
PBP	Payback period
PDE	Partial differential equation
PPA	Power purchase agreement
PPM	Pearson product-moment
RC	Rank correlation
RMSE	Root mean square error
RD	Regenerative drive
RTP	Real-time pricing
SPE	Sequential parameter estimator
SS	Steady-state
TBP	Time based programme
TOU	Time-of-use
VSC	Variable speed control
VSD	Variable speed drives
WACC	Weighted average cost of capital

LIST OF SYMBOLS

A	Cross-sectional area of bulk material
$\mathbf{b}_n$	New energy model vector parameter
$C_1 - C_9$	Conveyor friction resistance parameters
Cost^{FP}	Scheduling energy cost derived from a flat price
Cost^{PP}	Scheduling energy cost derived from predicted prices
d	Electricity price discount factor during non-critical days
D_n	Bulk material demand during a sample period n
$\widehat{D}_n$ & $\overline{D}_n$	Random normally distributed and mean components of D_n
$\mathbb{E}\{\}$	Mathematical expectation function
f	Conveyor friction coefficient
$\mathbb{F}^{-1}$	Inverse of the standard normal cumulative distribution
F_H	Primary resistance
F_N	Secondary resistance
F_U	Conveyor driving force
F_S	Special resistance
F_{St}	Slope resistance
g	Acceleration due to gravity
G_n	New energy model matrix parameter
h_c & h_p	MPC's control and prediction horizons
H	Height difference between conveyor's head and tail
I	Material feed-rate, (in tonnes/hour)
L	Belt conveyor length, (in metres)
LP	Electricity load profile of a BCS with N_B conveyors
M_n	Mass of bulk material in storage during a sample period n, (in Kg)
M_{out}	Mass of bulk material coming out of the conveyor
$\mathcal{N}(\cdot, \sigma^2)$	Normal distribution function with standard deviation σ
N_{crit}	Number of critical days declared by the electricity supplier in a month
N_B	Number belt conveyors
n_{neg}	The first year that makes the LCC negative
N_t & N_x	Number of time and spacial samples
N_T	Number of days under the CPP-F programme
N_{life}	Useful lifetime of an asset, (in years)

LIST OF SYMBOLS (continued)

P	Electrical power required by belt conveyors
Pr	Probability
$q(x,t)$	Bulk material mass per unit length at position x at time t, (in Kg/m)
$\bar{q}$	Average material mass per unit length, (in Kg/m)
q_B	Conveyor belt unit mass per metre, (in Kg/m)
q_{RO} & q_{RU}	Carry-side and return-side unit mass per metre
$\bar{q}_{ss}$	Average material mass per unit length during steady-state operation, (in Kg/m)
$\mathbf{q}_n$	Vector of $q(x,t)$s at multiple spacial sampling points during a sampling time instance n
s_n	Belt conveyor start-up occurrence indicator, (a binary variable)
$\mathbb{S}$	A set of feasible BCS schedules defined by operational constraints
ST_L & ST_U	Lower and upper bulk material storage limits
u_n	Belt conveyor on-off control input, (a binary variable)
v	Belt speed, (in m/s)
$\mathbb{V}\{\}$	Variance function
T_{crit}	Duration of the critical period
Greek letters	
α	Chance-constraints confidence level
α_c	Critical value of a chance-constraints confidence level
η	Belt conveyor motor and drive efficiency
δ	Belt conveyor's inclination angle
θ_j	Zhang & Xia's conveyor energy model parameters
λ & $\hat{\lambda}$	Post-implementation BCS load profiles during normal & critical days
ν_j & ν_{max}	Daily & maximum volatility value during an assessment period (e.g. a season)
π_n	Electricity price during a sampling period n, (in ZAR/kWh)
π_n^{PP} & π_n^{AP}	Predicted & actual electricity price during a sampling period n, (in ZAR/kWh)
$\pi_{AS}, \pi_{NA}, \pi_{RC}$	Electricity price charges (Administration, Network access & Reliability), (in ZAR/Month)
$\hat{\pi}$	Electricity price during a critical day, (in ZAR/kWh)
φ_k	New conveyor energy model parameters
ω	Objective function weighting factor
ω_{VSC}	Objective function weighting factor for variable speed control applications
Ω	BCS operational constraints

TABLE OF CONTENTS

CHAPTER 1 INTRODUCTION **1**
1.1 MOTIVATION 1
1.2 PURPOSE OF THE RESEARCH 3
1.3 RESEARCH CONTRIBUTIONS AND OUTLINE OF THE THESIS 4

CHAPTER 2 BACKGROUND **7**
2.1 ENERGY CONSUMPTION OF BELT CONVEYOR SYSTEMS 7
2.2 DEMAND-SIDE MANAGEMENT AND ELECTRICITY PRICING 11
2.3 OPTIMAL SCHEDULING 13

CHAPTER 3 A NEW ENERGY MODEL FOR LONG BELT CONVEYORS **18**
3.1 INTRODUCTION 18
3.2 CONVEYOR MODEL 21
3.2.1 Conveyor resistances 21
3.2.2 Modelling energy consumption 24
3.2.3 Modelling bulk material flow 26
3.3 MODEL VERIFICATION 28
3.3.1 Steady-state power calculations 28
3.3.2 Variable loading calculations 30
3.4 PARAMETER IDENTIFICATION 36
3.4.1 Parameter estimation 37
3.5 APPLICATION CASE-STUDY 39
3.6 CONCLUSION 42

CHAPTER 4 ENERGY MANAGEMENT IN SYSTEMS WITH DOWNHILL CONVEYORS **44**

4.1 INTRODUCTION . . . 44
4.2 BACKGROUND . . . 46
4.2.1 Conveyor drive technology . . . 46
4.2.2 Energy model . . . 48
4.3 ENERGY AND COST OPTIMISATION . . . 49
4.3.1 Case-study plant . . . 49
4.3.2 Electricity pricing . . . 50
4.3.3 Drive configuration options . . . 51
4.3.4 Optimal scheduling . . . 53
4.4 COST ANALYSIS . . . 56
4.4.1 Sensitivity analysis . . . 58
4.5 CONCLUSION . . . 60

CHAPTER 5 OPTIMAL SCHEDULING WITH UNCERTANITY IN MATERIAL DEMAND . . . 61
5.1 INTRODUCTION . . . 61
5.1.1 Critical peak pricing . . . 63
5.1.2 Model predictive control . . . 64
5.2 CASE-STUDY MODEL . . . 65
5.3 OPTIMAL MPC SCHEDULES . . . 66
5.3.1 Simulation results and discussions . . . 69
5.4 CHANCE-CONSTRAINED MPC . . . 73
5.4.1 Chance-constraints . . . 74
5.4.2 Storage sizing based on confidence level . . . 75
5.4.3 Simulation results and discussions . . . 76
5.5 CONCLUSION . . . 78

CHAPTER 6 THE BENEFIT OF PRICE FORECASTS IN CONVEYOR SCHEDULING . . . 80
6.1 INTRODUCTION . . . 80
6.2 PRICE DATA, CASE STUDY AND BENEFIT INDEX . . . 82
6.2.1 Variable speed control . . . 82
6.2.2 On-off control . . . 83
6.2.3 Typical plant schedules . . . 85

6.2.4 Forecast economic benefit index 85
6.3 METHODOLOGY 86
6.3.1 Rank correlation as an indicator of economic benefit 87
6.4 ELECTRICITY PRICE FORECASTING 89
6.5 SIMULATION RESULTS AND DISCUSSIONS 90
6.5.1 Effect of price volatility on economic benefit 90
6.5.2 Indicators of economic benefit 91
6.5.3 Using an artificial forecast 94
6.5.4 Sensitivity analysis 96
6.6 CONCLUSIONS 98

CHAPTER 7 SUMMARY 99

REFERENCES 102

CHAPTER 1 INTRODUCTION

Belt conveyor systems (BCSs) are a widely used versatile means of transporting bulk material. These systems are made-up of a series of conveyors, feeders and storages. Technological advances are leading to increasingly long conveyors being commissioned. Thus, conveyance is becoming more energy intensive. This together with increasingly expensive and sophisticated electricity tariffs makes it necessary to implement energy efficient technologies and to optimally schedule the operation of belt conveyors so as to minimise energy cost. This thesis focuses on the optimal scheduling of belt conveyor systems in order to reduce energy costs. The research-work advances knowledge in energy management of BCS operating under time-based demand-side management (DSM) programmes.

1.1 MOTIVATION

Figure 1.1 shows an overview of the issues motivating the work undertaken in this thesis. Figure 1.1 shows a BCS applied within an industrial process. The BCS transports bulk material coming out

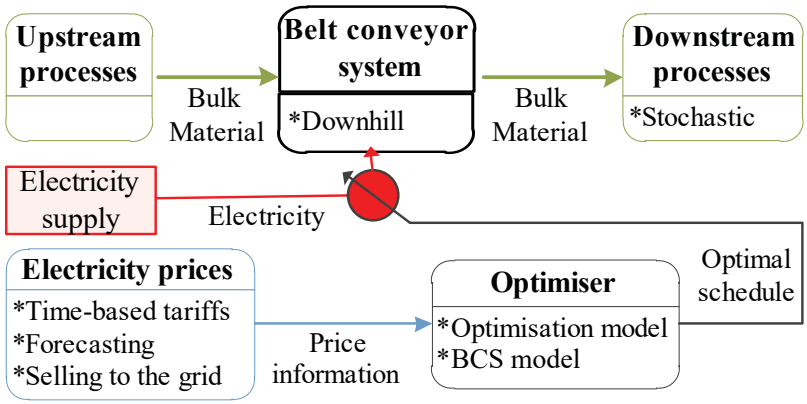

Figure 1.1. A summary of the issues motivating the research work in the thesis.

of up-stream processes and feeds it into down-stream processes. In the case of a lime stone mine supplying a cement factory, the up-stream processes include mining and crushing, while some of the down-stream processes are blending and heating in the kiln. Figure 1.1 shows that a schedule computed by the optimiser controls the operation and, hence, the energy consumption of a BCS, while taking the electricity price information into account. The availability of input material to the conveyor and the requirement for output material to be delivered by conveyors is dictated by up- and down-stream processes, respectively. In practice, these amounts of material can be uncertain depending on the nature of up- and down-stream processes involved. Therefore, scheduling algorithms able to handle uncertainty of bulk material flow are necessary.

Depending on the BCS drive technology, the schedule controls the BCS by either switching the belt on/off or varying the belt speed and feed-rate. The use of variable speed drives (VSD) in place of fixed speed drives has been studied and implemented extensively with the aim of improving energy-efficiency. Other less studied emerging options for improving efficiency is the use of regenerative drives on downhill conveyors. A better understanding and modelling of BCSs that incorporates regenerative drives is required.

The current trend of electricity market deregulation ushers in the use of demand-side management (DSM) programmes where electricity prices change in-order to regulate demand. Many of these DSM programmes use time-based electricity prices and some incentivise small generators to sell power to the grid. The variability of time-based prices ranges from seasonal to hourly price changes such as the real-time price (RTP) tariff. There is a need to further explore the scheduling of conveyor-belts under these new tariffs.

Moreover, the use of RTPs in schedules makes price forecasting necessary. The majority of literature on this subject tends to focus on improving the accuracy of forecasts based on commonly used accuracy metrics. However, a thorough understanding of the economic benefit of the forecast's accuracy when applied to belt conveyor scheduling is necessary.

Standard belt conveyor(BC) models show that the terrain where the BCS is installed has a big influence on the BC's energy consumption. It is also known that some downhill conveyors are capable of generating energy with the help of regenerative drives. The currently available research focuses on the design of electronic power circuits that connect regenerative drives to the grid and the associated power

quality issues. Thus, there is a need for investigating the less researched issue of energy management of BCS with regenerative drives, more so in relation to the new DSM programmes that allow selling power to the grid.

1.2 PURPOSE OF THE RESEARCH

The purpose of this work is to model the energy consumption and energy related cost of operating troughed belt conveyor systems under different electricity pricing tariffs. This work addresses the following issues:

- The inadequacies of the currently available conveyor energy models in modelling energy consumption and bulk material flow of long belts
- The energy management of BCSs with downhill conveyors (DHCs)
- The economic viability of energy efficiency improvement in BCSs based on the pricing schedule that allows for the selling of electricity into the grid
- The demand-side management of BCS's electricity load using time-based electricity tariffs, namely; Time-Of-Use (TOU), Critical-peak-pricing (CPP) and RTP
- The impact of the size of bulk material storage, available within the BCS, on the energy operating cost under DSM programmes
- The scheduling of BCS when the output material required from the system is uncertain.

The work presented here is intended for application in supervisory control of BCS with time intervals ranging from between 10 minutes to 1 hour. For this reason, the modelling assumes that the changes in energy consumption caused by the transient behaviour of the motor driving the conveyor are negligible. Moreover, the motor is modelled at a steady state assuming and that the motor's efficiency is constant. The required technical capability for conveyor drives to achieve the schedule speed ramps and the intricacies on how to achieve these transitions are not within the scope this work. Many of the methods

proposed and principles applied in this work can be directly applied to other industrial electricity loads capable of load-shifting. It will be indicated in the subsequent chapters, whenever this is the case.

1.3 RESEARCH CONTRIBUTIONS AND OUTLINE OF THE THESIS

The rest of the text is divided into 6 chapters. Chapter 2 gives a concise summary of the background literature relevant to the content of this thesis. This summary is divided into three themes, namely; energy consumption of BCS, electricity pricing and optimal scheduling. Each of the subsequent Chapters, apart from Chapters 7, advances a given set of objectives. These Chapters, 3-6, are formatted as manuscripts that can be read independently. The bulk of the content in Chapters 3, 5 and 6 has been published, while the content of Chapter 4 is currently in the printing process.

The focus of Chapters 3 and 4 is on energy-efficiency while Chapters 5 and 6 are inclined more towards energy-cost minimisation and DSM. Chapter 3 develops a new model for long belt conveyors where energy efficiency can be archived by matching the input feed-rate and belts speed. Chapter 4 considers the energy efficiency that can be archived by capturing the energy generated by downhill conveyors as opposed to wasting this energy on a braking resistor. Chapters 5 and 6 generally consider the impact of uncertainty in practical implementations of energy-cost optimal schedules. Chapter 5 focuses on uncertainties in bulk material demand due to down-stream processes, while Chapter 6 focuses on the uncertainty in electricity pricing. Chapter 7 summarises the results of the thesis.

A detailed account of this work's contributions is as follows:

In Chapter 3, a new conveyor energy model for long conveyors is proposed. The energy model is described by two equations; the first equation captures the flow of bulk material on the belt, while the second two-parameter equation quantifies the power requirements of the belt conveyor. The key contributions related to the new model in Chapter 3 are:

- The new model is able to account for varying amounts of mass per unit length throughout the length of the belt to give more accurate power calculations compared to previously proposed models

- A recursive parameter estimating algorithm and identification set-up is proposed. Simulations are used to show case this set-up's ability to identify parameters from noisy measurement data

- A sensitivity analysis of the power equation is used to justify the different parameter convergence rates.

Chapter 4 considers the energy efficiency improvements resulting from harnessing the energy generated by DHCs and an economic analysis of various belt conveyor drive configurations. The key contributions of Chapter 4 are:

- A novel optimisation model that can optimally schedule BCSs with DHC under a TOU tariff that allows for selling power to the grid. The proposed optimisation model is generic and its application is demonstrated for different conveyor drive configurations

- A cost analysis of energy efficient conveyor drive technologies retrofits and their sensitivity to financial variables and storage size. The analysis quantifies the amount of cost saving and/or profit that can be made under three different scenarios to help the BCS operator evaluate the economic viability of investing in regenerative drive technology.

Chapter 5 considers the benefit of changing from a TOU to a CPP tariff while using a model predictive control (MPC) approach to scheduling. The key contributions of Chapter 5 are:

- An MPC based optimal scheduling model for BCS under the CPP tariff. An analysis considering different amounts of storage capacities and MPC prediction horizons is also given

- The introduction of a stochastic MPC scheduling algorithm based on chance-constraints in order to cater for the uncertainty in the demand of material from the BCS

- A formula that gives the minimum size of storage required for the BCS to reliably deliver required bulk material is proposed. This formula is shown to be related to the prediction horizon of the stochastic MPC and the standard deviation of the material uncertainty.

Chapter 6 presents an economic assessment of real-time electricity price forecast accuracy on day-ahead scheduling of two types of BCS. The two types considered are those running VSDs and fixed-speed motors.The key contributions of Chapter 6 are:

- The analysis shows that the economic benefit of price forecasts is proportional to the amount of price volatility
- A case study and artificial forecast data is used to illustrate and explain the inappropriateness of maximum absolute percentage error (MAPE) and root-mean square error (RMSE) as indicators of economic benefit
- The introduction of Kendall's rank correlation (RC) between the predicted and actual prices as an indicator of the economic value of a forecast method. Case study data is used to show that RC is much better than MAPE and RMSE.

CHAPTER 2 BACKGROUND

This Chapter provides a summary of the relevant literature background on three key themes of the thesis. Firstly, Section 2.1 describes the components and operation of a BCS in order to provide a basis of how and where the energy of the BCS is consumed. Secondly, Section 2.2 provides background on DSM and how it is leading to a variety of electricity price tariffs. Finally, Section 2.3 explains the basic terminology and concepts of optimisation which is the basis of the optimal scheduling applied in this thesis.

2.1 ENERGY CONSUMPTION OF BELT CONVEYOR SYSTEMS

A troughed belt conveyor system, composed of a series of belts and storage containers, is operated to transport bulk material between two points. The distance between the points varies, ranging from a few metres up to as many as 20 kilometres. Over long distances, conveyors may need to traverse rugged terrain and avoid certain obstacles, such as protected natural reserves, power grid and very steep hills. However, there is a limitation on the sharpness of the horizontal curve a conveyor can withstand. This is mainly imposed by the ability of the belt material to bend without any excessive damage. A commonly used way around this limitation is to have several belts connected by transfer stations zig-zag the terrain as opposed to a single long flight. The inclination angle of the belt is also limited because material tends to slide back to the loading point when the belt is too steep [1].

Figure 2.1 shows a longitudinal section of a BCS, with two belt conveyors. The feed chute releases bulk material onto the surface of the belt that is usually made up of rubber materials. The feed chute has loading 'skits' attached to it output end in order to guide the bulk material as it enters the belt. The belt rolls over the carrying idlers from tail to head to discharge material into a transfer chute and onto the next belt. The belt surface is cleaned by a scrapper/belt cleaner to remove any residue as it

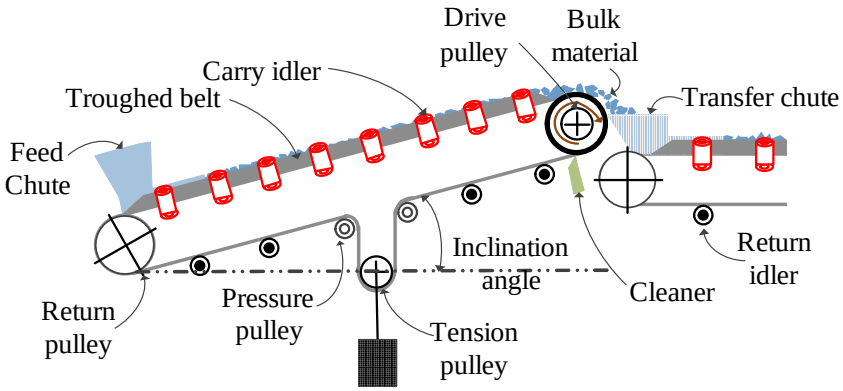

Figure 2.1. belt conveyor system.

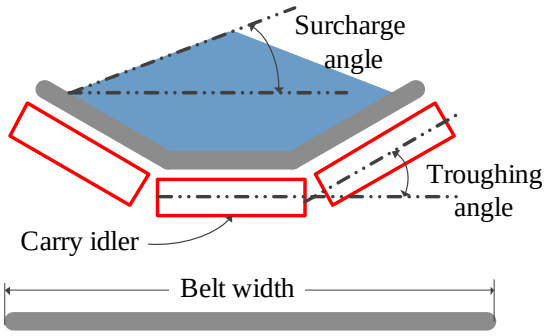

Figure 2.2. Cross-section of a troughed belt conveyor.

rolls back on return idlers. A system made-up of a counter weight, a tension pulley and some pressure pulleys is used to ensure adequate tension in the belt. This is to ensure that the belt remains in its track and avoids spillages.

Normally, the rate at which material enters the belt, the feed-rate, is regulated by a belt feeder pouring material into the feed chute. A number of different feeder designs exist including the screw feeder, belt feeder, single-plate feeder. The angular speed of the screw, the speed of a miniature belt and the deflection of the reciprocating plate control the feed-rate of the screw, belt and single plate feeders, respectively. A metal shaft connects the drive pulley to a system driving the belt conveyor. This mechanism is typically constituted of a gear-box, an electric alternating current motor, a motor drive and a braking mechanism. The belt speed is controlled by the turning motion of the motor [1, 2].

Figure 2.2 shows the cross-section of the belts' carry-side compared to the flat full width of a belt. The carrying idlers are troughed for most of the belts length so as to contain the bulk material, as shown by

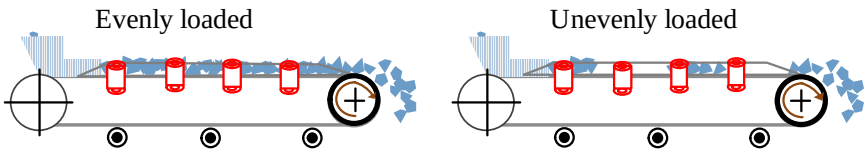

Figure 2.3. Longitudinal profile of the amount of material on the belt.

Figure 2.2. The properties of the bulk material transported comes in a wide variety of particle sizes, density, abrasiveness and corrosiveness. The selection of belt material and choice of the troughing angle are dictated by the bulk material's physical and chemical properties. For example, transporting corrosive sulphur powder requires a corrosion resistant belt material but sand does not. Similarly, a fine and smooth material such as grain has a smaller surcharge angle of 20^o-29^o compared to 35^o-39^o of an irregular and rough material such as bituminous coal. This implies that steeper troughing angle and/or a wider belt is required to transport grain than bituminous coal [1, 2].

The amount of material transferred through the BCS is controlled by manipulating the belt speed and feed-rate. The maximum speed of the miniature conveyor of the belt feeder and the size of the feeding aperture in the case of the single-plate feeder, account for the upper limit of the feed-rate, I_{max}. The two key contributing factors to the maximum belt speed, v_{max}, are the bulk material properties and the inclination angle. The important material properties for v_{max} are the particle size and abrasiveness of the material. Lumpy and abrasive material such as unscreened rock requires low speeds in order to minimise the damage on the belt especially around the loading area of the belt. However, light material such as cereal and beans can be transported at higher speeds. Increasing belt speed on an incline belt causes greater turbulence at the loading point, which leads to more abrasions [2]. Varying belt speed and feed-rate independently changes the mass per unit length of material on the belt , q. That is, the kilograms of material per meter of belt length. Figure 2.3 shows the effect of varying speed and feed-rate on linear mass density. The carrying capacity of the belt, q_{max}, is limited by its width and the troughing angle, as illustrated in Figure. 2.2. Thus, increasing q beyond q_{max} results in spillages.

The moving conveyor belts in the BCS are the main energy consumers. There are generally two widely used approaches to modelling energy consumption of a belt conveyors, namely; the energy conversion and the resistance based approaches. The energy conversion approach divides the energy consumption of the conveyor into energy required for moving an empty belt, energy required to move

belt horizontally, and vertically. The intuitive resistance based approach is the most widely used approach. This approach focuses on the individual sources of the resistance to the belts motion [3]. The motion of an upward inclined belt is resisted in different areas of the belt. The contact friction between the idlers and the belt, as well as the rolling friction of the idler resisting the belts motion throughout its length. These normally account for the largest potion of the total resistance and it occurs in all belts. A second group of resistances are those due to inertia of material loaded on to the belt and the resistance due to belt wrapping around the pulleys. There is also a special type of resistance that occurs due to a certain kind of additional fittings to some belts. This includes resistance due to parts of the loading skits touching the belt at the tail end and the scrappers cleaning the belt at the head end, just below the drive pulley. By virtue of its inclination, the force of gravity works against the motion of the belt lifting material from tail to head. This is also another type of resistance occurring in inclined belts. Thus, the effective force driving the conveyor, F_U, to overcome the various resistances is related to properties of the conveyor and the amount of material being transported. Therefore, the amount of energy, E, consumed by the conveyor, with motor and drive efficiency η, in the time interval $[t_1, t_2]$ is,

$$E(t_1,t_2) = \frac{1}{\eta}\int_{t_1}^{t_2} F_U(t)\cdot v(t)\,dt. \tag{2.1}$$

The Conveyor Equipment Manufacturing Association (CEMA), ISO 5048 and DIN 22101 define the three key standard ways of using resistances to calculate energy consumption [1, 4, 5]. These standards group the resistances experienced by the motion of the belt into appropriate classes. Their choice of groupings is fundamentally what makes these standards different. According to CEMA, resistance is due to four sources, namely; gravity when lifting material, material being conveyed horizontally, conveyor components and acceleration/deceleration of material being feed by the chute [1]. ISO 5048 and DIN 22101 consider resistances according to where they occur. The first is primary resistance occurring throughout the conveyor on both the carry and return sides. Secondly, secondary resistances occurring at the head and tail ends of the conveyor. Thirdly, special resistance occurring in particular installations of the belt and finally resistance due to height difference between the tail and head [4, 5]. The standard ISO 5048 provides the most intuitive method of modelling energy consumption and it is therefore chosen as the basis of the model proposed and used in Chapters 3 and 4. Chapters 5 and 6 employ an older model proposed in [6] that is also derived from ISO 5048.

Unlike the upward inclined, downhill conveyors are capable of generating energy. The energy management of BCS with downhill conveyors is not well researched. The currently abundant research literature on downhill conveyors is focused on the design of power electronic components and power quality issues of capturing their energy. Research into energy management of BCS with downhill conveyors is important for providing tools to assess the economic viability of capturing energy and advocating the implementation of relevant technologies. This is the theme of Chapter 4.

Traditionally, BCS are design to operate at maximum speed and capacity. It is common practice to oversize belt conveyor systems for three practical reasons. Firstly, the operation of down-steam processes being fed by a BCS may be so critical that the BCS operator cannot risk shortage of material. This would lead to an over design so that the BCS can be operated at above average throughput to recover from unforeseen up-stream system failures. Secondly, the over-sizing occurs in anticipation of short-term capacity expansions of the plant that sometimes may not be realised. Lastly, some sections of the BCS may be oversized as the BCS operator attempts to standardise the whole BCS's component sizes so as to lower maintenance costs [7]. In other applications such as mining BCS are loaded directly using excavators [8]. For these reasons, many conveyor belts operate with their q lower than q_{max} and in extreme cases some sections of the belt may be empty, as illustrated in Figure 2.3. However, studies have shown that energy efficiency is achieved by insuring that q is as close as possible to q_{max} [6, 9, 7, 10, 11]. Thus, the value of q is a very important contributor to energy efficiency of belts, especially when the belts are long. The proposed energy model in Chapter 3 considers this.

2.2 DEMAND-SIDE MANAGEMENT AND ELECTRICITY PRICING

Plants with BCS usually run on electricity from the grid. The rapidly increasing cost of electricity prices make it necessary to find more energy efficient ways of operating energy intensive industrial plants such as BCS.

Electricity is supplied through the grid from sources (power stations) with varying costs of generation. The grid normally has no storage for electricity. Thus, the cheapest power stations are dispatched first. The total real-time power usage of the grid (in watts), normally fluctuates cyclically within a day, week and year. The total system load (in watts) follows a nearly predictable pattern of relatively short peak usages on top of an almost flat and persistent base load [12]. As a result, it is cheaper to supply the base

load than the peak loads. For this reason, demand-side management (DSM) programmes are being introduced in order to reduce and flatten the total system load. DSM programmes can either be incentive based or time based. An incentive based programme (IBP) encourages the electricity consumer to reduce their consumption during peak usage times by offering monetary rewards proportional to their power reduction. Alternatively, a time based programme (TBP) discourages the electricity consumption during peak times by imposing high electricity prices at these times [13, 14].

TBPs are being applied more widely than IBPs because they are easier to implement. This thesis therefore focuses on TBP. Time-of-use (TOU), Critical peak pricing (CPP) and real-time pricing (RTP) are some of the commonly used tariff structures, within the TBP [14, 15, 16]. Under TOU, prices of electricity are fixed for each period of the day during the whole year or season. On the contrary, in RTP, the price of electricity changes frequently, usually every hour. Under CPP, the discounted TOU prices are normally applied and relatively higher prices are used during critical days, at the utility's discretion [14, 17]. Eskom, the South African state-owned power utility, is also moving towards more dynamic pricing schemes [18]. One of Eskom's recent initiatives is the implementation of a critical peak pricing (CPP) pilot project currently under way[1]. Chapters 4 and 5 use a TOU tariff. Chapter 5 also focuses on CPP, while Chapter 6 deals with RTP.

DSM programmes are useful to a power utility since it improves the reliability of the power system [13]. On the other-hand, dynamic prices expose electricity consumers to the risk associated with frequently changing prices [14] . This is particularly true for RTP. The best way of risk mitigation is electricity price forecasting. There is significant interest in the accurate prediction of electricity prices [19, 20, 21, 22, 23]. The techniques used for prediction include game theory, simulation models, statistical analysis and data mining models [19].

The main focus of research in the price forecasting front is to improve the forecast accuracy in terms of the commonly used performance metrics. However, the practical benefit of a price forecasting scheme and the ability to foretell its economic benefit when it is applied remains a challenge. A number of research reports indicate that the most accurate price forecast method does not necessarily provided the best economic benefit to the energy consumer or producer [24, 23, 25, 26]. It is, therefore, necessary to assess the economic benefit of price forecasting on BCS plants operating under the RTP tariff. This is the theme of Chapter 6.

[1] http://www.eskom.co.za/c/article/975/critical-peak-day-pricing-pilot-project/

A logical extension to the DSM programmes is to also allow consumers that are able to generate electricity to feed it into the grid to earn income. The key enabling technology is a smart meter that tracks the bi-directional flow of energy and facilitates communication between the consumer and utility. From a financial point of view, this bi-directional flow of energy can be implemented using one of the following three trading methods, namely; feed-in tariff (FiT), power purchase agreement (PPA) and net metering [27]. Under the FiT method, the utility is mandated to buy all the electricity generated by the IPP at a fixed price. This method is usually meant to encourage the production of energy from sustainable sources such as solar-PV and wind [28]. The PPA method covers a wide range of contractual agreements, such as wheeling agreements. Wheeling allows for the generating customer to use the grid, for a fee, to supply another customer with their excess electricity. A power purchase agreement between the generating and buying customer, and a wheeling agreement with the utility are usually required in this case [29]. On the contrary, net metering is such that the generating customer sells excess electricity to the grid whenever it is available and buys electricity whenever it is needed. Thus, the electricity meter effectively runs in reverse when the customer is generating excess. These options are being considered and implemented by utilities around the world. As an example, Eskom is also working on a newly proposed tariff called “Genflex” in order to facilitate wheeling [30, 31]. The introduction of net metering in Germany allows for house-hold electricity consumers to sell excess electricity from their roof-top solar panels to the utility, effectively using the grid as a form of electricity storage [28]. Apart from the usual renewable sources, many of the industrial and commercial consumers already produce excess heat that can be captured to generate electricity that is fed back to the grid. For example, heat from the electric arc furnace in steel making plants. These developments raise the need for a thorough understanding of how DSM programmes such as these can be exploited for the benefit of conveyor belt operators. The analysis in Chapter 4 focuses on the issue of capturing energy from downhill conveyors under the "Genflex" tariff.

2.3 OPTIMAL SCHEDULING

Optimal scheduling of BCSs informs the supervisory control of a BCS operator on when to change the BCSs’ belts speeds and feed-rates to gain maximum benefit from the DSM programme. The optimal schedule allocates most power usage of the BCS to periods of low electricity prices and if necessary some to periods of high electricity consumption while also meeting the operational constraints. The schedule also matches the belt speeds to feed-rates in order to reduce the energy consumption of the

BCS. This optimal schedule is calculated by solving an optimisation problem [6, 32, 33, 34]. An optimisation problem is written as shown by Equation (2.2).

$$\begin{aligned} &\min_{y_1,y_2,\ldots y_n} f_{\text{Obj}}(y_1,y_2,\ldots y_n) \\ &\text{such that,} \\ &y_1,y_2,\ldots y_n \in \mathbb{S}, \\ &g_i(y_1,y_2,\ldots y_n) = 0 \; \forall i \in \{1,2,\ldots m\}, \\ &h_j(y_1,y_2,\ldots y_n) \leq 0 \; \forall i \in \{1,2,\ldots l\}. \end{aligned} \tag{2.2}$$

Equation (2.2) is an example of an optimisation problem, characterised by the variables y_k, objective function $f_{\text{Obj}}(\cdot)$ and, constraints $\mathbb{S}$, $g_i(\cdot)$ and $h_j(\cdot)$. $\mathbb{S}$ is a set defining a range of permissible values of the optimisation variables. The functions $g_i(\cdot)$ and $h_j(\cdot)$ are the equality and inequality constraints that must be met by the variables. A solution, $\{y_1,\ldots y_n\}$, is said to be feasible if it satisfies all constraints. A mathematically rigorous definition of optimality explains it in terms of derivatives of a Lagrangian combining the objective and constraints functions [35]. For the purpose of this thesis, a much simpler treatment shall suffice. Therefore, an optimal solution $\{y_1^*,y_2^*,\ldots y_n^*\}$ is simply defined as a feasible solution that gives the lowest value of the objective function.

The type of an optimisation problem depends on the types of variable and the nature of the constraints and objective function. For example, a problem is called binary when $\mathbb{S} = \{0,1\}$ and it is called mixed-integer when $\mathbb{S}$ contains integers and real numbers. In a similar manner, a problem is said to be linear when all function $f_{\text{Obj}}(\cdot)$, $g_i(\cdot)$ and $h_j(\cdot)$ are linear and it is called non-linear whenever one of these functions is non-linear. For example, the majority of the optimisation problems in Chapters 4, 5 and 6 are non-linear optimisation problems. The problem in (6.2) of Chapter 6 is a linear binary integer problem. Optimisation problems can also be classified as either stochastic or deterministic. Unlike their deterministic counterparts, the objective functions and/or constraint functions of stochastic problems depend on random parameters whose value can only be known after the optimisation problem is solved. A chance-constrained optimisation problem formulated in Chapter 5 is an example of a stochastic optimisation problem [35, 36].

Figure 2.4 shows the general approach adopted for solving BCS optimal scheduling problems. The first step is to analyses the system with the purpose of identifying the objective, variables that can

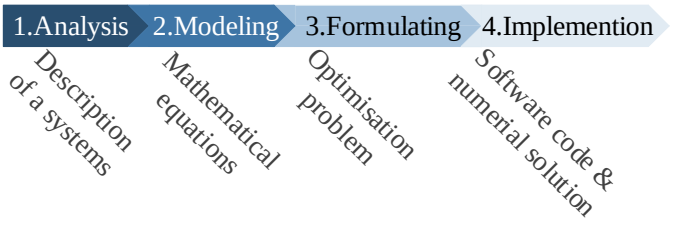

Figure 2.4. General approach for formulating and solving BCSs optimal scheduling problems.

be manipulated to influence the objective, limitations and the interactions between the individual sub-systems. For industrial energy management purposes, the primary objective can be to reduce energy consumption and energy costs. The output of this step is a concise description of the systems, its operation and what objectives need to be achieved. There may also be other objectives needed for proper operation of the system such as lowering maintenance costs. In the case of BCS, the constraints include actuator limits, belt capacity, storage capacity and, plant specific operational requirements such as maintaining a minimum level in storage bins. The possible optimisation variables are on-off status of the belt conveyor drives, belt speed and hopper feed-rate. For example, the on-off status of the belts and pumps are used as variables in [32] and [34].

The purpose of the second step of the procedure in Figure 2.4 is to derive mathematical models from the description obtained in step 1. A real system such as a BCS is infinitely complex and cannot to be completely described by mathematical equations. This being the case, a balance has to be struck between accuracy and complexity. Moreover, care must be taken that only the relevant processes of the system are modelled. For example, the analysis in [32] models the BCS and associated train schedule. Dynamic systems such as the belt conveyors are modelled using differential equations or partial differential equations (PDEs). The proposed new energy model in Chapter 3 uses a PDE. While the mathematical equations describing dynamic systems are continuous-time in nature, optimisation algorithms are able to easily tackle discreet-time equations. Therefore, the equations describing systems have to be discretised. In fact, the model in Chapter 3 is discretised in both time and space. Pseudospectral methods and the finite difference methods (FDMs) are some of the commonly used ways of discretisation [32, 37]. FDMs approximate the differential equation using the finite differences to approximate derivatives. Only FDMs are used in this thesis.

In step 3, the mathematical equations from step 2 are posed as an optimisation problem in the format given by (2.2). The formatting of the optimisation problem may involve using some constraints to

eliminate redundant variables and relaxing some constraints by adding them to the objective as penalty functions. Sometimes scaling of the variables is necessary [35]. This process is intended to create an optimisation problem that can be solved as easily as possible.

Generally the objective function for scheduling BCS is a weighted sum of two components as expressed in (2.3), namely; the energy cost component f_{Energy} and the mechanical cost f_{Mech}.

$$f_{\text{Obj}} = f_{\text{Energy}}(P, \pi, t) + \omega f_{\text{Mech}}(v) \tag{2.3}$$

The weighting parameter, ω, is set according to the desired trade-off between the two cost components. Equation (2.3) shows that f_{Energy} is a function of electrical power drawn by the conveyor, P, electricity pricing, π, and time. Extreme changes in belt speed causes high amounts of longitudinal stress on the CB and may lead to system failure [38]. Thus, it is advisable to avoid large velocity ramp rates. This will lead to reduced conveyor maintenance costs. This cost is represented by f_{Mech} that is dependent on belt speed, v. The most commonly applied way of representing f_{Mech} is using the sum of belt speed ramp squares at sampling instances 1, 2, n, $n+1$, ..., i.e, $f_{\text{Mech}} = \sum_n (v_n - v_{n+1})^2$ [33]. This techniques has been applied in Chapters 3 - 6 where variable speed control of conveyors is concerned.

In step 4, the optimisation problem is translated into a software code that is executed to obtain a numerical solution. During this step care must be taken to ensure that the relevant solver software is selected. For example, a non-linear program solver such as *fmincon*[2] can solve a quadratic problem but not a mixed-integer linear problem. The problems in this work are solved on the Matlab software platform using native solvers and others from a toolbox called *OPTI*[3].

The solver software is an implementation of an optimisation algorithm. These algorithms solve optimisation problems iteratively by improving an initial guess of the solutions. Existing algorithms can be divided into two broad categories based on their underlying theories. The first category relies on heuristics such as mimicking biological processes and the second on mathematical analysis [35, 36]. The work in this thesis uses algorithms of the second category because they have been proven to converge when solving well-posed problems. Algorithms mimicking biological processes such as the Genetic Algorithm (GA) have not been proven to be convergent. However, they are easy to implement and are able to solve some problems more quickly than those of the second category [36]. The majority of the problems encountered in this work is nonlinear. Therefore, algorithms such as interior-point

[2] A Matlab package solver

[3] http://www.i2c2.aut.ac.nz/Wiki/OPTI/

and sequential quadratic programming methods are used. The interior-point method searches for the optimal solution by moving within the set of feasible solutions. Alternatively, sequential quadratic programming methods model the non-linear problem as a sequence of quadratic problems.

The scope of the current work is restricted to the formulation of energy optimisation challenges into optimisation problem. That is, the primary focus of this work is on the first three steps shown in Figure 2.4. The optimisation software implementing the various algorithms is employed as black-boxes accepting a problem and providing an optimal solution. Therefore, the details of how optimisation algorithms work are also beyond the scope. The technicalities of varying belt speed are an important consideration since such variations can lead to problems such as excessive belt tension and motor damage during deceleration [38, 39]. This is an active area of research that is also beyond the scope of the current work.

CHAPTER 3 A NEW ENERGY MODEL FOR LONG BELT CONVEYORS

The need for energy efficiency and energy cost savings requires a better understanding of BCS energy models. This chapter proposes an energy model for long troughed belt conveyors. The new model is necessary because of the conveyor technological advances that are currently leading to increasingly long belt conveyors being commissioned. The model is based on resistances and it captures the flow of the conveyor's load using a partial differential equation. Unlike, the previously proposed models, the proposed model accounts for the different amounts of material mass per unit length throughout the whole of the conveyor's length and so it is able to give a more accurate estimate of the belt's energy consumption. The proposed model is verified by comparing it to a model proposed by Zhang and Xia in [6]. Verification results show that the power consumption calculations of the newly proposed simpler model are consistent with those of a known non-linear model with an error of less than 4%. An identification procedure for estimating the two model parameters is given. Simulations indicate that the parameters can be identified successfully from data with up to 15% measurement noise. The proposed model gives better predictions of the power consumed and material delivered by a long belt conveyor than the steady-state models in the current literature.

3.1 INTRODUCTION

The rising electricity prices and changing tariff structures are driving an increasing need for efficient and cost effective use of electricity, especially in energy intensive industrial applications such as bulk material transportation [40, 41, 42, 43]. Electricity remains an important source of energy for industries. Large electricity consumers need an accurate understanding of their operations in order to take advantage of the increasing number of tariff structures being rolled-out [40, 42]. The efficient

and cost effective running of belt conveyors, like any other application, requires accurate plant models to be used by optimising algorithms such as that demonstrated in [43]. This chapter proposes a new energy model for belt conveyors (BCs) with long, troughed belts. This model is suitable for conveyors longer than 1 km. The ultimate goal is to use the proposed model for accurate assessment of the energy consumption and cost of operating long BCs.

Troughed conveyor belts are a widely used method of bulk material transportation. They are used in power plants, mining and mineral processing, food and chemical industry as well as in ports [44, 45]. The bulk material transportation industry generally regards conveyance distances over 1 km as long and thus this definition is adopted in this chapter. The current technological trend sees increasingly longer belts being deployed, with lengths up to 20 km on a single flight [46, 10]. A conveying system can also be further elongated in applications that connect several belts in series, so as to navigate a rough terrain [10]. However, long belts are more technically challenging to control at high speeds and so many are relatively slow with a typical speed of less than 8 m/s [47].

Energy efficiency in belt conveyors is achieved by matching belt speed to the input material feed-rate in order to maximise the mass of material conveyed per unit length and consequently, per unit of energy [6]. The mismatch between speed and the feed-rate exists because in practice conveyors tend to operate at slightly below full capacity. BCs are usually oversized during design to cater for anticipated capacity expansions and sometimes to standardise component sizes in an effort to lower maintenance costs [7]. In mining applications, conveyors maybe loaded by an excavator resulting in an uneven loading of the belt so that the overall material flow rate is 50-70% of full capacity [8].

The majority of the current literature in belt conveyor modelling focuses on dynamic modelling of the belt tension, elastic properties of the belt material and modelling individual types of resistances [47, 45, 48]. However, there is also a need for the energy model to capture the quantities of material transferred by conveyors for the purposes of energy cost optimisation, as demonstrated in [43]. The current models assume a steady-state condition with a uniform material density through-out the whole belt [33, 32]. On very long belts, the effect of variable mass per unit length can be significant, because it takes a significant amount of time for material to move from a loading point (at the tail) to a discharge point(at the head). The model proposed in this chapter is able to accurately capture the amounts of material loaded on each section of the conveyor belt and, hence, to calculate an accurate value of power required by the conveyor.

The ISO 5048, DIN 22101 and CEMA modelling standards provide a concise analytical model based on resistances, in particular the primary resistance [1, 4, 5, 6]. The CEMA model requires knowledge of three friction coefficients accounting for, namely; ambient temperature correction, belt-idler friction and belt-load flexure [1]. Unlike CEMA, ISO 5048 and DIN 22101 require only one primary friction coefficient and a more generic means of calculating other resistances [4, 6, 7]. As a result, they form the basis of the model proposed in this chapter. However, all modelling standards are based on typical values of friction coefficients that require rules of thumb and an experienced engineer to estimate. A parametric model that can be estimated using field measurements, therefore, becomes a more useful and practical option for accurate predictions of energy consumption.

The proposed energy model uses a first-order partial differential equation (PDE) to capture the state of material on the belt and a two-parameter equation derived from established industry standards to quantify the conveyor's power requirements. Unlike the previously proposed models, our model accounts for the different amounts of mass per length throughout the whole of the conveyor's length, and it is therefore able to give a more accurate estimate of the belt's energy consumption. The proposed model is verified by comparing its steady-state calculations to a model proposed by Zhang and Xia in [6]. The model in [6] is used for comparison, because it is also derived from ISO 5048. The results show that the proposed energy model gives power values close to those obtained from [6], under maximum loading conditions. A novel system identification set-up using a recursive algorithm to estimate the model parameter is proposed. The variables required for measurement on the proposed set-up are identified. A sensitivity analysis of the power equation is used to justify the different parameter convergence rates, and their practical implications are discussed. The proposed model is useful in applications when the conveyor speed is controlled, as shown in the case-study application. The case-study simulation of the proposed model is shown to perform better than the steady-state approach in scheduling of a BCS under a time-of-use tariff.

The remainder of the chapter is organised as follows: Section 3.2 presents the derivations of the proposed model. Section 3.3 verifies the proposed model by comparing its BC power consumption calculations to those of an existing model. Section 3.4 investigates the accuracy of the proposed model's calculations and presents a parameter identification procedure. Section 3.5 presents a simulation example illustrating the use of the proposed model on the day-ahead scheduling of a BCS. Section 3.6 presents the conclusions.

3.2 CONVEYOR MODEL

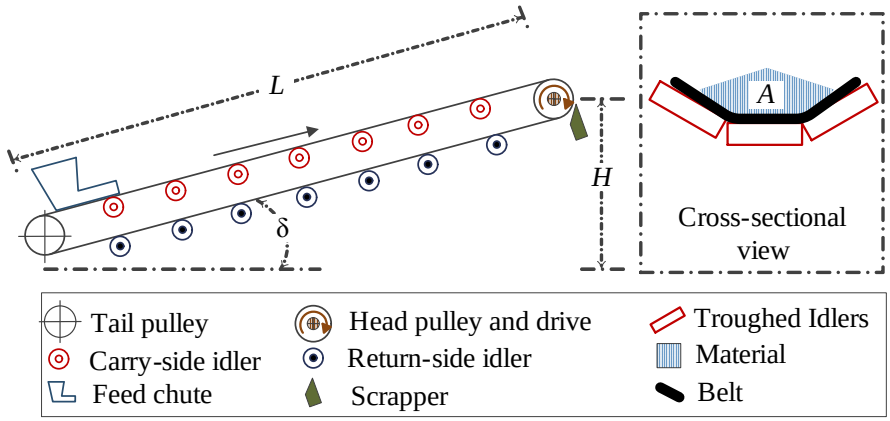

Figure 3.1. Simplified sketch of a conveyor.

A troughed conveyor is powered by an electric motor driven system and supported by a system of pulleys, as shown in Fig. 3.1. The conveyor carries the bulk material on top of a troughed surface of a rubber belt. The troughed structure of the belt is maintained by sets of evenly spaced idlers (see cross-sectional view of Fig. 3.1). Proper idler spacing is determined during the design phase as recommended by industry guidelines such as [1] and [5], to avoid excessive belt sag and potential spillages. This ensures that the cross-sectional area of the belt is fairly constant. The belt is usually fitted with accessories such as a feed chute at the tail end and a scrapper below the head end.

3.2.1 Conveyor resistances

The electrical power required by a BC, P, is a product of the required peripheral driving force, F_U, the belt speed and drive system efficiency, η, i.e., $P = \frac{1}{\eta} F_U \cdot v$ [6]. The peripheral driving force is given by,

$$F_U = F_H + F_N + F_{St} + F_S, \tag{3.1}$$

where F_H, F_N , F_{St} and F_S, are the primary, secondary, slope and special resistances [4].

All resistances are dependent on the amount of material that the conveyor belt is carrying. By convention, this amount is specified in mass per unit length, $q(x,t)$. Thus, $q(x,t)$ is the mass of material per unit length of a conveyor belt section located at position x during time t in kg/m. Let:

$$\bar{q}(t) = \frac{1}{L}\int_0^L q(x,t)dt, \tag{3.2}$$

be the average mass per unit length over the total length, L, of the belt conveyor. When the flow of material on the BC is steady, $q(x,t)$ is uniform and constant. That is, $\bar{q}(t) = q(x,t)$ and $\bar{q} = \bar{q}(t)$. In order to obtain an energy model based on amount of material, we begin by relating $\bar{q}$ to all of the resistances given in (3.1).

Primary and slope resistances

Consider an L meters long belt with an artificial coefficient of friction f, inclined at an angle δ and operating under the Earth's gravitational constant g. Supposing the unit mass per meter of the belt, carrying-side revolving idlers and return-side revolving idlers unit mass are, q_B, q_{RO} and q_{RU}, respectively. Then, the primary resistance is given by,

$$F_H = C_1 + C_2 \cdot \bar{q}, \tag{3.3}$$

where $C_1 = fLg[q_{RU} + q_{RO} + 2q_B\cos\delta]$ and $C_2 = fLg\cos\delta$.

$$F_{St} = C_7 \cdot \bar{q}, \text{ where } C_7 = gH. \tag{3.4}$$

The slope resistance in (3.4) is dependent of the height difference, H, between the tail and head ends of the conveyor. The slope and primary resistances account for the majority of the energy consumption, and they are easy to calculate [7]. For temperatures above 0 ^oC, the ISO and DIN standards prescribe a basic value of friction coefficient is 0.020 [5]. The exact value of f varies per installation, and a detailed account of its determination is given in [49]. For long conveyors, f is even lower than 0.016, a typical minimum value for short conveyors [7].

Special resistance

Special resistance, F_S, depends on the special accessories fitted on the belt. Depending on the installation, the accessories may include; friction due to idler tilting, contact with skirt-board, contact with chute flaps and contact with discharge ploughs. F_S is described by,

$$F_S = C_4 \cdot \bar{q} + C_5 \cdot \bar{q}^2 + C_6, \tag{3.5}$$

where $C_4 = c_\varepsilon \mu_0 L_\varepsilon g \sin\varepsilon \cos\delta$, and $C_6 = \mu_0 L_\varepsilon g \sin\varepsilon \cos\delta\,(c_\varepsilon + \cos\gamma)\, q_B + A_s p \mu_3 + BK_a$. Resistance from the material due to carry-side idler tilting is given by $C_4\bar{q}$. C_4 depends on the toughing factor c_ε, length of belt with tilted idlers L_ε and ε idler tilt angle. L_ε is equal to L minus the transition length at the tail and the head ends of the conveyor where the belt is guided towards/from a pulley. Usually the transition length is small and thus, $L \approxeq L_\varepsilon$ [5]. The resistance due to return and carry-side idlers, scraper and contact with skit-plates is C_6. C_6 depends on the contact area of the scraper A_s, pressure applied by the scraper p, scraping factor K_a and the toughing angle γ as shown in (3.5). $C_5 = \mu_2 g l/(b_1^2 \rho)$ is the friction due to contact on the skirt-plates [4]. C_5 depends on the skirt-plate length l and width b_1 between the skirt-plates. The skirt-plates are installed over a very short length at the head of the conveyor so as to guide material from the feeder and avoid spillages. Thus, $l \ll L$, and the effect of $C_5\bar{q}^2$ is local, independent of L and small compared with the overall resistance value [7]. C_4 ,C_5 and C_6 are equivalent to k_1 , k_2 and k_3 of [6], respectively.

Secondary resistance

Secondary resistance has three sub-components, namely; the resistances occurring at the pulley, C_8, resistance due to acceleration of material at the tail end, F_{NL}, and resistance due to acceleration of the material on the skirt plate, F_{NS}. Thus,

$$F_N = F_{NL} + F_{NS} + C_8, \tag{3.6}$$

where $F_{NL} = v^2\bar{q}$, $F_{NS} = C_3 \cdot v^2\bar{q}^2$ and $C_3 = 2\mu_2/(\mu_1 b_1^2 \rho)$. Normally, material is launched at none zero speed onto the conveyor. However, this speed is taken to be zero for the purposes of calculating accelerations relating to F_{NL} and F_{NS}. In this case, the maximum amount of secondary resistance is assumed, risking a slight over estimation of the power consumption. F_{NS} depends on the width between the skirt-plates, b_1, the loose bulk density of the material, ρ (in kg/m^3), material friction coefficient on

the belt μ_1 and the skirtplates μ_2, as shown in (3.6). C_8 depends on a number of parameters including the material composition of the belt, belt width B and average tension at the pulley. The measurement or calculation of the average tension is complex and, therefore, C_8 is difficult to calculate. Nevertheless, the modelling error will be small because the amount of secondary resistance is small compared with the primary. The modelling error becomes even smaller as the conveyor's length increases.

An easier alternative of calculating F_N, more suitable for long conveyors, is provided by [4] and shown in (3.7).

$$F_N = F_H(C_9 - 1). \tag{3.7}$$

ISO [4] indicates that for conveyors longer than 80 m, the secondary resistance is related to the primary resistance by a main resistance factor, C_9, as shown in (3.7). For example, the values of C_9 for 100 m and 1 km long conveyors are about 1.8 and 1.1, indicating that the secondary resistance is 44% and only 9% of F_H for the two lengths, respectively. The approximation of F_N suggested by (3.7) shows that the contribution of F_N on the total resistance is generally lower than 10% of F_H when the belt length is 1 km or longer. For this reason, we consider belts of length 1 km or more as long BC and suitable for the model being proposed.

3.2.2 Modelling energy consumption

Substituting for the secondary resistance and resistances from (3.3) to (3.5), into (3.1) leads to,

$$F_U = C_9C_1 + C_6 + (C_9C_2 + C_4 + C_7)\cdot\bar{q} + C_5\cdot\bar{q}^2. \tag{3.8}$$

Let the no-load and density parameters be $\varphi_1 = C_9C_1 + C_6$ and $\varphi_2 = C_9C_2 + C_4 + C_7$, respectively. Due to the influence of C_1 and C_2, the value of parameters φ_1 and φ_2 increase quickly with increasing L. On the contrary, C_5 is independent of the belt length and its value is much smaller than φ_1 and φ_2, since it is a component of F_S. As a result, C_5 is much smaller when compared with both φ_1 and φ_2, for long conveyors. For example, a 2 km conveyor with specification similar to those specified in [3] will have a φ_1 =380 kN, φ_2 =685 $\mathrm{m^2s^{-2}}$ and C_5 =4.01×10^{-2} $\mathrm{m^3s^{-2}kg^{-1}}$. Thus, for long conveyors, the total resistance is given by,

$$F_U = \varphi_1 + \varphi_2 \cdot \bar{q} + C_5 \cdot \bar{q}^2 \approx \varphi_1 + \varphi_2 \cdot \bar{q}. \tag{3.9}$$

For long conveyors, the approximation in (3.9) is possible because all the non-linear components are from F_S, whose contribution is very small and, therefore, can be ignored. This means that for long belts, the total resistance can be approximated as linearly dependent on the average linear mass density with a fair amount of accuracy. Moreover, F_S does not occur in all conveyor belt installations. However, the power model in (3.9) is generic and applies to all long conveyors because, the length-dependent coefficients of F_S (C_4 and C_6) are incorporated into the parameters φ_1 and φ_2, so the presence or absence of F_S would be easily accounted for by a parameter identification procedure.

For variable loading, $q(x,t)$ varies throughout the length of the belt. Therefore, according to (3.2) and (3.9), the amount of power required to drive a long conveyor is,

$$P(t) = \frac{1}{\eta}(\varphi_1 + \frac{\varphi_2}{L}\int_0^L q(x,t)\,dx) \cdot v(t). \tag{3.10}$$

Motor and drive mechanism efficiencies vary with changing motor speed and load [7]. However, variations become small for very large motors, such as those used to drive long conveyors. Thus, a constant value of η can be used and the rest of the small efficiency variations will be incorporated within the modelling parameters. Eqn. (3.10) implies that calculating the energy consumption of a long conveyor requires the knowledge of only two parameters. Therefore, the energy consumed over a time interval $[t_1, t_2]$ is given by,

$$E(t_1,t_2) = \frac{1}{\eta}\varphi_1 \int_{t_1}^{t_2} v(t)\,dt + \frac{\varphi_2}{\eta L}\int_{t_1}^{t_2}\left[\int_0^L q(x,t)\,dx\right] v(t)\,dt. \tag{3.11}$$

It is worth noting that relating the BC resistances to $\bar{q}$, in the derivation of (3.9), introduces an error in power calculations when $q(x,t)$ varies. This error underestimates and overestimates the power requirement of different sections of the conveyor where $q(x,t)$ is higher and lower than $\bar{q}$, respectively. However, the overall error is reduced as the individual errors are summed in a long BC. Moreover, the impact of these errors becomes small for steep belts where F_{st} is dominant.

3.2.3 Modelling bulk material flow

The material mass per unit length is limited by the maximum carrying capacity of the belt, q_{max}. It can be understood from the cross-sectional view of the BC in Fig. 3.1 that increasing $q(x,t)$ on a section of the belt would increase the height of material above the belt's bottom surface until the material spills over when it can no-longer be contained by the troughing.

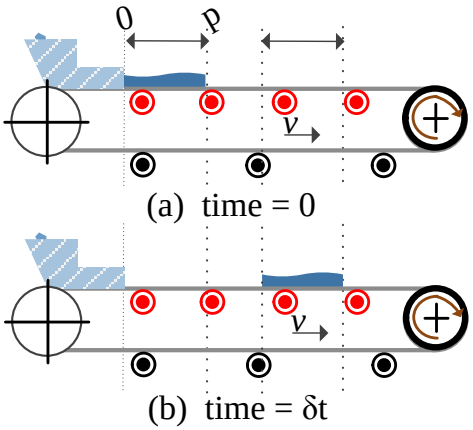

Figure 3.2. Wave-like property of material flow on the conveyor belt.

Figure 3.2 represents a longitudinal view of the material traveling at v m/s on an L meters conveyor belt, where the height of material above the bottom belt surface represents the magnitude of $q(x,t)$. Fig. 3.2(a) shows the BC initially at time 0 seconds, just as the outlet of the chute is being stopped. Fig. 3.2(b) shows the status of the same mass, M, of material on the belt after time δt seconds. The bulk material on the conveyor flows from tail to head with negligible amount of diffusion. Therefore,

$$M = \int_0^p q(x,t)dx = \int_{v\delta t}^{p+v\delta t} q(x,t+\delta t)dx. \tag{3.12}$$

Thus, after δt seconds, all of the mass of the material that was located before the position p or in the interval $[0,p]$ meters is now located within the interval $[v\delta t,\ p+v\delta t]$ meters. This implies that material on the belt behaves like a wave travelling at a constant speed until it is spilled at the head of

the conveyor. According to the fundamental theorem of calculus, differentiating M given in (3.12) with respect to p gives,

$$q(p,t) = q(p + v\delta t, t + \delta t). \tag{3.13}$$

Differentiating (3.13) with respect to δt and then letting $\delta t = 0$ results in the partial differential equation (PDE) (3.14) [50].

$$\frac{\partial}{\partial t} q(x,t) = -v(t) \frac{\partial}{\partial x} q(x,t), \tag{3.14}$$

where $v(t)$ is the belt speed. The modelling in [51] also confirms that this wave-like motion of material, where the mass balance equation in (3.12) holds, can be modelled using a one-dimensional transport equation (3.14).

The total amount of material discharged by the conveyor, M_{out}, and the total amount of material entering the conveyor, M_{in}, during the time interval $[t_1, t_2]$ are,

$$M_{\text{out}} = \int_{t_1}^{t_2} v(t) q(L,t)\, dt \text{ and } M_{\text{in}} = \int_{t_1}^{t_2} v(t) q(0,t)\, dt = \int_{t_1}^{t_2} I(t)\, dt, \tag{3.15}$$

where $I(t)$ is the input feed-rate of the conveyor. For computational purposes the model can be discretised to using a finite difference method (FDM). FDMs offer a simple way of calculating numerical solutions of partial differential equations [37]. The model is discretised into N_x samples in space and N_t samples in time over a given total time period TD. The space sampling points are located at points $i \cdot \Delta x$ (where $\Delta x = L/N_x$) and time sampling points occur at instances $n \cdot \Delta t$ (where $\Delta t = TD/N_t$). Using the discretisation, the mass per unit length of material located at a point $i \cdot \Delta x$ on the belt during a time sample $n \cdot \Delta t$ is denoted by $q(i,n)$, i.e.

$$q(i,n) = q(i \cdot \triangle x, n \cdot \triangle t). \tag{3.16}$$

For brevity, the average and individual mass per length at different points at times $t = n \cdot \Delta t$, are represented by $\bar{q}_n$ and $\mathbf{q}_n$, respectively. That is, $\mathbf{q}_n = [\ q(1,n) \quad \ldots \quad q(N_x,n)\ ]^T$ and $\bar{q}_n = \sum_{i=1}^{N_x} q(i,n)$. Usually, for scheduling, the modelling assumption is that both the input feed-rate and belt speed are constant over a single time sample period, e.g., $v(t) = v_{n-1}$ and $I(t) = I_{n-1}$, for $t \in [(n-1) \cdot \Delta t, n \cdot \Delta t]$. It, therefore, follows that the discrete representation of the initial densities of material on the belt, $q(x,0)$, is $\mathbf{q}_0$. Using the above notation, the boundary conditions at the tail become,

$$q(0,n) = I_{n-1}/v_{n-1}. \tag{3.17}$$

The implicit Backward Euler (BE) method is selected for solving (3.14). This FDM method is unconditionally stable when solving the first order wave equation such as (3.14) [37]. The BE method uses a backward and a centred difference to approximate the time and space partial derivatives, respectively. A backward difference on the space derivative is used for the head of the conveyor because $q(N_x+1,n)$ is invalid. Applying this method to (3.14) results into the following N_x equations,

$$q(i,n+1) = \begin{cases} 2\{q(i-1,n) - q(i-1,n+1)\}/\gamma_i + q(i-2,n+1) & i = 1,2,3,\ldots N_x - 1 \\ \{q(N_x,n) - q(N_x-1,n+1)\}/(\gamma_i+1) & i = N_x \end{cases}, \tag{3.18}$$

where $\gamma_n = v_n \frac{\triangle t}{\triangle x}$. Equation (3.18) can also be represented in matrix and vector form as,

$$G_n \mathbf{q}_{n+1} = \{\mathbf{q}_n + \mathbf{b}_n \cdot I_n/v_n\} \text{ where } G_n \in \Re^{N_x \times N_x}, \mathbf{b}_n \in \Re^{N_x \times 1}, \tag{3.19}$$

The elements of the matrix G_n and vector $\mathbf{b}_n$ n are given by (3.20).

$$G_n = \begin{bmatrix} 1 & \gamma_n/2 & 0 & \cdots & 0 & 0 & 0 \\ -\gamma_n/2 & 1 & -\gamma_n/2 & & 0 & 0 & 0 \\ 0 & -\gamma_n/2 & 1 & \ddots & 0 & 0 & 0 \\ \vdots & & \ddots & \ddots & \vdots & \vdots & \vdots \\ 0 & 0 & 0 & & 0 & 0 & 0 \\ 0 & 0 & 0 & & -\gamma_n/2 & 1 & \gamma_n/2 \\ 0 & 0 & 0 & & 0 & -\gamma_n & (1+\gamma_n) \end{bmatrix}, \mathbf{b}_n = \begin{bmatrix} \gamma_n/2 \\ 0 \\ 0 \\ 0 \\ \vdots \\ 0 \\ 0 \end{bmatrix}. \tag{3.20}$$

3.3 MODEL VERIFICATION

3.3.1 Steady-state power calculations

For verification, the 325 metre long conveyor example given in [3] is used but with different lengths beginning from 500 m to 3 km in steps of 500 m. The maximum power required by the conveyor

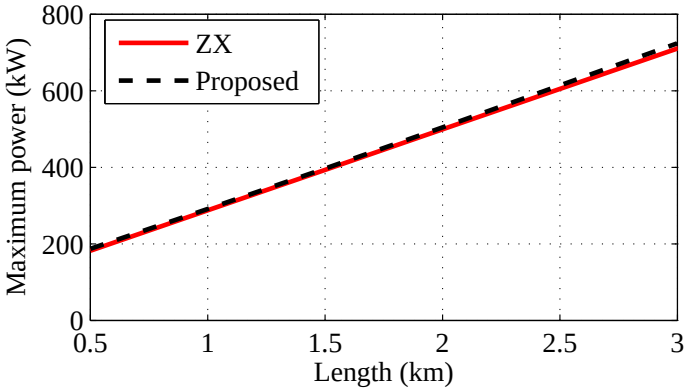

Figure 3.3. Maximum capacity power calculations for both models.

Table 3.1. Contributions of individual components to the total power required.

Unit	Component			
	Total	φ_1	$\varphi_2 \cdot \bar{q}$	$C_5 \cdot \bar{q}^2$
		L =500 m		
kW	191.3	41.7	145.7	3.9
%	100.0	21.8	76.1	2.1
		L =2 km		
kW	508.1	123.7	380.4	3.9
%	100.0	74.9	28.7	0.8

operating at full carrying capacity is calculated analytically, for both the proposed linear model of (3.10) and the model from [6], labelled as ZX. Fig. 3.3 shows that the maximum capacity power calculation values of the proposed linear model are close to those of ZX model for short and medium length belt conveyors.

The key assumption of the parametric power model in (3.10) is that the non-linear components of the resistance are sufficiently small for long conveyors. The model in [6] and (3.10) are both based on ISO 5048 even though (3.10) is linear with two fewer parameters. In order to verify the linearity assumption, resistance values of each summation of (3.9) are calculated, and their contribution to the total power consumption assessed, for two belts with lengths 500 m and 2 km.

Table 3.1 gives typical values of power and their percentage contribution to the total power when a belt

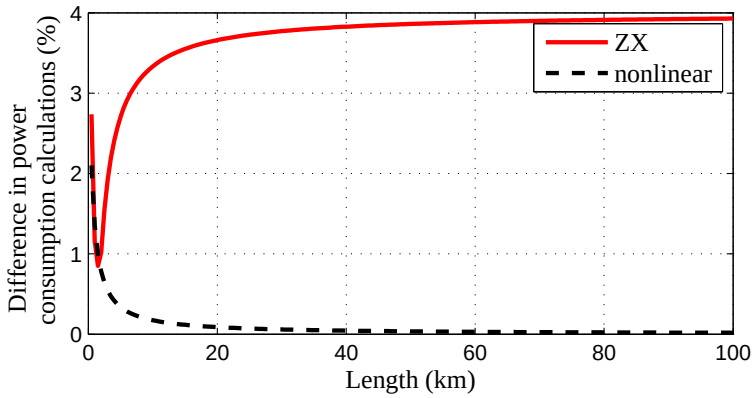

Figure 3.4. Percentage differences in power consumption calculations for the ZX and non-linear models relative to the proposed model.

given in [3] is operated at maximum speed and capacity. The calculations in Table 3.1 show that the non-linear component's contribution is much smaller than that of the linear component. The effect of the non-linear component diminishes with increasing conveyor length, *i.e.,* it decreases from 2.1% to 0.8% as the length is increased from 500 m to 2 km. Therefore, the linear simplification in (3.9) is justified.

Fig. 3.4 shows the percentage difference in maximum power calculations obtained by the linearised model's compared to the proposed nonlinear model and the model of [6], for various lengths of the conveyor. The results show that the linearisation error diminishes to 0% with increasing distance. The results also show that maximum power calculations from the proposed linear model deviate slightly from those of the model in [6], with an error that is generally less than 4%. Compared to the model in [6], the power calculation difference fluctuates for short distances below 2 km. The reason for this fluctuation is that the proposed model uses the DIN 22101 recommended values of C_9. These values are variable below 2 km, but a constant value of $C_9 = 1.05$ is used beyond the 2-km length.

3.3.2 Variable loading calculations

The real advantage of the proposed PDE model, described by (4.1) and (4.2), is its ability to capture the changes in the amount of material mass per unit length on the belt as the input feed rate and belt speed vary. The approach in [6] is that of a steady-state (SS) situation where the belt loading resulting from the current input feed-rate is assumed to instantaneously apply to the whole of the belt. An 8 km

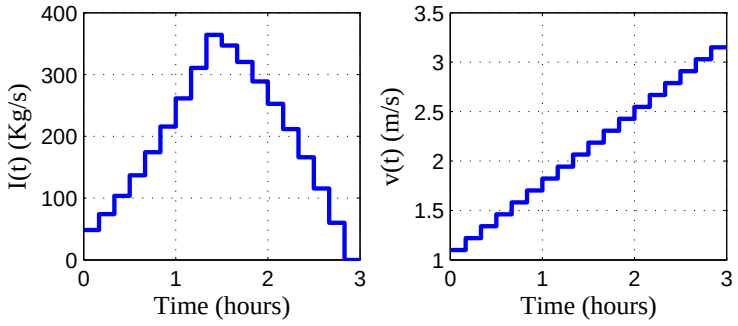

Figure 3.5. Input feed-rate and belt speed.

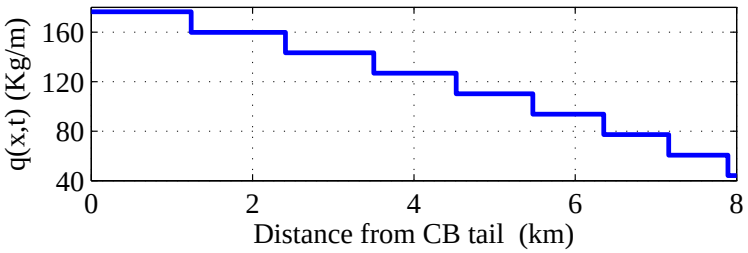

Figure 3.6. First-in-first-out (FIFO) queue model of the actual $q(x,t)$ on the belt after 1.5 h.

long belt with input feed-rate and belt speed shown in Fig. 3.5 is considered, in order to investigate the difference between the SS and PDE models.

The inputs in Fig. 3.5 cover a duration of 3 hours and they vary every 10 minutes. The actual belt mass per length at the end of each sampling time can be calculated precisely because the inputs are known. This is possible because the belt conveyor effectively operates as a first-in-first-out (FIFO) queue of $q(0,t)$'s, whose lengths are obtained by multiplying their corresponding speeds by the 10 minute sampling time (*i.e.*, $\tilde{L}_n = v_{n-1} \cdot \triangle t$). Fig. 3.6 shows the positions of the different mass per lengths on the 8-km belt after 90 minutes when the inputs shown in Fig. 3.5 are applied. For example, the mass per length at 4 km corresponds to the inputs $v = 1.70$ m/s and $I = 216$ kg/s applied 50 to 60 minutes after running the belt. Thus, q(4 km,1.5 h) = 216/1.70 = 127 kg/m, as illustrated in Figure 3.6.

Fig. 3.7 shows the simulation results of the proposed PDE model described by (3.19) for the 8 km-long conveyor with inputs shown in Fig. 3.5. The temporal and spatial resolutions used for the simulation are 5 minutes and 250 m, respectively. Fig. 3.7 illustrates the wave-like flow of material on the belt

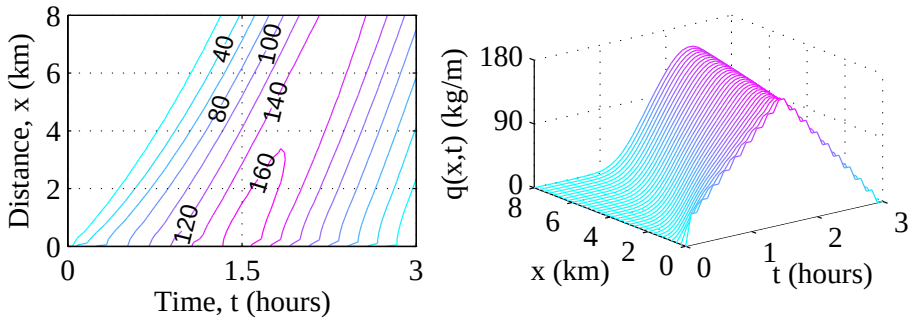

Figure 3.7. Three-dimensional view of $q(x,t)$ on the 8 km-long conveyor.

described in Section 3.2.3. During simulation, the system of linear equations obtained from the model in (3.19) is solved in the least-squares sense whenever the equality cannot be satisfied exactly. The good accuracy of the proposed flow model can be seen by comparing the actual $q(x,t)$ in Fig. 3.6 to the data on the contour map of Fig. 3.7 along t = 1.5 h. For example, the contour map in Fig. 3.7 shows that the q(4 km,1.5 h) is just above 120 kg/s, q(6 km,1.5 h) is in the range [80,100] kg/s and q(8 km,1.5 h) is marginally above 40 kg/s. These simulated model values correspond closely to the actual values of q(4 km,1.5 h) = 127 kg/s, q(6 km,1.5 h) = 93.7 kg/s and q(8 km,1.5 h) = 44.1 kg/s, shown in Fig. 3.6.

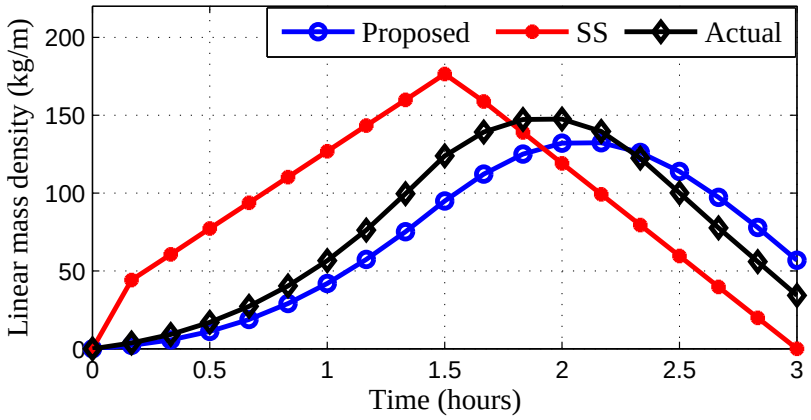

Figure 3.8. Calculated (Algorithm 1) and modelled values of the conveyor's average unit mass per length.

Algorithm 1 implements the principle of the FIFO queue illustrated in Fig. 3.6 to calculate the actual average mass per length on the belt, $\bar{q}(n)$. Algorithm 1 is also used to calculate the total amount of material received at the tail end of the conveyor after each sampling time n, $\sum_{i=1}^{n} M_{\text{out}}(i)$, given the initial uniform density of material on the belt $\mathbf{q}_0$. Algorithm 1 is based on the assumption that the belt

Algorithm 1: Calculating the actual average mass per unit length and total amount of material discharged.

Input: $v(n)$.

Output: $\sum_{i=1}^{n} M_{\text{out}}(i)$ and $\bar{q}(n)$.

Distance travelled by the belt, $D_1(n) \leftarrow \triangle t \cdot \sum_{i=1}^{n}(v_i)$.
if $D_1(n) \leq L$ **then**
  $\bar{q}(n) \leftarrow \frac{\triangle t}{L} \sum_{i=1}^{n}(q_0 \cdot v_i)$ and $\sum_{i=1}^{n} M_{\text{out}}(i) \leftarrow D_1(n) \cdot q(i,0)$
else
  Initialise, $j \leftarrow 1$ and $D_j(n) \leftarrow \triangle t \cdot \sum_{i=j}^{n}(v_i)$.
  while $D_j(n) > L$ **do**
    $j \leftarrow j-1$ and $D_j(n) \leftarrow \triangle t \cdot \sum_{i=j}^{n}(v_i)$.
  end
  Length of the last mass per unit length $L_{j-1} \leftarrow L - D_j(n)$ and
  $\bar{q}(n) \leftarrow \frac{1}{L}\left\{\triangle t \sum_{i=j}^{n}(q(0,i) \cdot v_i) + q(0,j-1) \cdot L_{j-1}\right\}$.
  if $j > 2$ **then**
    Length of the last mass per unit length that has been spilled, $L_e \leftarrow D_{j-1}(n) - L$.
    $\sum_{i=1}^{k} M_{\text{out}}(i) \leftarrow L_e \cdot q(0,j-1) + \triangle t \cdot \sum_{i=1}^{j-2}(q(0,i) \cdot v_i) + L \cdot q_0$.
  else
    Length of the last mass per unit length that has been spilled, $L_{ex} \leftarrow D_1(n) - L$.
    $\sum_{i=1}^{k} M_{\text{out}}(i) \leftarrow L_{ex} \cdot q(0,1) + L \cdot q_0$.
  end
end

is relatively flat and that there is an insignificant amount of material trampling backward or forward on the belt.

Fig. 3.8 shows the actual and model calculated average mass per unit length. These results show that the proposed model's calculations are closer to the actual values than those of the SS approach. Fig. 3.9 shows the power calculations at a 10 minute sampling interval for the input shown in Fig. 3.5. The proposed PDE model closely approximates the actual power requirement. The proposed PDE model performs better because it is able to estimate $\bar{q}(n)$ with a small error compared to the SS approach. The proposed model's calculated power values are on average 10.8% different from actual power. On the contrary, the SS model's calculations give a very large difference with an average absolute percentage

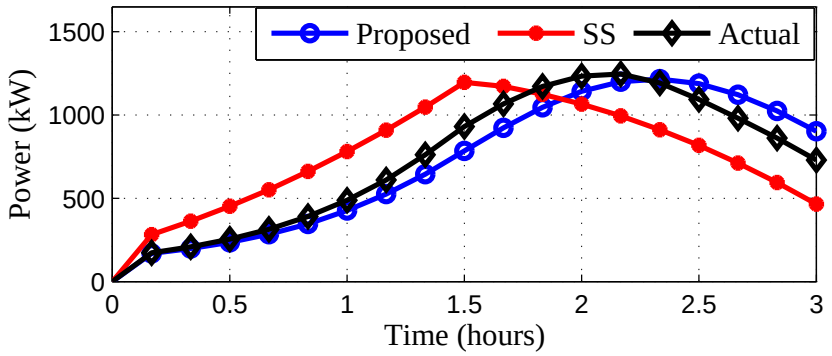

Figure 3.9. Calculated (Algorithm 1) and modelled values of the conveyor's power consumption.

error of 40.4%. The accuracy of the PDE model can be improved by simply increasing the number of space discretisation points, N_x, at the cost of having more model variables.

Fig. 3.9 shows the power calculations at a 10 minute sampling interval for the input shown in Fig. 3.5. The proposed PDE model closely approximates the actual power requirement. The proposed model's average absolute percentage error is a relatively small value of 10.8% over the 3 hour duration. On the contrary, the SS modelling approach gives a very large average absolute percentage error of 40.4%.

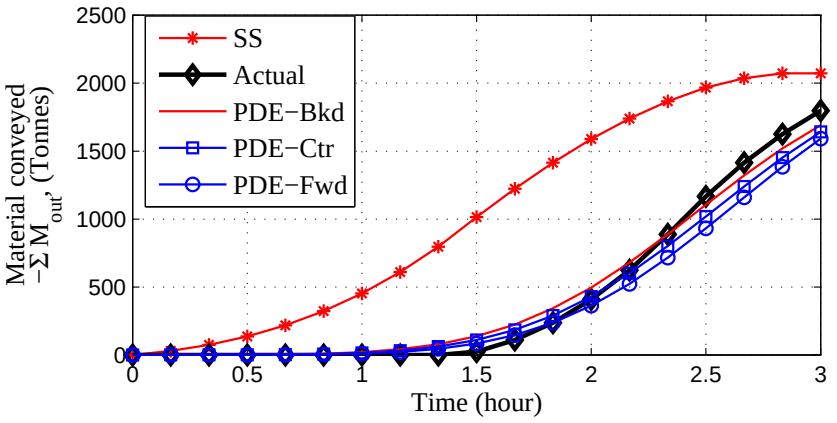

Figure 3.10. Calculated (Algorithm 1) and modelled amounts of material delivered by the conveyor after a given amount of time.

The amount of material entering the conveyor over a time interval is easily calculated from the input feed-rate using (3.15), as $M_{\text{in}}(n) = I_n \cdot \triangle t$. However, the material delivered at the head-end of the conveyor can only be estimated using a general formula. (3.21) shows the three different estimates of

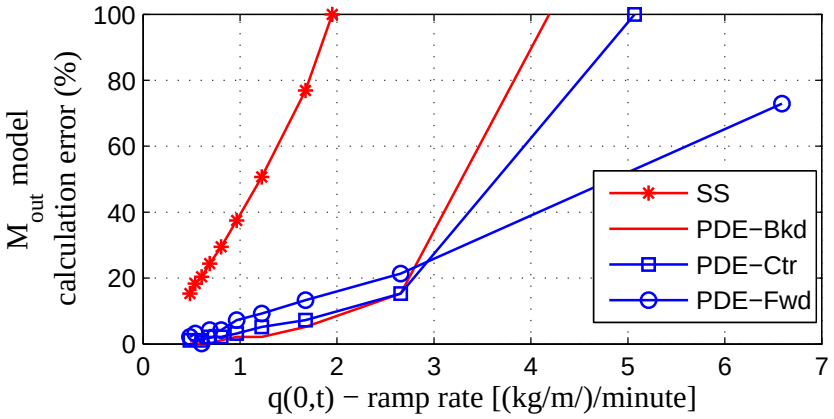

Figure 3.11. Effect of variation in $q(0,t)$ on the error when calculating M_{out}.

M_{out} using backward, forward and centred integrations of the conveyor model's last node. Algorithm 1 can be used to verify the exact value of M_{out}.

$$\begin{aligned} M_{\text{out}}(n) &\approx \triangle t \cdot v_n \cdot q(N_x, n) \text{ (Bkd)}, \\ M_{\text{out}}(n) &\approx \triangle t \cdot v_n \cdot q(N_x, n-1) \text{ (Fwd)}, \\ M_{\text{out}}(n) &\approx \triangle t \cdot v_i \cdot \tfrac{q(N_x,n)+q(N_x,n-1)}{2} \text{ (Ctr)}. \end{aligned} \tag{3.21}$$

Fig. 3.10 shows the performance of each of the integration strategies as well as the SS model when calculating the material delivered by the conveyor, over a period of 3 hours. All the methods from (3.21) give close estimates of M_{out}, but the SS approach always over-estimates the amount of material delivered. However, the PDE model using a backward integration gives the closest final calculation of the material delivered and it is therefore adopted for the rest of the chapter. The SS model's estimation is expected to improve with increasing belt speed and the performance of all methods improve with decreasing rate of variation in I_n and v_n. Fig. 3.11 shows that the mean percentage modelling error for calculating M_{out} decreases with decreasing ramp rate of $q(0,n)$. The results in Fig. 3.11 show that the modelling error is below 10% for all integration methods when the ramp rate is below 1.2 kg/m/minute. The accuracy of calculating M_{out} can also be improved by decreasing the sampling time at the expense of degrading computational speed.

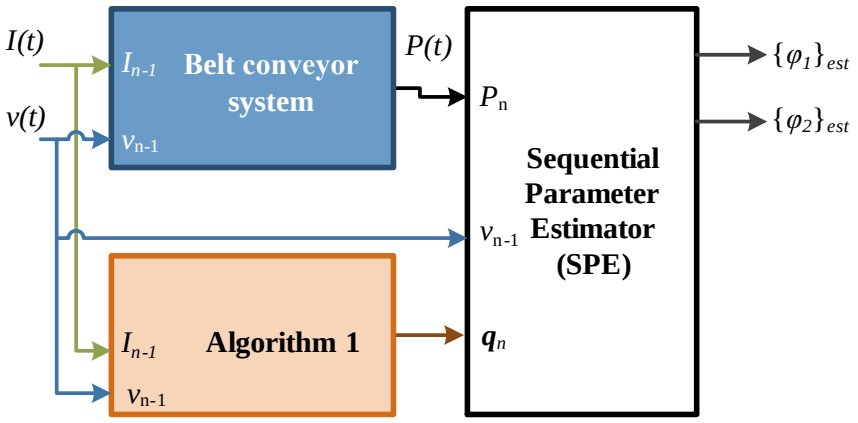

Figure 3.12. Parameter identification set-up.

3.4 PARAMETER IDENTIFICATION

Fig. 3.12 shows the set-up recommended for online estimation of the model parameters. This proposed online parameter identification requires the knowledge of three variables, namely: power consumption, belt speed and input feed rate. The feed rate, if not controlled, has to be measured at the tail-end of the conveyor. The purpose of Algorithm 1 is to keep track of the mass per unit length on the whole of the belt. The use of Algorithm 1 eliminates the expensive alternative of installing multiple sensors throughout the length of the belt. The identification process uses knowledge of the initial material distribution on the conveyor $q(x,0)$, continuous measurement and sampling of the feed rate and belt speed in order to estimate $q(x,t)$. It is important to note that $q(x,0)$ does not necessarily need to be measured. If it is unknown, any valid value, such as $q(x,0) = 0$, can be used as an initial guess, and the Algorithm 1 would be able to reach an accurate estimate of $q(x,t)$ after some time when the effect of the guess has been eliminated. For example, it would take at most 30 minutes for the effect of the initial guess to be eliminated in a 2 km-long belt running at a minimum speed of 1.11 m/s.

Alternative to measuring $I(t)$ and $v(t)$, the mass per unit length at the tail-end of the conveyor, $q(0,t)$, can be measured. Due to an effectively constant cross-sectional area, the height of evenly-spread material above the belt provides a good estimate of $q(x,t)$, at any point x of the belt. However, there are even more accurate methods of measuring $q(x,t)$ using specialist belt weighing equipment or high-speed cameras and laser scanners coupled with advanced signal processing technologies [7, 52].

The set-up in Fig. 3.12 assumes that $I(t)$, $v(t)$, $M_{out}(t)$ and $P(t)$ can be measured from the BC.

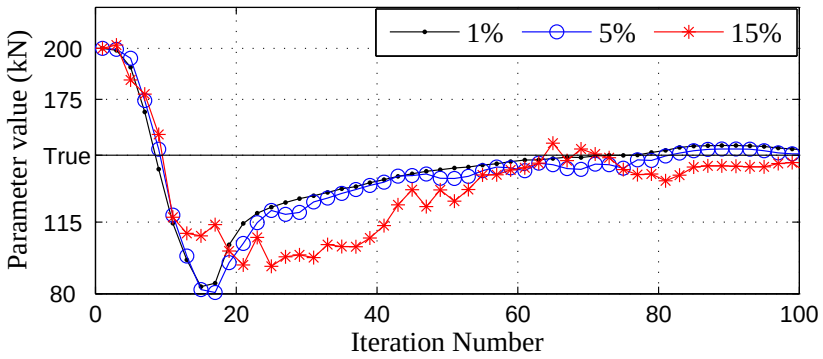

Figure 3.13. Convergence of the no-load parameter, φ_1, for different measurement noise levels.

Algorithm 1 and the sequential parameter estimator (SPE) take synchronised samples of $v(t)$ and $I(t)$ as input to their calculations. The SPE uses the calculated mass per length $\mathbf{q}_n$, measured power output and input speed to approximate the belt energy model parameters.

3.4.1 Parameter estimation

Algorithm 2: Sequential parameter estimation.

Input: P_n, v_n and $\{\mathbf{q}_n\}_{\text{est}}$.

Output: $\{\varphi_1\}_{\text{est}}$,$\{\varphi_2\}_{\text{est}}$ and Ω_n^{SPE}.

$n \leftarrow 0$, assign initial values $\{\boldsymbol{\varphi}(0)\}_{\text{est}}$ and Ω_0^{SPE}.

for $n \leftarrow 1$ ***to*** N_t **do**

  Calculate the estimation error, $\varepsilon^{SPE} \leftarrow \mathbf{y}_n^T \cdot \widehat{\varphi}(n-1) - P_n$.

  Update parameter estimate, $\widehat{\varphi}(n) \leftarrow \widehat{\varphi}(n-1) - \Omega_{n-1}^{SPE} \cdot \mathbf{y}_n [1 + \mathbf{y}_n^T \cdot \Omega_{n-1}^{SPE} \cdot \mathbf{y}_n]^{-1} \varepsilon^{SPE}$

  Update covariance estimate, $\Omega_n^{SPE} \leftarrow \Omega_{n-1}^{SPE} - \Omega_{n-1}^{SPE} \cdot \mathbf{y}_n [1 + \mathbf{y}_n^T \cdot \Omega_{n-1}^{SPE} \cdot \mathbf{y}_n]^{-1} \mathbf{y}_n^T \cdot \Omega_{n-1}^{SPE}$

end

The SPE algorithm recursively improves its estimated parameter values and their error covariance matrix by implementing a recursive least-squares algorithm listed as Algorithm 2. Such an algorithm can be easily implemented into a hardware device to improve execution speed as shown in [53]. At each time instance $t = n\triangle t$, the SPE uses the $\mathbf{q}_n$, as well as the measured belt speed and power output samples, to calculate the current estimate of parameter values $\{\boldsymbol{\varphi}(n)\}_{\text{est}} = \begin{bmatrix} \{\varphi_1\}_{\text{est}} & \{\varphi_2\}_{\text{est}} \end{bmatrix}^T$. The SPE uses the discrete version of the power equation (3.10), $P_n = \mathbf{y}_n^T \cdot \{\boldsymbol{\varphi}(n)\}_{\text{est}}$, where $\mathbf{y}_n^T = \eta \cdot \begin{bmatrix} v(n-1) & v(n-1)\bar{q}(n) \end{bmatrix}^T$.

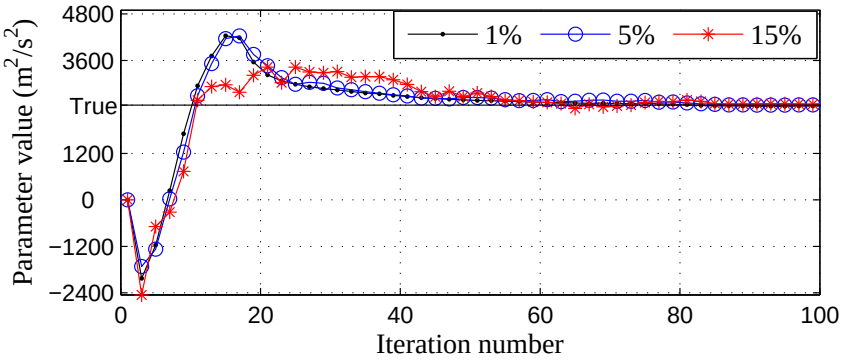

Figure 3.14. Convergence of the density parameter, φ_2, for different measurement noise levels.

In practice, the measurement of variables required for parameter estimation is likely to contain noise. Figs. 3.13 and 3.14 show the effect of measurement noise on the estimation of parameters. This simulation considers a belt with specifications similar to those found in [33], so that the true parameter values are $\varphi_1 = 147.72$ kN and $\varphi_2 = 2445.5$ m^{2}s^{-2}. The true value of a parameter is labelled as "true" on the y-axis. The results are shown for simulations with varying sizes of percentage noise errors. The measurements used are sampled at 10-minutes interval, while the inputs are varied as shown in Fig. 3.5. Figs. 3.13 and 3.14 show that the SPE algorithm takes longer to converge as the magnitude of noise increases. Thus, using precise measurement instruments will result in quicker estimation of the energy model parameters.

A comparison between the Figs. 3.13 and 3.14, shows that the estimation of φ_2 converges to its true value faster than that of φ_1. The rate of convergence in parameter estimation is related to its the sensitivity to the output [54]. Since, the state equation is independent of the parameters, the parameter output sensitivities, $S^P_{\varphi_1}$ and $S^P_{\varphi_2}$, are given by,

$$\begin{aligned} S^P_{\varphi_1} &= dP/d\varphi_1 \quad = v(n-1), \\ S^P_{\varphi_2} &= dP/d\varphi_2 \quad = v(n-1)\cdot \textstyle\sum_{i=0}^{N_x} q(i,n)/N_x. \end{aligned} \tag{3.22}$$

In a typical operation, the average mass per unit length of a conveyor is a large value, bigger than about 50% of the belt's $q_{\max}$, and so usually $\sum_{i=0}^{N_x} q(i,n)/N_x \gg 1$ kg/m [8]. Therefore, generally the power used by the conveyor is more sensitive to φ_2 than φ_1, i.e., $S^P_{\varphi_1} < S^P_{\varphi_2}$. This explains the different convergence rates shown in Figs. 3.13 and 3.14. Therefore, for this model, it is easier to identify the

true value of φ_2 than that of φ_1. This implies that, in practice, the time it takes to get convergence of φ_1 will determine the duration of a successful identification exercise.

3.5 APPLICATION CASE-STUDY

Consider the day-ahead optimal scheduling of the an 8 km-long coal conveying belt transporting coal from a stockyard to storage silos feeding the boilers of a power plant, explained in [40]. Assuming that the belt is initially empty (*i.e.*, $\mathbf{q}_0 = \begin{bmatrix} 0 & 0 & \dots & 0 \end{bmatrix}^T$) and operating under Eskom's RuralFlex, the time-of-use (TOU) electricity tariff is given by Equation (21) [55]. The objective of the schedule is to find an energy-cost effective way of replenishing the silos as the power plant consumes the coal. Thus, the coal conveying process is restricted to maintaining the amount of coal in the silos between the lower ST_L and upper ST_U storage limits of 1958 and 4756 tons, respectively. The silos initially have M_0= 2460 tons of coal. The electricity load supplied by the power station determines the rate at which the coal is being consumed from the silos [40].

$$\pi_n = \begin{cases} 0.44 \text{ R/kwh, off-peak } n \in [1-6, 23-24] \\ 3.27 \text{ R/kwh, peak } n \in [7, 11-18, 21-22] \\ 0.84 \text{ R/kwh, standard } n \in [8-10, 19-20] \end{cases} . \tag{3.23}$$

The optimal schedule has to optimise the energy and mechanical costs, while meeting the hourly coal demand (D_n) and operating within storage (ST_L, ST_U), belt capacity ($q_{\max}$) and actuator limits ($I_{\max}, v_{\max}$). The SS approach scheduling optimisation is given by (3.24).

$$\begin{gathered} \mathbf{min}_{\{v_n, I_n\}} \sum_{n=1}^{N_t} P(n) \cdot \pi_n + \varpi \sum_{n=2}^{N_t} (v_n - v_{n-1})^2 \\ \mathbf{s.t} \\ ST_L \leq M_n = M_{n-1} + \triangle t \cdot I_n - \tfrac{\triangle t}{3600} \cdot D_n \leq ST_U, \\ v_n \in [0, v_{\max}], I_n \in [0, I_{\max}], \bar{q}_n \in [0, q_{\max}], \\ \text{Given } M_0, \\ \text{where } \bar{q}_n = I_n / v_n \text{ and } P(n) = \tfrac{1}{\eta}(\varphi_1 + \varphi_2 \cdot \bar{q}_n) \cdot v_n, \ \forall n \in [0, N_t] \end{gathered} \tag{3.24}$$

The first addend of the objective function in (3.24) quantifies the energy cost and the second is meant to limit extreme belt speed changes so as to minimise maintenance costs, as explained in Section 2.3.

The biggest source of error for the SS approach in belt conveyor optimal scheduling comes from its failure to account for the transition time from the initial condition where the belt's $q(x,t)$ may be less than ($q_{\max}$). It has already been illustrated in Section 3.3.2 that this may lead to miscalculations of the power usage and the amount of material delivered. An alternative is to use the proposed model as shown in (3.25). The added accuracy of the proposed model comes with an added computational cost, since more variables have to be added to the optimisation problem. This is because the proposed model discretises the conveyor in both space and time, while the SS approach only involves time discretisation. As a result, the SS approach in (3.24) has $2N_t$ unknowns while the PDE formulation in (3.25) has $2N_t + N_x \cdot N_t$ unknowns. This makes the PDE model problem much more involving and harder to solve. The

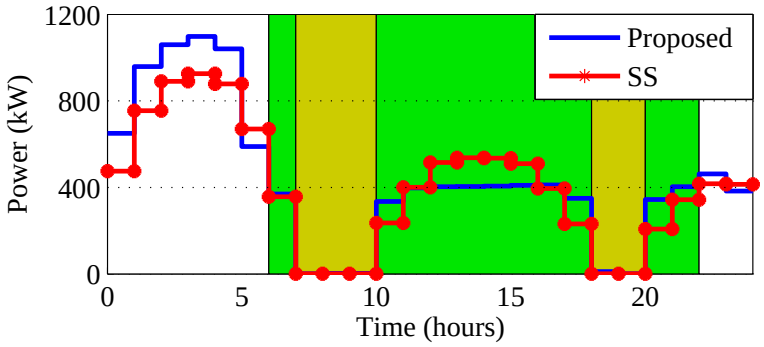

Figure 3.15. Power consumption of optimised schedules.

optimisation problem in (3.25) is solved using active set methods solver implemented in MATLAB. The optimisation of Equation (3.25) converges quickly when a feasible sub-optimal starting point is provided. This initial starting point can be easily generated by simulating the belt first with inputs that obey the storage bound constraints.

$$
\begin{gathered}
\mathbf{min}_{\{v_n, I_n, \mathbf{q}_n\}} \sum_{n=1}^{N_t} P(n) \cdot \pi_n + \varpi \sum_{n=2}^{N_t} (v_n - v_{n-1})^2 \\
\mathbf{s.t} \\
G_n \cdot \mathbf{q}_{n+1} = \mathbf{q}_n + \mathbf{b}_n \cdot q(0,n), \\
ST_L \leq M_n = M_{n-1} + v_n \cdot q(N_x, n-1) - \tfrac{\triangle t}{3600} \cdot D_n \leq ST_U, \\
v_n \in [0, v_{\max}], I_n \in [0, I_{\max}], q(i,n) \in [0, q_{\max}], \\
\text{Given } \mathbf{q}_0 \text{ and } M_0, \\
\text{where } P(n) = \tfrac{1}{\eta} \varphi_1 v_n + \tfrac{1}{\eta L} \varphi_2 v_n \sum_{i=1}^{N_x} q(i,n), \\
\gamma_n = v_n \tfrac{\Delta t}{\Delta x} \text{ and } q(0,n) = I_{n-1}/v_{n-1}, \\
\forall n \in [0, N_t], \text{ and } \forall i \in [0, N_x]
\end{gathered}
\tag{3.25}
$$

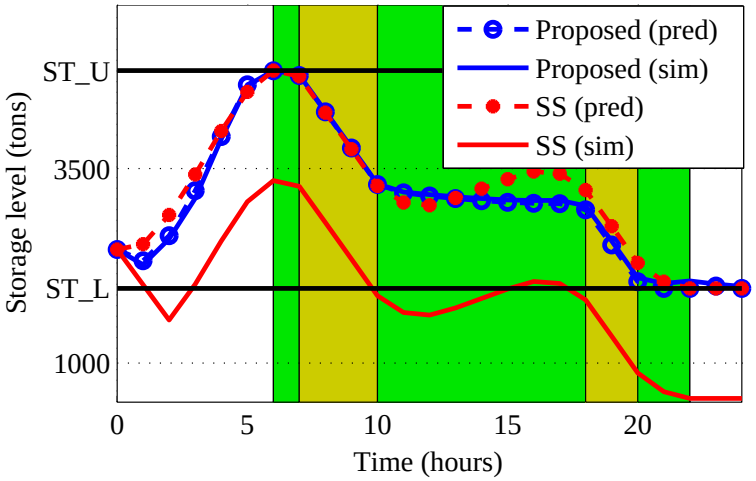

Figure 3.16. Predicted (pred) and flow model simulated (sim) storage level for both optimisation solutions of (3.25) and (3.24).

The optimal day-ahead schedules of both the SS approach and PDE model are shown in Fig. 3.15. The background colours of Fig. 3.15 correspond to the different TOU tariff rates given in (4.4). The proposed model estimates that the BC consumes 10.49 MWh, while the SS approach gives 9.69 MWh, and the resulting energy cost calculations of the proposed model are 6.4% higher. In Fig. 3.15, the prominent difference between the two schedules occurs during the first 5 hours of the day, where the PDE schedule requires more power than the SS model. The difference is caused by the fact that the SS model assumes that the conveyor begins delivering material into the storage from the first second. This is, however, not true, since the belt is initially empty, and so, coal has to travel from the loading point to the tail end, which is 8 km away. Thus, the SS approach wrongly underestimates the energy consumption and cost of the BC's operation.

Both solutions obtained from solving (3.24) and (3.25) are feasible. That is, both solutions predict that $ST_L \leq M_n \leq ST_U, \forall n \in [0, N_t]$. However, simulating the optimisation solutions with the PDE flow model of (4.1) illustrates that the SS approach's solution violates the storage bounds, as shown in Fig. 3.16. The results in Fig. 3.16 show that the level of storage predicted by the proposed model is relatively accurate. However, the SS approach creates a schedule that actually violates the storage bound constraints.

3.6 CONCLUSION

This chapter has proposed an energy model with two parameters based on the belt resistances for long belt conveyors with troughed belts. The model uses a partial differential equation to capture the varying amounts of mass per unit length on the belt in order to give a more accurate representation of the transported bulk material. The proposed model provides steady-state power calculations that are close to models found in the current literature. The proposed model is shown to estimate power usage of a long belt conveyor more accurately than the existing steady-state power models. The proposed model's ability to accurately account for the amount of material being transferred by the conveyor makes it more useful in practice than the steady-state models currently available in literature. An online identification set-up for estimating the true values of the model's parameters is proposed and simulated for an 8 km-long conveyor. The identification of results show that precise measuring equipment is required for speedy identification and that it is easier to estimate the true value of the model density parameter than that of the no-load parameter. The proposed model is applied in a case-study application simulation to demonstrate its superiority over the steady-state approach. Simulations show that, unlike the SS approach, the proposed model is able to provide a schedule that does not violate storage level constraints.

Accuracy of the newly proposed model can be improved by increasing the number of sampling points in space (i.e. along the conveyor's length). This, however makes the model more computationally expensive and the optimal scheduling problem becomes harder for the computer to tackle. It is possible that introducing alternative discretisation methods apart from the currently used BE method, may alleviate this. These alternative discretisation methods need to be investigated further in future works.

Future work on the model should also consider calculating the power requirement of the BC by summing the resistances of shorter sections of the conveyor's length. This approach is likely to improve the calculation of the primary and secondary resistances' contributions to the overall power requirement of BCs. Future work should also consider incorporating the use of multiple drives on a single conveyor since this is very common in long conveyors.

CHAPTER 4 ENERGY MANAGEMENT IN SYSTEMS WITH DOWNHILL CONVEYORS

Downhill conveyors are important potential energy sources within belt conveyor systems (BCSs). Their energy can be captured using regenerative drives. This chapter presents a generic optimisation model for the energy management of BCSs that have downhill conveyors. The optimisation model is able to optimally schedule three configurations of a case-study BCS that is connected to the grid and operated under a time-of-use demand-side management programme. The three suggested drive configurations showcase potential energy savings/profits that can be obtained from implementing; (a) variable speed control, (b) internal use of downhill conveyor energy and (c) the export of energy to the grid. The results show that a BCS with a daily energy consumption of 924 kWh can be reconfigured and controlled to reduce consumption by 53% or 100% or be made to generate 1,984 kWh, depending on the configuration. Analysis of the investment in each of the three configurations is assessed using a life-cycle cost and payback period (PBP). The daily operation simulation results show that the use of regenerative drives and variable speed control are able to provide energy savings in BCSs. The cost analysis shows that the configuration that enables sale of energy to the grid is the most profitable arrangement, for the case-study plant under consideration. The sensitivity analysis indicates that the PBPs are more sensitive to the annual electricity price increase than the discount rate. Combining regenerative drives and optimal operation of BCS generates energy savings that give attractive PBPs of less than 5 years.

4.1 INTRODUCTION

Belt conveyor systems (BCSs) are used in a variety of industries for bulk material transportation [33, 56]. It is a well known fact that energy consumption of belt conveyor systems (BCSs) is lowered

by implementing variable speed drives (VSDs) instead of fixed speed drives [7, 9, 10, 11, 32, 33, 40]. BCSs are typically made up of storage units and a series of belts, some of which may be downhill. Downhill conveyors (DHC) tend to require a constant braking force in order to maintain a required operating speed. In addition to the required mechanical safety brakes, an electrical braking system is used [57, 58, 59]. In general, the braking process is undesirable because it wastes energy, presents a fire risk and reduces the motor's lifespan. An efficient alternative is to capture the braking energy and convert it into useful electrical energy [59, 60].

Apart from VSDs, further attempts to achieve energy efficiency are leading to the introduction of regenerative drives (RDs) on downhill belts [31, 57, 58]. DHCs have long been seen as potential sources of energy [57, 58]. The use of a 20 MW thyristor-based active front end (AFE) drive system to harness the power of DHCs in an iron-ore mine is reported in [57]. An insulated-gate bipolar transistor (IGBT) based AFE drive is also applied on conveyors of a cement plant to potentially generate over 700 kW of power [58]. The application of RD technology is increasingly gaining interest in the power and energy research community. Its other application areas include passenger transportation and overhead cranes [60, 61, 62, 63]. The current research on the application of RDs tends to focus on power quality related issues and not enough attention has been given to energy management and cost issues [57, 58, 63]. The latter two issues are the theme of this chapter.

Changes in tariffs towards dynamic electricity pricing are one of the dominant trends in the electricity markets. This trend is motivated by the increasing need for utilities to influence demand and offer the most equitable prices for electricity [40]. Some of the progressive tariffs, such as Eskom's[1] newly proposed Genflex allows consumers to sell power back to the grid [55]. Tariffs such as this make energy efficiency interventions capable of producing power even more attractive. Thus, VSDs and RDs can be used in combination with optimal scheduling to derive further cost benefit from BCSs under price-responsive demand-side management (DSM) programmes [64, 65].

Predictably, the decision to install VSDs/RDs is motivated by their economic viability within a particular plant and this depends on the amount of potential energy savings or profits. It is therefore necessary to accurately model and predict the amount of savings/profits to be made from the energy saved/generated by investing in VSDs and RDs.

[1] www.eskom.co.za (a South African state-owned utility)

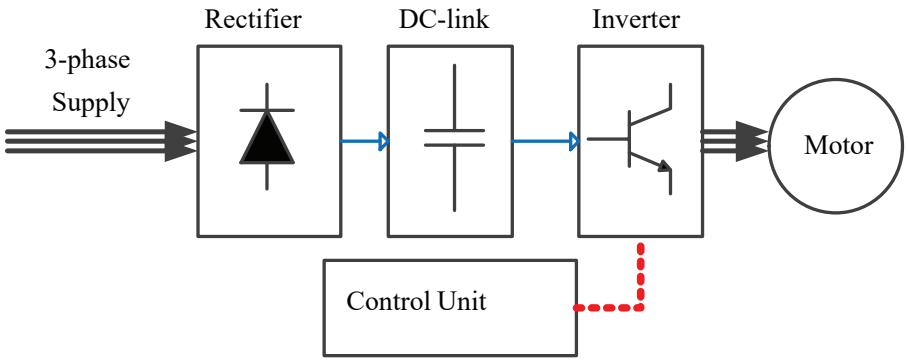

Figure 4.1. Components of a variable speed drive.

This chapter presents an optimal scheduling model and three drive configuration options that can be used to improve the energy efficiency of BCSs with DHCs. The proposed generic optimisation model can calculate optimal schedules for three different configurations of drives while taking into consideration the BCS's operational constraints. Besides improving energy efficiency, the model also minimises the electricity cost by taking advantage of the electricity tariff. The economic benefit of implementing VSDs and RDs on BCS with DHCs are analysed for a case study plant. The proposed model quantifies the potential amount of energy savings or profits and can be used to help a BCS operator decide on the economic viability of investing in regenerative drives. The analysis in this paper is novel because the newly proposed optimisation model facilitates energy management of BCSs that are able to sell electricity to the grid.

4.2 BACKGROUND

4.2.1 Conveyor drive technology

For variable speed control (VSC), a belt conveyor's alternating current (AC) motor is driven by a VSD fed by a three-phase supply. The VSD is made-up of four sub-components as shown in Fig. 4.1. The diode/IGBT rectifier converts the incoming AC to direct current (DC). The DC-link has a capacitor bank that filters the DC from the rectifier. The inverter then converts the filtered DC back to an AC, the frequency of which is dictated by the control unit. The control unit produces a pulse-width modulation PWM signal that sequentially switched the transistors of the inverter to produce AC power of a desired frequency. The AC motor is energised by the inverter to rotate at the speed proportional to the output

AC frequency. In this way, the speed of the motor is controlled by varying frequency of the output AC [9, 11, 59, 63].

The load on a DHC produces a torque that rotates the motor's shaft to generate electrical energy. This energy is transmitted back into the drive to charge the DC-link's capacitor. This results in a raised DC-bus voltage because the energy cannot flow out through the rectifier. To avoid equipment failure, the DC voltage has to be restored to its normal level. A dynamic braking unit connected to the VSD achieves braking by absorbing the energy on the DC-bus and, hence, lowering the DC voltage. The braking unit is made up of a chopper and a power resistor. The copper is an electronic switch that connects a resistor to the DC-bus in order to dissipate the energy into heat whenever the DC voltage increases beyond the required level. During braking, the resistor becomes hot and so an investment into a well functioning ventilation system is sometimes needed to reduce the heat [59, 63].

Active front end (AFE) is one of the prominent regenerative drive technologies [57, 58, 63]. In the AFE configuration, the VSD's input diode rectifier is replaced by a bi-directional voltage source rectifier capable of directing power from the conveyor motor into the grid [57, 58, 63]. The regenerative energy from a DHC can either be used by other motors within the plant or sold to the grid. Not all power from the bulk material load is converted into electrical energy due to friction in the motor and mechanical subsystems attached to the shaft. A utility may also impose a transmission charge when the conveyor feeds power into the grid. The implementation of this technology is commonly packaged in AFE units that also include line filter and choke modules to improve the quality of power [63, 66].

In practice, multiple options for configuring AFE and VSD units are available to application engineers. For instance, a single VSD unit can be used to drive multiple motors. A common DC-bus can also be used to connect DC-links of multiple VSD units so that a regenerating motor simply injects energy into the DC-bus where other motors can use it, to reduce the load on the grid. The use of RD and choice of configuration needs to be justified by operational constraints and the amount of energy to be generated for a given plant layout. These considerations will be made so that investment into RDs/VSDs is economically viable for a belt conveyor operator [59, 63]. As a result, the ability to model the energy output of DHCs is crucial.

4.2.2 Energy model

The linear mass density $q(x,t)$ of material at a given point, x, on the conveyor belt at a time, t, is related to the speed of the belt $v(t)$ by,

$$\frac{\partial}{\partial t}q(x,t) = -v(t)\frac{\partial}{\partial x}q(x,t). \tag{4.1}$$

The electrical power required by the motor driving an L meters long belt is given by,

$$P(t) = \frac{1}{\eta}(\varphi_1 + \frac{\varphi_2}{L}\int_0^L q(x,t)\,dx)\cdot v(t), \tag{4.2}$$

where $\varphi_k \quad k \in [1,2]$ are the modelling parameters and η is the overall motor drive efficiency [56]. In [56], the energy model parameters are shown to be related to the physical properties of the BCS by parameters $C_k \quad k \in \{1,2,4,6,7,9\}$ and an artificial coefficient of friction f, as shown in (4.3). Parameter C_9 depends on the belt's length and C_7 depends on the inclination height H, while C_4 and C_6 are derived from special friction of the conveyor whose contribution is usually small for long conveyors. The parameters C_1 and C_2 are derived from the primary friction of the conveyor and they are directly proportional the coefficient f [56, 1, 6].

$$\varphi_1 = C_9\cdot C_1(f) + C_6 \text{ and } \varphi_2 = C_9\cdot C_2(f) + C_4 + C_7. \tag{4.3}$$

For DHCs H is considered negative, thus $C_7 = gH < 0$. For belts with sufficiently steep profiles, the force of gravity on the bulk material dominates φ_2, and so $|C_9\cdot C_2(f) + C_4| < |gH|$. In such cases, the belt is capable of rolling downhill and turning the motor without any input power. This occurs whenever the mass of the material on the belt exceeds a critical value, $M_{\text{crit}} = L\cdot\varphi_1/|\varphi_2|$, and the conveyor is said to be operating in a regenerative mode.

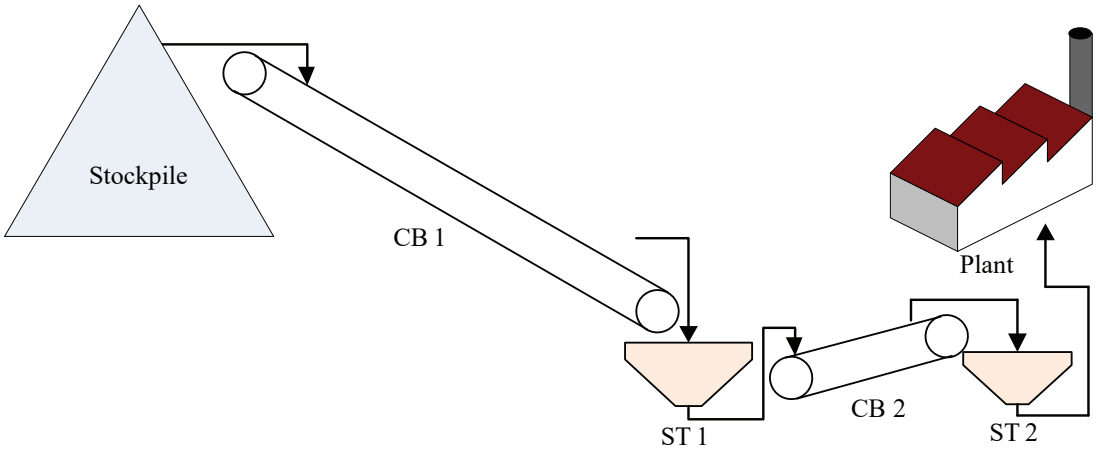

Figure 4.2. Conveyor in a cement making plant.

4.3 ENERGY AND COST OPTIMISATION

4.3.1 Case-study plant

For a case study, consider a BCS designed to transport limestone and clay from a mining area stockpile to a cement making facility similar to that in [58], located in the Waterberg region of South Africa. Fig. 4.2 shows a layout of the plant where BCS is run at a fixed speed. In many countries, the cement making industry accounts for a significant portion of national energy consumption. Raw material processing consumes about 28% of electricity, therefore, DSM is important in this industry [67]. Due to the rugged terrain, a long conveyor system is used. The system operates at a maximum speed of 3.1 m/s to transport bulk material to a plant 280 m below the crushing station. In our model, we consider the 2.4 km long DHC that receives quarry from the crusher and feeds it to a 0.6 km long inclined conveyor that delivers material to a storage in a cement plant as shown in Fig. 4.2.

The BCS considered is set to feed an annual production capacity of 1,400,000 tons which requires about 280 t/h of raw material. The system shown in Fig. 4.2 has a normal maximum throughput of 850 t/h and the plant silos, ST2, have a 6 hours buffer storage of 1680 tons. The energy model parameter values (φ_1, φ_2) are (25.0 kN, -1.58×10^3 m^2/s^2) for CB1 and (9.78 kN, 105 m^2/s^2) for CB2. CB1 is capable of generating 296 kW and CB2 can consume 55 kW of power at a speed of 3.1 m/s and throughput of 850 t/h. The intermediate bulk storage ST1 is typically negligible in size and it is located at a transfer station to facilitate the exchange of material between two belts.

4.3.2 Electricity pricing

In this section, we consider the operation of the plant in Fig. 4.2 under a Time-Of-Use (TOU) tariff similar to those offered by Eskom's demand-side management programmes. Mining operations are normally based in the rural areas, thus the tariff called Ruraflex given by (4.4) is used to estimate the cost of energy consumption [55].

$$\pi_n = \begin{cases} 0.40 \text{ R/kwh, off-peak } n \in [1-6, 23, 24] \\ 2.41 \text{ R/kwh, peak } n \in [7, 11-18, 21, 22] \\ 0.73 \text{ R/kwh, standard } n \in [8-10, 19, 20] \end{cases} . \tag{4.4}$$

The proposed Genflex tariff is used for calculating the profit made from generating energy as well as cost of consumption. Under the Genflex tariff, independent power producers (IPPs) are able to use the utility's network to wheel their energy to a third-party. The utility charges the IPP a use-of-system (UoS) charge for the use of its network. The IPP is able to get revenue for energy sales to a third-party according to their power purchase agreement (PPA) [30]. The selling price of the IPP's energy has to be less than that of the utility by some factor Sf_n, in-order to make it attractive to the third party.

The energy from the IPP is also subject to a flat-rate reliability charge π_{RC} and a time-dependent system loss charge. The reliability charge compensates the utility for providing good quality power and security of supply. The loss-charge accounts for the inevitable transmission losses incurred by the utility as it transmits the IPP's energy to loads connected to the utility. In Eskom's case, the utility simply assigns a loss-factor Lf_n based-on the distance between the IPP's generator location and the location of utility's major load. This effectively reduces the IPP's output from a monetary perspective. Considering the selling price, reliability and loss charges, the TOU energy costs for an IPP are,

$$\text{EC}_n = \begin{cases} \pi_n \cdot P_n^d \cdot \triangle t, & \text{when } P_n^d \geq 0 \\ (\pi_n \cdot \text{Sf}_n \cdot \text{Lf}_n - \pi_{RC}) \cdot P_n^d \cdot \triangle t, & \text{when } P_n^d < 0, \end{cases} \tag{4.5}$$

where P_n^d is the magnitude of average power produced or consumed by the IPP during a time period n. Negative and positive values of P_n^d correspond to the generation and use of power, respectively.

In addition to the energy cost (4.5) , the UoS charges are billed depending on whether the IPP is connected to the distribution or transmission network. Firstly, a standard administration and service charge π_{AS} is billed monthly per point-of-delivery and account. Secondly, the IPP incurs a network access charge π_{NA} based on the maximum power exported to the grid (or maximum demand required by the IPP) within a billing period. Hence, the monthly network access cost (NAC),

$$\text{NAC}(P_n^d) = \max\left\{-P_n^d, P_n^d\right\} \cdot \pi_{NA} \tag{4.6}$$

For the purpose of our analysis, the following pricing values are used; π_{AS} =R512.10/Month, π_{NA} =9.40/kW, π_{RC}= 0.20/kWh. π_{AS} represents the administration and service charge billed per month for account services rendered by the utility on each working day of the month. That is, days excluding weekends. The BC plant is assumed to sell its energy at a 20% discount to the utility's TOU price, so $\text{Sf}_n = 0.9$. The Lf_n associated with peak, standard and off-peak times are calculated to be 0.85, 0.85 and 0.75, respectively [55].

4.3.3 Drive configuration options

In the following sections, we compare the optimal scheduling of the BCS under three different configuration options with the base case design. In the base case design, the downhill CB1 is fitted with a 315 kW VSD and a braking unit, while both conveyors are operated at a constant maximum speed to meet the hourly material demand. Electricity cannot be sold to the grid under the base case. The value of feed-rate that meets the material demand when operating at full speed is 280 t/h. Under these conditions, CB1 generates 1,095 kWh while CB2 consumes 923 kWh of energy. From the utility's perspective, the plant's load profile is flat with an hourly consumption of 38.47 kW. Therefore, the plant's daily electricity cost under the tariff in (4.4) is R895.62.

The three different alternative configuration options and their implications on the energy and network access costs are subsequently explained. All options have a 315kW VSD connected to CB1 and a smaller 75kW VSD connected to CB2. The equipment used in each option is summarised in Table 4.1. The detailed descriptions of the options are;

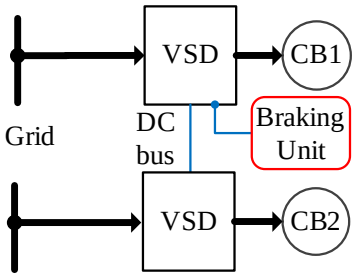

Figure 4.3. Option **B** drive configuration.

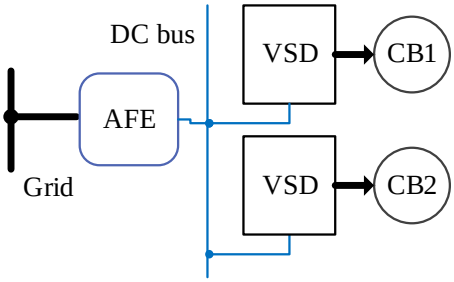

Figure 4.4. Option **C** drive configuration.

- **Option A** (VSC): The 315 kW VSD is connected to a braking unit connected and the two VSDs are isolated . Option A is similar to the base case and in that no electricity is sold to the grid. The only exception is the additional 75kW VSD on CB2. The electricity is continually being consumed by CB2, even when CB1 is produces more than the consumption of CB2. The only advantage over the base case is that this configuration is optimally operated using a variable speed. The energy cost, defined by (4.5), is modified to $\mathrm{EC}_n = \pi_n \cdot P_n^d \cdot \triangle t$, where P_n^d refers to the power consumed by CB2 only.

- **Option B** (VSC & internal use of energy): Each of the conveyors is connected to a VSD and both VSDs are in-turn connected by a common DC-bus, as shown in Fig. 4.3. This configuration is similar to that of option **A**,with the difference being the addition of the DC-bus. Option **B** is suitable when the individual belt conveyor drives are located in close proximity. Therefore, according to the layout in Fig. 4.2, the conveyor motors have to be located at the tail-end for CB1 and the head for CB2. The energy generated by CB1 can be used by CB2. Therefore, grid electricity is used only when the consumption of CB2 exceed the generation of CB1 (i.e. $P_n^d > 0$ and $\mathrm{EC}_n = 0$ whenever $P_n^d < 0$). So, (4.6) changes to $\mathrm{NAC} = \pi_{NA} \cdot \max\{P_n^d\}$ and (4.5) is modified to $\mathrm{EC}_n = \max\{0, \pi_n \cdot P_n^d \cdot \triangle t\}$.

- **Option C** (VSC & energy export): Each of the VSD driving the conveyors are connected to the grid through an AFE as shown in Fig. 4.4. Option **C** is also suitable for the conveyor drives that are located in close proximity to each other and when they are both close to the transformer. This reduces the length of connecting cables and hence the project costs. The braking unit is eliminated in this configuration because the AFE allows bi-directional transfer of power. When CB2 consumes more than what CB1 is producing, power P_n^d is purchased at a price π_n. Alternatively, when CB1 produces more power that the consumption of CB2, P_n^d becomes negative and the power is sold to a third-party via the grid. Thus, the energy and network access costs are as defined by (4.5) and (4.6), respectively.

Table 4.1. Summary of configuration options.

Option	Equipment/component available			
	VSDs	BU on CB1	Common DC bus	AFE
A	Yes	Yes	No	No
B	Yes	Yes	Yes	No
C	Yes	No	Yes	Yes

4.3.4 Optimal scheduling

For variable notation purposes, the super scripts 1 denote variables associated with the DHC and intermediate storage, while 2 is for those associated with CB2 and ST2. A generic daily cost function of operating the plant shown in Fig. 4.2 , incorporating all UoS charges, energy profits and belt mechanical costs is given by,

$$\text{OpCost}(v_n^j, I_n^j) = \sum_{n=1}^{N_t} \text{EC}_n(P_n^d) + \pi_{AS} \cdot \frac{1}{20} + \text{NAC}(P_n^d) \cdot \frac{1}{20} + \omega \sum_{n=1}^{N_t-1} \sum_{j=1}^{2} (v_n^j - v_{n+1}^j)^2, \tag{4.7}$$

where $P_n^d = P_n^1(\bar{q}_n^1, v_n^1) + P_n^2(\bar{q}_n^2, v_n^2)\ \forall n \in [0, N_t]$ is the power produced by the conveyor system, v_n^j, I_n^j & $\bar{q}_n^j\ \forall j \in \{1,2\}$ are the belt speed, feed-rates and average linear densities, respectively. The value $\bar{q}_n^j = \frac{1}{N_{xj}} \sum_{i=1}^{N_x} q^j(i,n), \forall j \in \{1,2\}$ is an average of linear densities sampled on N_{xj} equally spaced locations on each belt. The administration and service charge (π_{AS}) as well as NAC are spread over each of the monthly week days. The fourth addend of (4.7) represents the mechanical cost. The

mechanical cost ensures that the changes in belt speed are moderate to avoid excessive mechanical stress on the equipment.

The optimal operating schedule $\{v_n, I_n\}^*$, has to meet the following operating constraints,

$$\Omega_1 : \left\{ \begin{array}{c} G_n^j \mathbf{q}_{n+1}^j = \mathbf{q}_n^j + \bar{\mathbf{b}}_n^j \cdot (I_n^j / 3.6 v_n^j), \\ v_{\min}^j \leq v_n^j \leq v_{\max}^j, I_{\min}^j \leq I_n^j \leq I_{\max}^j \\ q(0,n) \leq Q_{\max}, \\ ST_L^1 \leq M_{n-1}^1 + v_n^1 \cdot q^1(N_{x1}, n-1) - \frac{\triangle t}{3.6} \cdot I_n^1 \leq ST_U^1, \\ ST_L^2 \leq M_{n-1}^2 + v_n^2 \cdot q^2(N_{x2}, n-1) - \frac{\triangle t}{3600} \cdot D_n \leq ST_U^2, \end{array} \right\}, \tag{4.8}$$

$\forall n \in [0, N_t]$ and $\forall j \in \{1,2\}$. The first row of (4.8) is a discretisation of (4.1) that caters for material flow. This row relates the linear density vectors $\mathbf{q}_n^j$ between time instances n and $n+1$ using the parameters G_n^j and $\bar{\mathbf{b}}_n^j$. The second and third rows of (4.8) define the actuator limits and belt carrying capacity, respectively. The last two rows of (4.8) ensure that storage limits are not exceeded. D_n represent the demand of bulk material and $\triangle t$ is the sampling time in the discrete domain. Therefore, the optimal operating schedule for the BC plant in Fig. 4.2 is the solution to the following optimisation problem,

$$\begin{array}{c} \mathbf{min}_{\{v_n, I_n\}} \text{OpCost}(v_n^j, I_n^j) \\ \mathbf{s.t} \\ \{v_n^j, I_n^j\} \in \Omega_1 \\ \Omega_2 : \{\sum_{n=1}^{Nt} v_n^2 \cdot q^2(N_{x2}, n-1) = \sum_{n=1}^{Nt} \frac{\triangle t}{3600} \cdot D_n\} \\ \text{given } \mathbf{q}_0^j \text{ and } M_0^j, \end{array} \tag{4.9}$$

where $\mathbf{q}_0^j$ and M_0^j are the initial belt linear density and amounts of material in storages. Each of the simulations begin with an empty storage. For the purpose of a fair analysis, an extra constraint, Ω_2, requiring that the storage level returns to zero at the end of the day is imposed.

Figs. 4.5 and 4.6 show the power and storage profiles for the three options. Fig. 4.5 shows that unlike option **B**, option **A**'s scheduling of CB2 avoids the peak times when electricity is most expensive. This is because all of CB1's energy is lost in option **A** and the utility always charges the plant for the

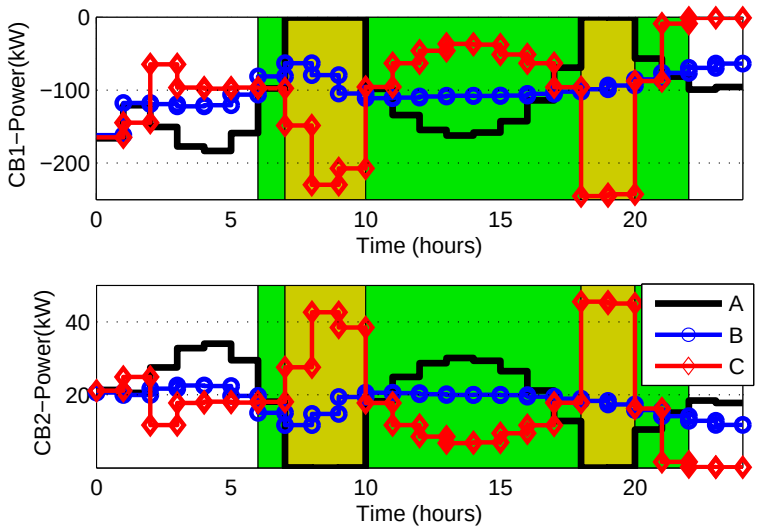

Figure 4.5. Power consumption of each belt for the three options.

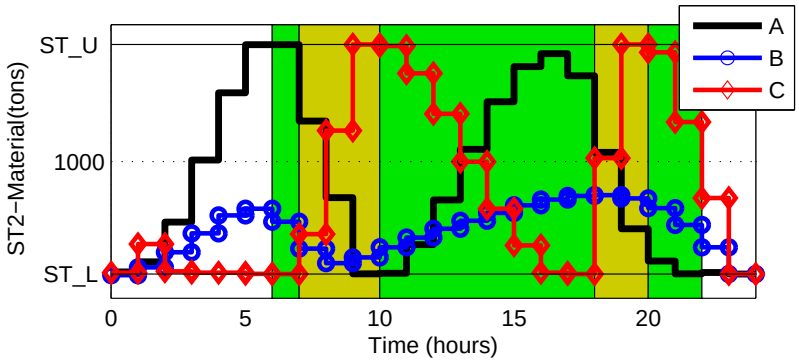

Figure 4.6. Storage profiles of ST2 for the three options.

consumption of CB2. However, option **B** uses the power generated by CB1 to power CB2. In contrast to both **A** and **B**, the scheduling under option **C** is shown to allocate most activity around peak times when the BCS can sell most of its energy at the maximum price. The storage profile on Fig. 4.6 shows that the capacity of ST2 restricts option **A** and **C** from avoiding and using peak times fully, respectively. However, option **B** does not fully use the storage capacity as it attempts maintain a balance of using CB2 to consume as much energy as CB1 produces. This is sensible because under option **B**, all of the excess energy is wasted by dynamic braking.

In general, the optimised process of moving the daily load of material generates a total of 1,984 kWh of energy. That is, CB1 generates 2,422 kWh of energy while CB2 consumes 437 kWh. The optimised

operation is more energy efficient than the full speed operation of the base case where CB2 consumes 923 kWh per day. As a result, the optimal scheduling of the plant saves energy under each of the three options.

The plant needs to pay the utility R253.13 under option **A**. However, the plant would not pay any money to the utility under option **B**. As for option **C**, the plant does not pay any money, it instead makes a profit of R1,452.43.

4.4 COST ANALYSIS

The life cycle cost (LCC) and payback period (PBP) of investing in an asset are the most commonly used values in determining the attractiveness and economic viability of an investment [68, 69]. The LCC is the discounted cumulative cost of owning, operating and disposing an asset. Thus,

$$\mathrm{LCC}(M) = CC + \sum_{j=0}^{N_{\mathrm{life}}-1} \frac{OPC_j}{(1+d)^j} - DSC, \tag{4.10}$$

where CC, OPC_j, DSC, d and N_{life} are the capital cost, operating cash-flows at the end of the j^{th} year, disposal cost, discount rate and the useful lifetime of the asset in years, respectively. PBP is the time required for the benefits from the assets to equal the expenditure incurred to own and operate the plant. That is, the number of years that make (4.10) equal zero. If n_{neg} is the first year that makes the LCC negative (i.e. $\mathrm{LCC}(n_{\mathrm{neg}}) < 0$), then according to the graphical method PBP is calculated by,

$$\mathrm{PBP} = n_{\mathrm{neg}} + \frac{\mathrm{LCC}(n_{\mathrm{neg}})}{\mathrm{LCC}(n_{\mathrm{neg}}-1) - \mathrm{LCC}(n_{\mathrm{neg}})} \tag{4.11}$$

The OPC_j is primarily the operating income/expenses because the power electronics components under consideration are hardly ever maintained. In contrast the motor is maintained at least twice a year [70]. Motor cost are not included in the current case study because the plant already has suitable AC motors and the energy saving interventions are restricted to electronic components running the motors. The electricity prices are subject to annual percentage increases r, mainly due to inflations. Thus, $\mathrm{OPC}_j = \mathrm{OPC}_0(1+r)^j$. The value of r is 13% in accordance with the latest multi-year price

determination plan by the South African regulator[2]. The electronic components of the VSD, AFE and BU are long-lasting, however they are more likely to be replaced at the end of the lifetime of the motors that they were connected to, mainly due to technological changes. Therefore, the residual value of the electronic components is taken to be zero, i.e DSC $= 0$. For the same reason, a 15 years lifetime period, M, commonly used for induction motors above 11kW, is adopted [70]. For calculations, the adopted discount rate is 2.45% (A 5 year bond interest rate[3] of 8.25% minus the consumer price index[4] of 5.8%) [70].

Table 4.2. Equipment prices and cost estimates.

Item	Amount (R$\approx$ 0.09 *US dollars as at 1 Jan 2015*)
VSD 75kW	114,695.00
VSD 315kW	394,352.00
Active Front End	278,538.00
Braking Unit (Chopper & Resistor)	64,367.00
Accessories (DC-bus)	65,590.00

For the purpose of the current analysis, the investment into a cooling system for the braking resistor is deemed unnecessary. A suitable distribution transformer that connects the plant to the utility is assumed to be available at no extra cost. The salvage value of the electronic equipment is ignored. Table 4.2 shows the equipment cost based on Altivar technology[5]. An installation cost of 10% of the cost of equipment is added to the CC for both options **A** and **B**. However, 20% is added for option **C** because it involves an AFE, which is a rarely used component.

Table 4.3 shows the economic data calculations for each option and the base case. The CC calculations are obtained by summing the cost of required components from Table 4.2 and adding the installation costs. Table 4.3 shows that options **A** and **B** consume less energy from the grid than the base case, while option **C** feeds energy back into the grid. Option **A** calculations show that simply installing VSDs and implementing VSC gives an attractive PBP of 3.56 years. A comparison of options **A** and

[2] www.nersa.org.za (Multi-year price determination 2 of 2015/16)
[3] secure.rsaretailbonds.gov.za
[4] http://beta2.statssa.gov.za
[5] http://www.schneider-electric.com/

Table 4.3. Benefit analysis of the different configuration options.

Item	Configuration option			
	Base case	**A**	**B**	**C**
CC (R)	504,591.00	630,755.00	685,755.00	949,768.00
Daily energy use from utility (kWh)	923	437	0	-1,984
Daily (cost) or savings (R)	(895.62)	642.49	895.62	895.62
Daily energy profits (R)	–	–	–	1,452.43
OPC_0(R)	214,949.00	-154,198.00	-214,949.00	-563,532.00
PBP (years)	–	3.56	2.88	1.62

B shows that improving energy efficiency by using the internally generated energy becomes a better investment option with a PBP of 2.88 years. The use of a RD in option **C** gives the quickest PBP of 1.62 years even thought the investment costs are almost twice that of the base case.

4.4.1 Sensitivity analysis

Discount rate and electricity price increase rate

The anticipated annual increase in electricity prices is based on the most recent increase. The calculations in Table 4.3 assume that the increase is maintained in the subsequent years. However, this may not be the case since it depends on future market dynamics. The discount rate values are also tricky to determine because they account for time value of money from the BCS operator perspective. Some analysis estimate it using the weighted average cost of capital (WACC) of the investing entity while others base it on the difference between interest rate and inflation [70, 71]. For this reason, there is an inherent uncertainty in values of both r and d. Therefore, a sensitivity analysis becomes necessary in order to validate the attractiveness of the investment options under consideration.

Fig. 4.7 shows the influence the value of r and d have on the PBP of all the three options. r and d are varied in the ranges [2,10] and [0,15], respectively. Generally, the changes in PBP are small, with the worst change being less than 10 months. This is a good indication showing that investing in any of the given energy saving options remains attractive in-spite of the likely changes in both r and d.

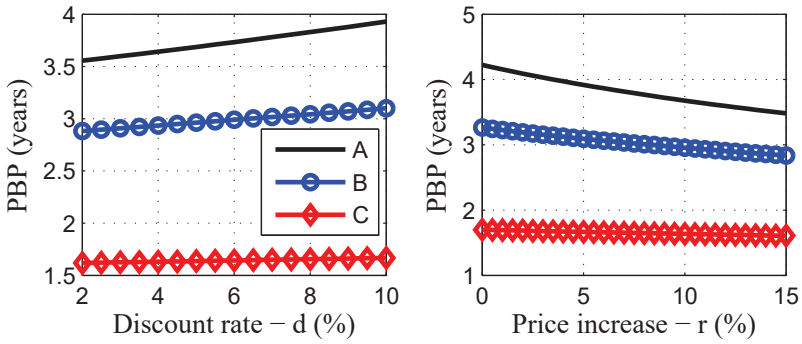

Figure 4.7. Sensitivity to discount rate and electricity price increases.

The results show that option **C** is the least affected by the changes, while option **A** is mostly affected. The long PBP of **A** makes it the most vulnerable to the changes. This means that investing in RDs (option **C**) is a better option than **A** or **B** when the required investment cash is available. Fig. 4.7 also shows that changes in r have a bigger impact on PBP than changes in d. For example, a 7% change in r results in about 5 months of change in PBP while a 7 % change in d gives less than a 3 months worth of change in PBP, for option **A**.

Intermediate storage capacity

The intermediate bulk storage, ST1, is a typically small storage located at a transfer station to facilitate the exchange of material between two belts. The use of transfer stations is usually discouraged in BCSs designs because they result in the loss of speed of material being transported and so reducing the efficiency. However, implementing a transfer station with a larger storage capacity introduces flexibility into the system and allows the system to take advantage of a time-of-use (TOU) tariff. Improved storage and feeder designs can also be applied to alleviate the problem of efficiency losses [72].

Fig. 4.8 shows option **C**'s PBP for different sizes of ST1 relative to the current size of ST2 (1680 tons). Results in Fig. 4.8 show that increasing the storage size reduces PBP, since the daily profits generally increase with storage size . However, increasing ST1 beyond 1680 tons (or 100%) results in a diminishing decrease in PBP until no further change happens. This is because the daily schedule cannot be optimised further to benefit from the tariff, within the given operational constraints. Therefore, an analysis similar to this required before a embarking on changing intermediate storage sizes with the aim of benefiting from the electricity tariff.

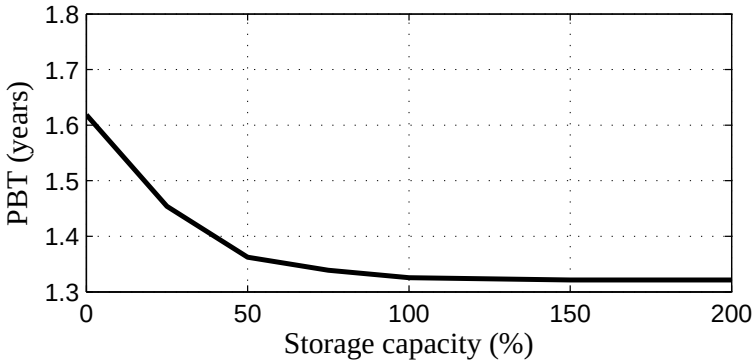

Figure 4.8. Sensitivity to changes in the intermediate capacity storage, ST1.

4.5 CONCLUSION

A generic optimal scheduling model for deriving energy efficient and cost effective schedules for belt conveyor systems (BCSs) with downhill belts is proposed and applied. The proposed optimisation model is able to control a BCS in order to save energy and cost within a TOU tariff that allows reselling of electricity to the grid. The model is applied on three proposed configurations to be retrofitted on an existing plant. These configurations use variable speed and regenerative drives. The results shows that the energy efficiency of BCS can be improved using variable speed drives (VSDs) and regenerative drives (RDs).

An economic analysis of investing in three proposed retrofit configurations is carried out, based on the payback period (PBP). The PBP's sensitivity to BCS storage sizes, increase in discount rate and electricity prices is assessed. The payback periods for all three energy saving configurations is found to be less than 5 years over a varying range of discount rate and electricity increases. Increasing the size of BCS storages is shown to provide a limited benefit towards cost saving on the given TOU tariff. The sensitivity analysis indicates that a careful study of the effect of storage size must be carried out because increasing storage capacity results in economic gains that are generally not proportional to the size of increase.

A similar generic optimisation model and economic analysis can be performed for other similar motor driven applications capable of implementing RDs. These applications includes lifts and cranes where the loads lifted above ground level present a potential source of energy.

CHAPTER 5 OPTIMAL SCHEDULING WITH UNCERTANITY IN MATERIAL DEMAND

The growing interest in demand response brings about increasingly complex electricity pricing structures. Electricity providers advancing critical peak pricing (CPP) see it as a more advanced and dynamic tariff than the standard time-of-use (TOU). In practice, the requirement of bulk material by down-stream processes may also be stochastic. The increased uncertainty in electricity prices and bulk material demand requires an appropriate algorithm to mitigate associated operational energy cost risk. This chapter considers the optimal scheduling of belt conveyor systems (BCSs) under a CPP tariff and stochastic scheduling when material demand is uncertain, using a chance constraints model predictive control (MPC) algorithm. The results show the suitability of this scheduling strategy under critical peak pricing and the importance of the BCS's storage size in reducing electricity cost. A method of sizing BCS storage with the help of chance constraints is proposed. The proposed stochastic MPC algorithm is shown to be a cost effective and appropriate method of handling uncertainties.

5.1 INTRODUCTION

The global economic growth in both developed and developing nations results in rapid growth of electricity demand and puts an ever increasing pressure on electricity supply. Demand response (DR) is seen as an increasingly good mechanism of improving the efficiency and reliability of electricity supply.

DR aims to control the load profile by changing the electricity consumption pattern of consumers ([13]). In this way, electricity can be supplied reliably and cheaply. DR program can either be incentive

based or time based ([13, 73]). Time based programmes (TBPs) offer different electricity prices, during different times (hours/half-hours) of the day, depending on the demand. The objective of these programmes is to reduce electricity usage during high price periods and encourage usage during low price periods, in order to flatten the user's load profile.

Time-of-use (TOU), critical peak pricing (CPP) ([19]) and real-time pricing (RTP) are some of the TBPs. Under TOU, prices of electricity are fixed for each period of the day during the whole year or season. On the contrary, in RTP, the price of electricity changes frequently, usually every hour. This is the most dynamic of the TBPs. CPP offers a compromise between TOU and RTP. Under CPP, the discounted TOU prices are normally applied and relatively higher prices are used during critical days decided by the utility ([14, 17]).

The general consensus amongst economist and engineers is that RTP will be the most beneficial pricing scheme for the utility and customers. Thus, CPP can be seen as an intermediate step towards the ultimate migration of utilities to RTP. Therefore, there is growing interest amongst utilities in CPP. For example, the state-owned South African utility, mentions its intention to implement CPP in its 2007 strategy document[1]. A number of utilities around the world currently offer CPP ([14, 15, 18, 74]).

Unfortunately, the increasing variability in TBPs shifts increasing electricity cost risk towards the customer's side ([14]). Thus, the use of energy cost optimal schedules becomes increasingly important especially for large industrial sector energy consumers. Deriving cost optimal operating schedules is an involving task because it has to take into account both electricity and operating costs, together with practical uncertainties involved in the operations. Due to its robustness and ability to handle constraints, model predictive control (MPC) provides a suitable solution to optimal scheduling.

Belt conveyor systems are used extensively in industrial applications for bulk material handling, to transfer material from one point to the other. Application areas include transporting material between plants in the mining industry and pulp-paper production, as well as for coal and ash handling systems

[1] http://www.eskom.co.za/c/article/975/critical-peak-day-pricing-pilot-project/

in thermal power plants ([32, 75]). In all the operations the material transferred has to meet some demand, which may be random, depending on the downstream processes.

This chapter considers two overall issues. Firstly, the benefit obtained through the use of MPC scheduling to operate a BCS on a CPP programme. The system is assumed to have initially been scheduled using optimal control under TOU tariff. Secondly, the use of a robust MPC schedule based on chance-constraints is presented. The control of variable speed drive BCs given in [6] is used as a case study. Although, a case study and a BC model from [33] are used, the work in this chapter is unique in four ways. Firstly, the use of a robust MPC strategy with chance-constraints is introduced. Secondly, CPP tariff structure is considered in this work while only TOU is considered in [33, 76]. Thirdly, the current analysis considers the original BC plant in [76] under different storage sizes and the relationships between storage size and the MPC's prediction horizon are explored. Lastly, the method of sizing the storage based on confidence level is derived. It is worth noting that the application of the strategy proposed in this chapter can be easily adapted for different industrial loads that are able to time-shift their operations such as water pumping systems in [34].

5.1.1 Critical peak pricing

Under a CPP tariff, the electricity provider issues a pricing signal to declare a critical period during which the price of electricity goes very high ([14, 74]). The critical period is usually declared a day before it occurs. The CPP contract allows the supplier to declare a limited number of critical days, N_{crit}, in a month. For example, Eskom's pilot project limits the number to 17 days per annum. There are a number of variants of CPP, but the three most common are: fixed-period CPP (CPP-F), variable period CPP (CPP-V) and extreme day CPP (CPP-ED) ([3, 14]).

Under the CPP-F, the timing, duration T_{crit} and price $\hat{\pi}_n$ of the critical period are fixed. However, under CPP-V, the notification period, T_{crit} and $\hat{\pi}_n$ can vary within predetermined limits. CPP-ED is a slightly different version of CPP, where a flat tariff is normally used and a TOU with high critical peak prices and low off-peak prices are used on extreme days. The consumer benefits from reduced electricity prices, discounted by a stipulated rate during the standard and peak periods ([3, 15]). For example, the California's statewide pricing pilot project sets the peak period price to five times the standard rate, a

day ahead notification is given and only 15 critical days are allowed per year, under CPP-F. While the critical period varies from one to five hours and the notification time can be as short as four hours, under CPP-V ([15]). The analysis in this chapter will consider CPP-F, other variants of CPP will be considered in future work.

5.1.2 Model predictive control

MPC is a control strategy whereby the control actions are obtained from a repetitive on-line solution of an optimal control problem. First, the MPC algorithm begins from the present state of the process and solves an optimal control problem over a finite-horizon, known as the prediction horizon h_p. Then, only the first portion of the resulting control sequence is applied to the system. This procedure is repeated, each time beginning from the current state of the process. The duration of the control sequence used is called the control horizon h_c [77, 78].

The superiority of MPC as a control strategy lies in its ability to easily handle constraints and multiple variables. The fact that the state is repeatedly measured, that is feedback, allows MPC to be robust against modelling uncertainties and disturbances [77, 79]. MPC has been applied to a wide range of practical problems and there is also growing interest within the power and energy sector [34, 80, 81, 82, 83, 84].

In [80] and [34], the authors show the suitability of MPC for pump scheduling under TOU and maximum demand tariff structure. Zhang in [76] shows the advantage of standard closed-loop MPC over open-loop optimal control on conveyor scheduling. Široký in [81] develops an MPC framework for minimising energy consumption in buildings. While, Ma argues that MPC is best suited for optimising energy use when the controller needs to incorporate prediction of weather variables, occupancy, renewable energy availability, and energy price signals [82]. MPC schedules are applied in generator maintenance and dynamic dispatch by [85] and [12], respectively. [79] proves the robustness and convergence of an MPC algorithm applied on a generic class of problems, that includes energy appliance scheduling.

The use of chance-constraints to enhance the robustness of the standard MPC algorithm has been demonstrated in [84, 86, 83]. The authors in [83] use chance-constraints to create a robust MPC

algorithm for a spacecraft rendezvous problem. Hovgaard and colleagues proposed an MPC-based power management scheme for optimising energy cost in supermarket refrigeration systems [84]. The chance-constraints are used to handle uncertainty in both process models and prediction of external variables, such as outdoor temperature. In [86] a chance-constrained MPC (cc-MPC) algorithm is used in the control of a high-purity distillation column to satisfy process output constraints.

5.2 CASE-STUDY MODEL

[33] has shown that the power used by the belt conveyor with variable-speed drives is related to the feed-rate I in tons per hour (t/h), and belt speed v in m/s. The speed and feed-rate are in turn related to the each other by unit mass of material q in kg/m. The relationships are given by,

$$P(I,v) = \frac{1}{\eta}(\theta_1 v I^2 + \theta_2 v + \theta_3 \frac{I^2}{v} + \theta_4 I + \frac{v^2 I}{3.6}), \tag{5.1}$$

and

$$I = 3.6 \cdot v \cdot q, \tag{5.2}$$

where θ_j are the design parameters unique to the system and η is the efficiency of the conveyor drive.

The amount of energy used to convey a given amount of material is constant, regardless of the time the conveying is done. However, under a CPP tariff, the conveying can be done during the cheapest time to reduce energy costs. Unfortunately, the demand has to be met at all times so the conveying has to be done whenever the material is needed. The storage is used to introduce some flexibility into the scheduling of the conveyor, because it can allow for the conveyance of material during cheap time slots before it is needed.

The amount of material in the storage (M_n), at a particular hour is related to the hourly feed-rate I_n and hourly demand D_n, as shown in (5.3). The other operating restriction is that the amount of coal in the storage must be maintained within safe limits. That is, the upper limit ST_U and lower limit ST_L. These constraints can be expressed as,

$$M_{n+1} = M_n + I_{n+1} \cdot \Delta t - D_{n+1}, ST_L \leq M_n \leq ST_U. \tag{5.3}$$

Both the speed and feed-rate of a given belt conveyor are physically limited. Thus,

$$I_{min} \leq I_n \leq I_{max} \text{ and } v_{min} \leq v_n \leq v_{max}. \tag{5.4}$$

For variable speed belts, the unit mass of the material on the belt should be less than the maximum value Q_{max}. Thus,

$$\frac{I_n}{3.6v_n} \leq q_{max}. \tag{5.5}$$

5.3 OPTIMAL MPC SCHEDULES

Consider a CBS with a series of N_B belts moving bulk material from point A to point B. Depending on the feed rate and belt speed, the j^{th} conveyor consumes $P^j(\cdot,\cdot)$ of power. Beginning at a time $l = t$, the MPC algorithm operates by repeating the following three steps, starting from the current amount in storage M_l.

Step 1: Predict the optimal schedule $(I_n^j, v_n^j)^*$, by solving the following optimisation problem over prediction horizon h_p,

$$\min_{(I_n^j, v_n^j)\in\mathbb{S}} \sum_{n=l+1}^{h_p+l} \{\sum_{j=1}^{N_B} P(I_n^j, v_n^j)\}\pi_n + \omega \sum_{j=1}^{N_B} \sum_{n=l+1}^{h_p+l-1} (v_n^j - v_{n+1}^j)^2 \tag{5.6}$$

where ω is a weighting parameter, π_n is the price of electricity and $\mathbb{S}$ is a set of feasible schedules constrained by the BC modelling equations (5.2)-(5.5). Variables I_n^j and v_n^j denote the feed rate and belt speed for the j^{th} conveyor during the n^{th} sampling period within the prediction horizon ranging from t to $t + h_p$. The first term of (5.6) optimises the energy. The second term optimises velocity ramps, $(v_{j,n} - v_{j,n+1})$, this is intended to reduce the excessive belt speed changes that are likely to damage the conveyor, as explained in Section 2.3.

Step 2: Implement only the first part of the optimal schedule, (I_t^j, v_t^j). Find the next state M_{l+1}, using (5.3) while noting that only the last conveyor feeds the storage. The material in storage and the CBS's electrical load LP_{l+1} are given by (5.7).

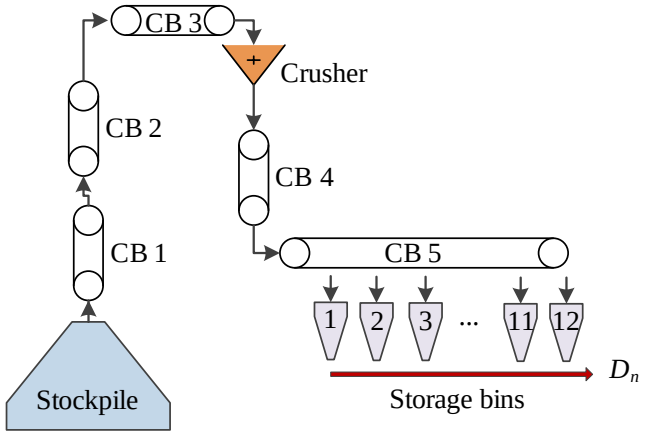

Figure 5.1. Process flow diagram of the coal conveying system.

$$\begin{aligned} M_{l+1} &= M_l + I_{l+1}^{N_B} - D_{l+1}. \\ LP_{l+1} &= \sum_{j=1}^{N_B} P^j(I_{l+1}^j, v_{l+1}^j). \end{aligned} \tag{5.7}$$

Step 3: Move to the next sample time, $l = t+1$ and repeat steps 1 and 2.

It is important to note that for every step of the MPC algorithm, the prediction horizon moves forward in time, even though h_p remains constant. On the other hand, an optimal control (OC) implements the whole of the schedule resulting from step 1, at once.

CASE STUDY: COAL-HANDLING PLANT

For a case study, the coal conveying system in a coal-fired power plant given by [33] and shown in Figure 5.1, is considered. A plant consisting of five belts and a crusher, moves coal from a storage yard to 12 coal bins of a power station. The storage bins have a total capacity M_{total} of 5595 tons. The ST_L and ST_U storage safety limits are set at 1855 and 4756 tons, respectively. The hourly demand for coal D_n can be calculated from the average power demand of the station. In reality, coal demand is random because the future amount of power required by downstream processes can never be predicted with certainty. This randomness is considered in detail in Section 5.4.

The plant is modelled as two belts with the same amount of feed-rate. The first belt (C1-C3) moves from the stockpile to the crusher at the speed of v^1 and the second (C4-C5) from the crusher to the storage running at v^2. The belt parameter values (θ_1, θ_2, θ_3, θ_4) are (2.38×10^{-4}, 6.34×10^{3}, 3.1×10^{-3}, 62.6) and (2.14×10^{-4}, 7.28×10^{3}, 2.8×10^{-3}, 77.9) for the first and second belt, respectively. A one hour sampling time has been used for simulations. The belt drive efficiency is 88.9%. The upper limits of the feed-rate and speed are q_{max} =1800 tons/hour and v_{max} =2.5 m/s, respectively.

The plant is assumed to initially operate under a TOU tariff where the hourly price is given by

$$\pi_n = \begin{cases} 0.35 \text{ R/kwh} & \text{for } t \in [0,8), \\ 0.70 \text{ R/kwh} & \text{for } t \in [8,9)\cup[12,19)\cup[22,24), \\ 1.11 \text{ R/kwh} & \text{for } t \in [9,12)\cup[19,22), \end{cases} \tag{5.8}$$

using OC schedules. R stands for South African currency, Rand. Under the CPP-F programme, the energy prices in (5.8) are reduced by a discount rate d during non-critical days. The CPP-F pricing is given by

$$\hat{\pi}_n = \begin{cases} \text{(critical)} \begin{cases} 3 \text{ R/kwh} & \text{for } t \in [15,22), \\ \pi_n \text{ R/kwh} & \text{for } t \in [0,15)\cup[22,24), \end{cases} \\ \text{(normal)} \begin{cases} (1-d)\pi_n \text{ R/kwh} & \text{for } t \in [0,24). \end{cases} \end{cases} \tag{5.9}$$

The monetary benefit to a belt conveyor operator switching to a CPP-F program over N_T days, is quantified by (5.10), assuming zero reservation capacity. The benefit depends on LP_n, λ_n, $\hat{\lambda}_n$ and CC, which are the load before CPP-F (baseline), load profile after CPP-F (post-implementation) during normal days and post-implementation load profile during critical days and investment cost, respectively. The first term of (5.10) quantifies the gain made through the discounted prices during non-critical days. The second term gives the cost saved by shifting the load away from critical hours.

$$\text{Benefit} = (N_T - N_C)\sum_{n=1}^{24}\pi_n(LP_n - d\cdot\lambda_n) + N_C\sum_{n=1}^{24}(\pi_{nn} - \hat{\pi}_n\cdot\hat{\lambda}_n) - CC \tag{5.10}$$

The CC is the money used to improve the plant in order to take advantage of the CPP programme. It could include the cost of installing BC with higher feed rates or increasing storage capacity. The scenarios explored in this chapter do not consider a retrofit, thus $CC = 0$.

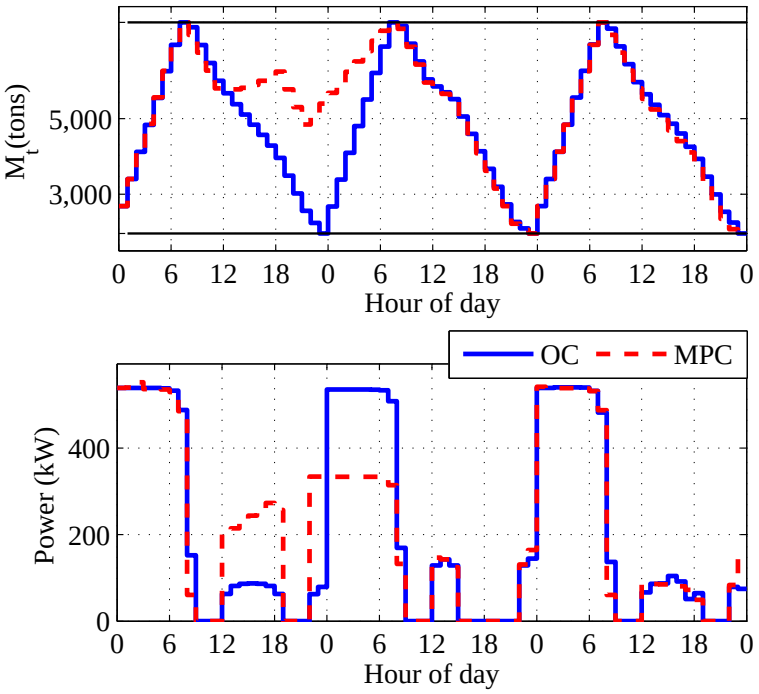

Figure 5.2. State of storage and load profiles for both MPC and OC schedules.

5.3.1 Simulation results and discussions

The following simulations consider the operation of the BCS over a period of 30 days with 2 critical days. The baseline is derived from OC schedules under TOU of (5.8) and the post-implementation schedules are obtained from MPC under CPP-F given by (5.9). Under CPP-F, the critical day is announced at 1500hrs the day before it occurs.

Figure 5.2 compares the behaviour of MPC and OC for the coal conveying system over 3 days, when the 2^{nd} day is a critical day. The simulation considers the BCS in the case with $1.5M_{total}$ of storage and a 50% discount rate. These settings are chosen because they amplify the differences between OC and MPC. The OC shifts the load within the day, by conveying more material over a shorter period of 1300-1500 hours while maintaining a daily energy consumption of 5.1 MWh. However, the MPC shifts some of the load backwards to the day before the critical day. For the MPC, the daily energy consumptions are 6.7 MWh, 3.5 MWh and 5.1 MWh, for days 1, 2 and 3, respectively. The level of storage in Figure 5.2 shows how MPC uses storage to shift load.

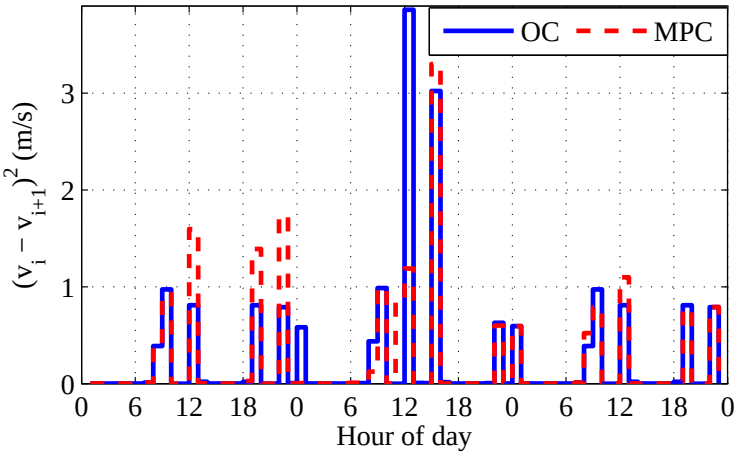

Figure 5.3. Belt speed changes for both MPC and OC schedules.

The ability of MPC to shift load between days makes it more appropriate for scheduling within the CPP program. OC cannot shift load between days because under OC the optimal schedule is solved for one day at a time. On the contrary, the receding horizon of MPC allows it to 'see' an impending price increase of a critical day and hence act to consider it for optimisation. The other advantage of the MPC schedule is its ability to limit extreme belt speed changes as shown in Figure 5.3.

When the discount rates are low and the storage size limited there is little difference in cost savings obtained from MPC as opposed to OC. Practically, the discount rates are usually, less than 10%. Thus, the subsequent simulations will consider the MPC schedules with a discount rate of 10%.

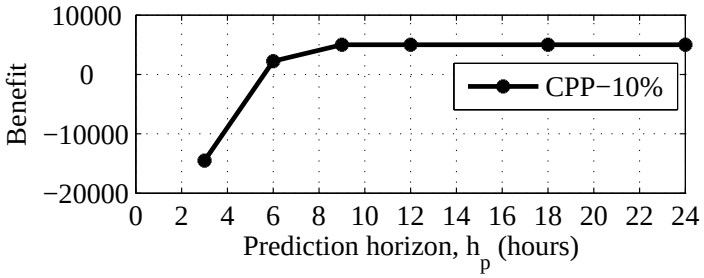

Figure 5.4. Influences of prediction horizon on the benefit.

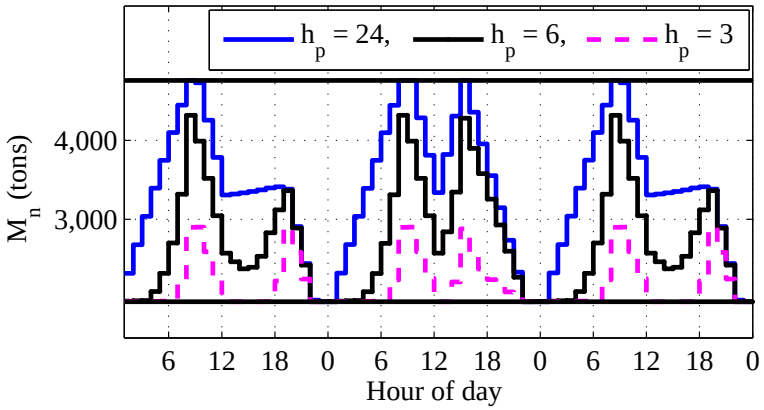

Figure 5.5. Storage usage for varying prediction horizons.

Figure 5.4 shows the benefit gained by implementing MPC with varying prediction horizons, for a 10% discount rate. Both the prediction and control horizons are kept at equal lengths in all simulations. The results show that it would be more costly to enrol into a 10% discounted CPP-F programme while the prediction horizon is less than 6 hours. Thus, as expected, increasing the prediction horizon increases the benefit gained from the CPP-F programme.

This observation is due to the fact that at shorter prediction horizons, MPC fails to 'see' impending high electricity prices in time and so it fails to use the storage to buffer against them. This reasoning is better illustrated in Figure 5.5. Figure 5.5 shows how the storage is being used by MPC for various lengths of the prediction horizons. The full capacity of storage is never used by MCP when the prediction horizon is 3 or 6. Moreover, the maximum capacity of storage used increases with increasing prediction horizon.

Figure 5.6 shows the total and disaggregated benefit of enrolling into the CPP program considering similar plants with different amounts of storage. The disaggregated benefit plot separates the benefit gained by the algorithms during critical days and non-critical days as given by (5.10). On the total benefit, the interesting observation about figure 5.6 is that; below the storage size of $1.5M_{total}$, a plant with larger storages would benefit more from the programme than those with smaller storage. Form $1.5M_{total}$ to $2M_{total}$, the opposite is true. Finally, beyond $2M_{total}$ the benefit remains the same regardless of the storage size.

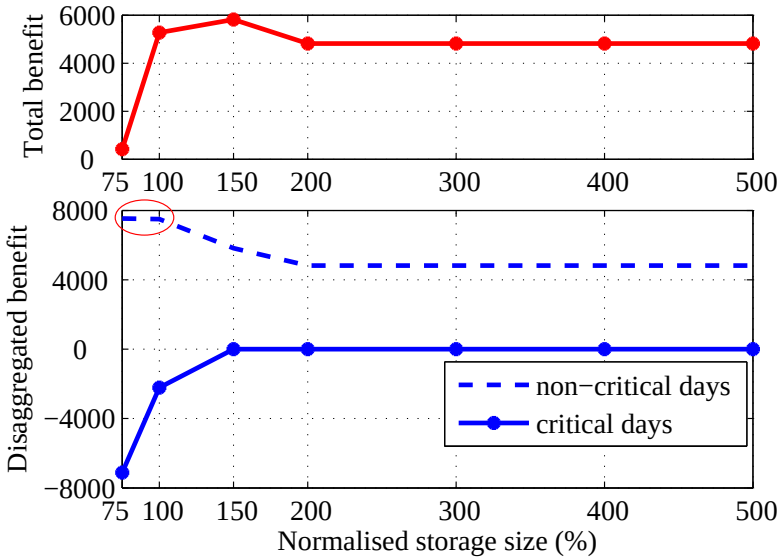

Figure 5.6. Influence of storage size on the benefit.

Analysis of the disaggregated plots is able to explain the behaviour of the total benefit plot. As the storage size increases, the benefit obtained by the MPC schedule during non-critical days diminishes because the storage becomes larger enough for the OC to successfully optimise the baseline. This is because the baseline L_i is from a plant being scheduled using OC already.

For plants with storage size less than $1.5M_{total}$, the storage is very small and so MPC fails to sufficiently shift the load within the day (intra-day) during the critical time. Thus, it is punished by very high costs during critical days. When the storage is very large (beyond $2M_{total}$), a very small benefit is gained by load shifting during critical days. This is because the baseline has been shifted very well due to the large storage, so the only benefit gained during non-critical days depends on the discount rate.

Figure. 5.7 shows the operating cost before and after the implementation of the CPP-F programme. The benefit of CPP-F can be seen from the reduced post implementation costs.

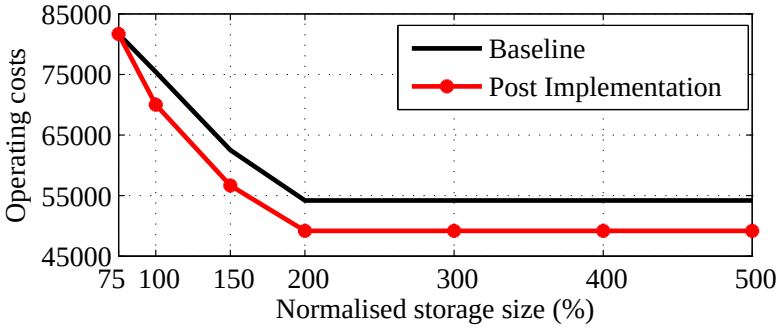

Figure 5.7. Operating cost for different storage capacities.

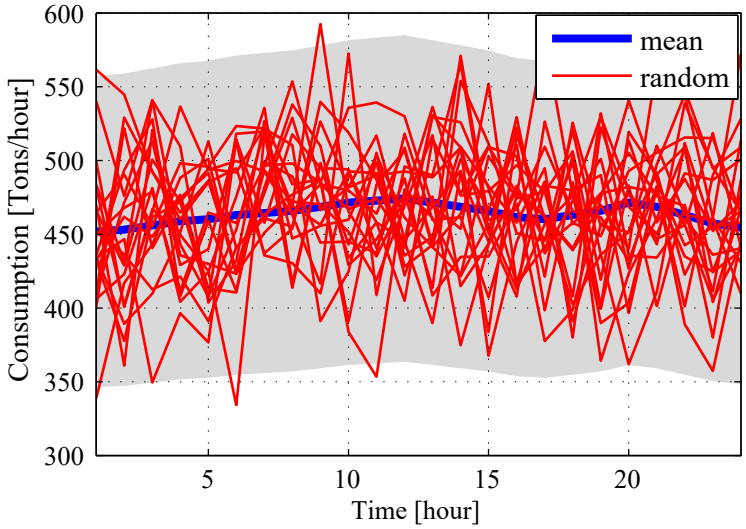

Figure 5.8. Random demands and 99% confidence bounds.

5.4 CHANCE-CONSTRAINED MPC

Simulations in Section 5.3 are based on the assumption that the material demand is known with certainty 24 hours ahead of time. In practice, this is not the case. For the case study considered in this chapter, the hourly coal demand depends on the power station's short-term load forecast. Load forecasts are known to be uncertain and research into load forecasting continues to be carried out ([87, 88]). Thus, an uncertain load forecast implies an uncertain coal demand.

A load forecast is usually expressed as a point forecast plus or minus a confidence level, based on the

Gaussian distribution ([89]). It is therefore reasonable to assume that the actual material demand can be modelled as a sum of a known mean demand $\overline{D}_n$ and random normally distributed component $\widehat{D}_n$. That is,

$$D_n = \overline{D}_n + \widehat{D}_n, \text{ where } \widehat{D}_n \sim \mathcal{N}(0, \sigma_n^2). \tag{5.11}$$

The $\widehat{D}_n$s are assumed to be independent of each other. Figure 5.8 shows a set of 20 random realization of the coal demand with a standard deviation that is 10% of the mean demand, to be used in the subsequent simulations.

The uncertainty in material demand will result in the violation of the storage safety limit, as described by (5.3). The practical purpose of the storage safety is to act as a buffer in-case of a BC failure. For example, the lower limit ensures that there is enough coal in the storage bins for the power plant to run in-case the belt conveyor breaks down and emergency maintenance has to be carried-out. The lower limit will also give the plant operators enough time to safely shut-down their down-stream processes. Similarly, the upper limit ensures that no spillages occurs in-case there is a problem with BC instrumentation and actuators, that may disable control signals.

To reduce the violation of constraints, a stochastic MPC algorithm is needed. The most common way of making a robust MPC is to tighten the constraints. That is, make the new lower bound bigger and the new upper bound smaller. This amount of tightening can be calculated well when the disturbance is bounded ([90]). In this case, tightening reduces the effective operating storage size and so according to analysis in Section 5.3, it has energy cost implications.

5.4.1 Chance-constraints

A systematic way of setting robust bounds can be obtained through the use of chance-constraints. Consider the lower limit constraint in (5.12) during the k^{th} sampling time of the MPC's prediction step.

$$ST_L \leq \sum_{n=1}^{k} I_n - \sum_{n=1}^{k} D_n + M_0, \tag{5.12}$$

where M_0 is the initial amount of material in the storage. It can be understood from the purpose of the storage limits that their violation presents an operational risk. Thus, the objective of the stochastic algorithm is to reduce this risk. That is, the lower bound constraint must be satisfied with a sufficiently high probability α (say $\alpha = 99\%$). Substituting for D_n translates (5.12) into,

$$Pr\{\sum_{n=1}^{k} \widehat{D}_n \leq \sum_{n=1}^{k} I_n - \sum_{n=1}^{k} \overline{D}_n - ST_L + M_0\} \geq \alpha, \tag{5.13}$$

where Pr denotes probability. (5.13) is known as a chance-constraint ([86]). The expected value $\mathbb{E}\{\}$ and variance $\mathbb{V}\{\}$ of the sum of error terms are given by,

$$\mathbb{E}\{\sum_{n=1}^{k} \widehat{D}_n\} = 0, \; \mathbb{V}\{\sum_{n=1}^{k} \widehat{D}_n\} = \sum_{n=1}^{k} \sigma_n^2. \tag{5.14}$$

By standardising the sum of $\widehat{D}_n$, the chance-constraint in (5.13) can be rewritten as,

$$ST_L + \mathbb{F}^{-1}(\alpha)\sqrt{\sum_{i=1}^{k} \sigma_n^2} \leq \sum_{n=1}^{k} I_n - \sum_{n=1}^{k} \overline{D}_n + M_0 \tag{5.15}$$

where, $\mathbb{F}^{-1}(\alpha)$ is the inverse of the standard normal cumulative distribution. Thus, the chance-constraints also tighten the lower bound with an amount of restraint related to a confidence level α. A similar analysis on the upper limit also results in the tightening of the bound. The new upper bound constraints are of the form,

$$\sum_{n=1}^{k} I_n - \sum_{n=1}^{k} \overline{D}_n + M_0 \leq ST_U - \mathbb{F}^{-1}(\alpha)\sqrt{\sum_{n=1}^{k} \sigma_n^2} \tag{5.16}$$

Thus, the cc-MPC is implemented using the three steps defined in Section 5.3 with the storage limits defined by (5.15) and (5.16) in place of (5.3).

5.4.2 Storage sizing based on confidence level

Figure 5.9 shows typical constraints during the prediction step of the MPC. The MPC with chance-constraints (cc-MPC) is compared with an MPC where the bounds have been restrained (r-MPC). cc-MPC has tapered constraints as predicted by (5.15). This also coincides with the fact that the effect of prediction error increases with increasing look-ahead time.

It is worth noting that increasing α for a given set of limits (ST_L and ST_U), prediction horizon and demand variances, will eventually result in equal lower and upper bounds. Thus, for some critical

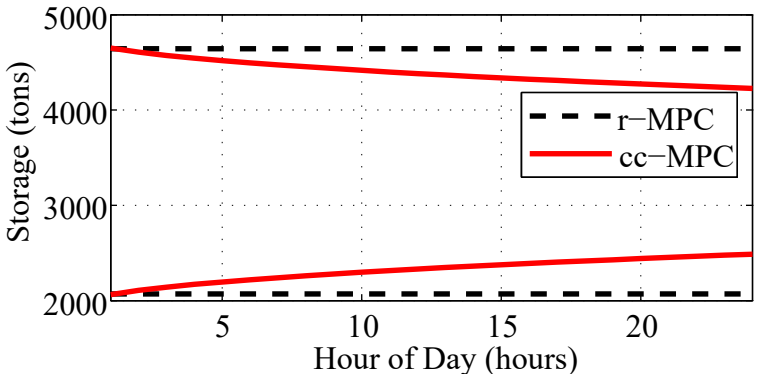

Figure 5.9. Constraints at the beginning of the day for restrained MPC (r-MPC) and chance constrained MPC (cc-MPC).

value α_c,

$$ST_L + \mathbb{F}^{-1}(\alpha_c)\sqrt{\sum_{n=1}^{h_p}\sigma_n^2} = ST_U - \mathbb{F}^{-1}(\alpha_c)\sqrt{\sum_{n=1}^{h_p}\sigma_n^2}. \tag{5.17}$$

Increasing the confidence level beyond α_c makes the open loop MPC problem infeasible. This implies that the amount of storage in the belt conveyor system cannot assure constraint satisfaction beyond α_c. That is, the operating risk can not be further reduced. Assuming a constant value of standard deviation, $\sigma_i = \sigma$, then (5.17) simplifies to,

$$ST_U - ST_L = 2\sigma\mathbb{F}^{-1}(\alpha_c)\sqrt{h_p}. \tag{5.18}$$

The right hand side of (5.18) is the effective storage size within which the scheduling algorithm is expected to operate. Therefore, (5.18) gives the minimum effective storage capacity that is able to provide safety confidence level α_c. Thus, it can be used for storage sizing when designing a BCS similar to the model in Section 5.2 with a specified value of reliability α_c.

5.4.3 Simulation results and discussions

The following simulations consider the robustness of scheduling algorithms over 100 days of random material demand under the tariff in (5.8). Initially, 100 realisation of material demands with a 10% standard deviation ($\sigma_n = 0.1\overline{D}_n$) are generated and then these realisations are used for simulating variants of OC and MPC algorithms. MPC, cc-MPC and r-MPC refer to the standard MPC, MPC

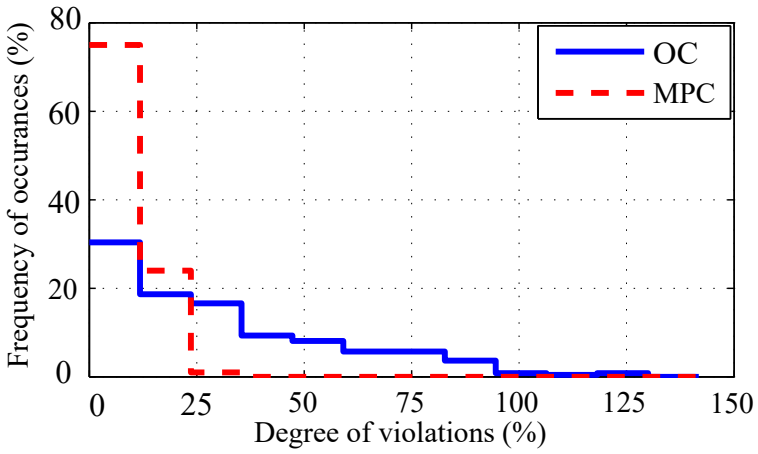

Figure 5.10. Distribution of constraint violations (absolute value) for both OC and MPC.

with chance constraints and MPC with tightened constraints, respectively. The same notation applies for OC. The amount of restraint on the constraints is calculated as a percentage of effective storage. So, r-MPC(10%) implies that the bounds are tightened by 10% of $(ST_U - ST_L)$. However, for the cc-MPC(99%), the 99% is the value of α.

Figure 5.10 shows the distribution of absolute values of bound violations for the standard MPC and OC. The degree of violations are given as a percentage of the mean hourly coal demand. Therefore, a violation of 100% means that the storage bound is breached by an amount equal to the average hourly coal demand. The results in Figure 5.10 indicate that the magnitude of violations resulting from MPC are smaller than those resulting from OC. Table 5.1 summarises the robustness and cost effectiveness of the scheduling algorithms. The cost effectiveness is measured by the mean daily energy cost (MDEC). r-OC(15%) is less robust that cc-OC(99%) because it results into larger violations even though the two algorithms have almost equal costs. Comparing r-MPC(15%) and cc-MPC(99%) shows that r-MPC achieives a marginally better performance at a high cost. Thus, chance-constraints algorithms are better than ones with tightened constraints. A comparison between cc-OC and c-MPC shows that MPC gives smaller magnitudes of violations at a lower cost than OC. For example, cc-MPC(99%) has a maximum of a 2% violation while cc-OC(99%) gives 13%, but cc-MPC(99%) achieves smaller violations at about a 4% cost reduction. Table 5.1 also shows that cc-MPC becomes more robust as the constraints are further tightened. This robustness is obtained at the cost of increasing average daily energy cost.

Table 5.1. Performance results. MDEC refers to mean daily energy cost.

Algorithm	MDEC	Number of violations	Biggest violation
OC	2261	247	126%
MPC	2264	200	27%
r-OC(15%)	2380	7	36%
r-MPC(15%)	2386	0	0%
cc-OC(90%)	2346	56	64%
cc-MPC(90%)	2277	42	12%
cc-OC(95%)	2346	30	46%
cc-MPC(95%)	2281	22	9%
cc-OC(99%)	2379	7	13%
cc-MPC(99%)	2290	2	2%

5.5 CONCLUSION

The analysis in Section 5.3 shows that the prediction horizon of the MPC is related to the amount of storage used and hence the amount of cost savings. MPC performs better when the prediction horizon is lengthened. It has also been observed that optimal control is capable of intra-day but not inter-day load shifting. The ability of MPC to perform inter-day load shifting makes it a better algorithm for energy cost optimisation under a CPP-F programme.

The amount of storage in the plant dictates the amount of load shifting that is possible. The bigger the storage the smaller the baseline cost and the harder it is for the MPC to benefit from the CPP-F programme. These conflicting situations mean that the benefit obtained from a CPP-F program is not linearly related to the amount of storage of the belt conveyor plant.

Analysis also shows that the larger the storage, the lower the operational cost of the belt conveyor plant. However, this cost ceases to decrease as the storage increases, for very large storages. Both utility and end-user can benefit from a CPP-F programme provided, the discount rates is attractive and the end-user's equipment has sufficient storage to facilitate load shifting.

The analysis in Section 5.4 shows that MPC is more robust than OC and that a robust schedule is obtained at the expense of higher energy costs. Chance-constraints have been shown to be an effective means of building robust conveyor schedules. The use of chance-constraints is meaningful because it is based on the desired confidence level. Chance-constrains also provide an intuitive formula for sizing the conveyor system's storage size.

For future work, the analysis in this chapter needs to consider other variants of the CPP tariff apart from the CPP-F. The current work assumes that the random components of the the stochastic demand are independent and are normally distributed. Thus, future work also needs to gather extensive data and investigate the practically occurring nature of these components.

CHAPTER 6 THE BENEFIT OF PRICE FORECASTS IN CONVEYOR SCHEDULING

The use of real-time pricing (RTP) tariff is increasing as increasingly more electricity markets become deregulated. Scheduling of belt conveyor system (BCS) under RTP requires electricity price forecasting. This chapter deals with quantifying the economic benefit of price foresting schemes used for a day-ahead scheduling of a BCS under the real-time pricing tariff. The case study considered uses three price forecasting methods on the PJM's market prices over a period of two years. A great deal of research literature related to price forecasts tends to focus on improving the accuracy of forecasts with little regard for their practical application. Quantifying the benefit of a forecasting scheme is a challenging problem and it important to operators of all large industrial loads, capable of load-shifting. Results in the current literature suggest that mean absolute percentage error (MAPE) is poor at indicating the economic benefit of a forecast. Rank correlation (RC) between the predicted price and the actual price is proposed as an indicator of economic benefit. The results show that RC is a better indicator of economic benefit than root mean square error (RMSE) and MAPE. They also show that potential economic benefit obtainable from forecasts depends on price volatility and not mean price. An artificial forecast is used to validate the superiority of RC over MAPE and RMSE. It is observed that the predictability of a forecast's economic benefit is largely dependent on how responsive the load is to electricity price changes.

6.1 INTRODUCTION

One of the currently dominant trends in the electricity markets is the move from fixed towards dynamic prices. This is driven by the introduction of price-responsive demand response (DR) in demand-side management (DSM) programmes. While, DR improves the power system's stability, tariffs such as

RTP impair the customer's ability to schedule most of its operations at times when electricity prices are low. This is because prices are given in real-time [13, 14]. The most appropriate strategy of mitigating the risk of high electricity cost is using cost-optimal scheduling with an accurate price forecasting method. The commonly used methods of quantifying forecasts' accuracy in literature are mean absolute error (MAE), mean absolute percentage error (MAPE) and root mean square error (RMSE) [19, 20, 21, 22, 23]. A great deal of literature related to price forecasts tends to focus on improving the accuracy of forecasts with little regard for their practical application.

However, there is a growing interest in the economic assessment of price forecast accuracy for specific applications [20, 23, 25, 26, 24]. The authors in [25] and [26] consider the effects of price forecast errors on the supply-side of the grid, while [24] deals with the demand-side. The authors in [25, 26, 24] illustrate the inadequacy of MAPE in indicating the economic value of a forecast method. The main contribution of this chapter extends this discussion by suggesting rank correlation (RC) as an alternative means of assessing economic impact and illustrating why the use of MAPE and RMSE is flawed.

This chapter presents the economic assessment of electricity price forecast accuracy using day-ahead scheduling of load-shifting industrial plants. Two types of load-shifting loads are considered; one with on-off control and the other with continuous motor speed control via variable speed drives (VSDs). Three methods of forecasting day-ahead electricity prices are used to schedule the operation of a coal-conveying industrial plant in a real-time electricity market. The price forecasts and the costs of resulting schedules are compared over a period of two years using PJM[1] market prices. The results show that the economic benefit obtained from the forecast is highly dependent on the volatility of the electricity price being predicted. The ability of RC, MAPE and RMSE to rank the economic benefit of different forecasts is compared. As in [24], the assessment illustrates the weakness of common forecast accuracy indicators in assessing the appropriateness of a forecast method. However, the results in this chapter further show that RC between the predicted and actual prices is a better indicator of the economic value of a forecast method. The chapter uses an artificial forecast to illustrate why MAPE and RMSE are poor indicators of economic benefit.

[1] (Monthly Locational Marginal Pricing) www.pjm.com

6.2 PRICE DATA, CASE STUDY AND BENEFIT INDEX

The data used in this chapter are the real-time hourly locational marginal pricing data of the PJM, for a period of 24 months from September 2010. Due to seasonal changes in the electricity prices, data is divided into four seasons of three months each. For each season, the three prediction methods are trained with data of the first two months and performance is evaluated on the remaining month.

On-off control (OOC) or variable speed control (VSC) are two common alternatives used for controlling industrial plants with motors for the purposes of energy efficiency and energy cost optimisation. Studies in [32] and [33] show the use of OOC in BCSs that transport coal. [34] shows both strategies for the control of pumping systems. [91] advocates the use of variable-speed drive technology for energy efficiency initiatives on cooling systems of 20 mines.

The case study industrial plant considered is a BCS transporting coal, as detailed in Figure 5.1 [33]. This industrial plant supplies a pre-determined series of hourly demand of coal D_n to a power station through storage bins. The coal-conveying system consists of a series of five belt conveyors and 12 storage bins. The system's control inputs consist of hourly feed-rates I_n and belt speeds v_n for variable speed drives driving the conveyors. The total capacity of the storage bins is 5595 tonnes. In this case, the upper limits of the feed-rate I_{max} and speed v_{max} are taken to be 1500 tonnes/h and 2.5 m/s, respectively. The hourly coal demand by the power station is obtainable from the predicted power demand [33]. The hourly demand data used in the subsequent simulations is D_n = [451.66, 453.07, 455.89, 458.72, 460.13, 462.95, 464.36, 465.77, 468.58, 471.39, 472.79, 474.19, 471.39, 468.58, 465.76, 461.54, 460.13, 462.95, 465.77, 471.39, 468.58, 462.95, 457.31, 454.48].

6.2.1 Variable speed control

The VSC schedule is obtained by solving the optimisation problem given by (6.1). Apart from optimising the cost of energy, (6.1) also attempts to reduce the stress on the belt and conveyor components by minimising the velocity ramp $(v_n - v_{n+1})$. ω and ω_{VSC} are weighting parameters that control the amount of trade-off between the two objectives. The N_t sampling points are obtained by dividing a 24-hour day into equal sampling periods of duration Δt. The power required by the

conveyor is modelled as a four-parameter nonlinear function $P(I_n, v_n)$ described in [6]. The variable π_n represents the real-time hourly electricity price.

$$\begin{gathered}\min_{I_n, v_n} \Delta t \cdot \sum_{n=1}^{N_t} \pi_n P(I_n, v_n) + \omega \cdot \omega_{VSC} \sum_{n=1}^{N_t - 1} (v_n - v_{n+1})^2 \\ \text{subject to:} \\ I_n / 3.6 v_n \leq q_{max}, \\ ST_L \leq M_0 + \Delta t \cdot (\sum_{n=1}^{m} I_n - \sum_{n=1}^{m} D_n) \leq ST_U, \\ \forall m \in \{1, 2, \ldots, N_t\}, \\ \text{where } I_n \in [I_{min}, I_{max}] \text{ and } v_n \in [v_{min}, v_{max}].\end{gathered} \tag{6.1}$$

To avoid spillages, the optimal schedule must ensure that the unit mass of material on the belt does not exceed the maximum q_{max}. It must also ensure that the amount of material in the storage, M, is constrained within the upper (ST_U) and lower (ST_L) storage limits. The optimisation is initialised with the amount of material in the storage (M_0) equal to ST_L. The lower bounds of the I_n and v_n are set to zero. The VSC scheduling problem is a nonlinear optimisation problem due to the conveyor power function and the nonlinear programming Matlab[2] toolbox is used to solve it.

6.2.2 On-off control

For the OOC in (6.2), the schedule is a series of the binary variables u_n that indicate by 1 when the plant is on and by 0 when it is off. In this case the objective is to minimize the cost of energy and the number of times the plant has to be switched on. Frequent on-off switching of motors is not advisable because it increases mechanical stress on the conveyor components. High start-up current of loaded motors also tends to reduce the motor's life span [33]. The OOC in (6.2) uses an auxiliary variable s_n to minimize the number of start-ups. s_n indicates by a value 1 whenever a start-up occurs. This so called 'Pretoria method' is implemented by two inequality constraints and an addend in the cost function, i.e. $\sum_{n=1}^{N_t} s_n$ [40, 92]. The generic inequality, $u_{n+1} - u_n - s_{n+1} \leq 0$, is meant to ensure that $s_{n+1} = 1$ whenever there is a start-up, i.e whenever $u_{n+1} > u_n$. The other inequality, $u_1 - s_1 \leq 0$, caters for the special case of the very first switching variable sample (u_1), when the motors are assumed to initially be off.

[2] http://www.mathworks.com/help/optim/

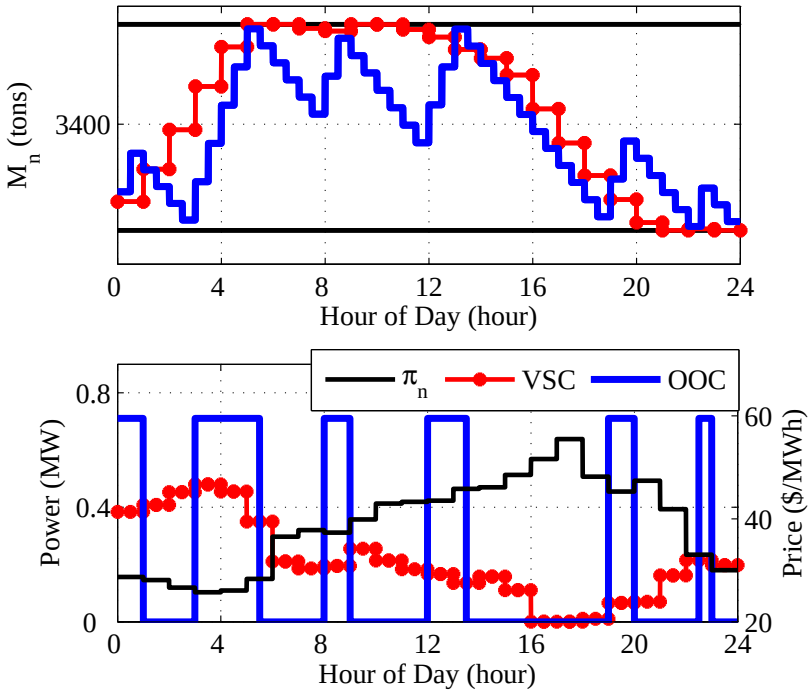

Figure 6.1. Typical usage of storage bins and power schedules.

$$
\begin{aligned}
&\min_{u_n,s_n} \Delta t \cdot P_{ON} \cdot \textstyle\sum_{n=1}^{N_t} \pi_n u_n + \omega \sum_{n=1}^{N_t} s_n \\
&\text{subject to:} \\
&ST_L \leq M_0 + \Delta t \cdot (F_{MAX} \cdot \textstyle\sum_{n=1}^{m} u_n - \sum_{n=1}^{m} D_n) \leq ST_U, \\
&u_1 - s_1 \leq 0 \ , \ u_{n+1} - u_n - s_{n+1} \leq 0, \\
&\forall m \in \{1,2,\ldots,N_t\}, \forall i \in \{1,2,\ldots,N_t - 1\} \\
&\text{where } u_n, s_n \in \{0,1\}.
\end{aligned}
\tag{6.2}
$$

The system is taken to deliver maximum feed rate and run at maximum speed when it is on. Thus, $P_{ON} = P(I_{max}, v_{max})$, when $u_n = 1$. A sampling time of 30 minutes is used for the simulations of OOC. The OOC is a linear binary optimisation problem that is solved using a mixed integer solver called Coin-or branch and cut (Cbc) found in the OPTI[3] Matlab toolbox.

6.2.3 Typical plant schedules

Fig. 6.1 shows the price schedule and SOS obtained for the biannual hourly mean price series using the same daily coal demand [33]. The selected settings are $\omega = 2$ and $\omega_{VSC} = 0.1$. The VSC and OOC objective function costs are 192 and 172, respectively, both with the mechanical cost contributing less than 10%.

The high prices are avoided by both the VSC and OOC plants. During the first six hours of the day the power usage of the VSC cannot be increased any further to take advantage of the low prices because the storage reaches maximum capacity. Fig. 6.1 shows that the OOC scheduled plant is on in spite of a period of relatively high prices between 12:00 and 13:30, because otherwise the storage level would go beyond the lower limit. The schedules shown in Fig. 6.1 are able to avoid the price peak well because the real-time market energy price used for scheduling is fully known. This is practically impossible for real-time pricing, therefore in practice scheduling will have to rely on predicted prices.

6.2.4 Forecast economic benefit index

Generally, an accurate forecast produces low scheduling cost because it correctly predicts hours with high prices to be avoided and hours with low prices to be used. A bad-case scenario is when the day-ahead price is assumed to be constant and the resulting schedule merely attempts to meet the operational constraints. In such a case the schedule is developed without any information on the future prices. Thus, the cost of a schedule using a flat price profile throughout the day is used as a basis for comparison. For the purpose of comparison, the economic benefit of a forecasting method is quantified by creating a forecast economic benefit index (FEBI) adapted from [24] and defined by (6.3).

$$\text{FEBI} = 100 \times (\text{Cost}^{FP} - \text{Cost}^{PP})/\text{Cost}^{FP} \tag{6.3}$$

where Cost^{FP} and Cost^{PP} are the plant's operational costs determined using a flat price (FP) and predicted price (PP) schedules, respectively. The FEBI is a big positive value when the PP schedule is a lot cheaper than the FP schedule. In this case, the magnitude of the FEBI quantifies how beneficial

[3] http://www.i2c2.aut.ac.nz/Wiki/OPTI/

the forecast is. On the contrary, the FEBI is negative when the PP schedule is more expensive than the FP schedule. This indicates that the forecasting is, in fact, counter-productive. Thus, a positive value implies that there is a cost advantage in using the PP while a negative value implies a loss incurred owing to the PP.

6.3 METHODOLOGY

The methodology for calculating performance of forecasts using scheduling costs and FEBI is summarised in Fig. 6.2. For each day of operation, the following three steps are carried out;

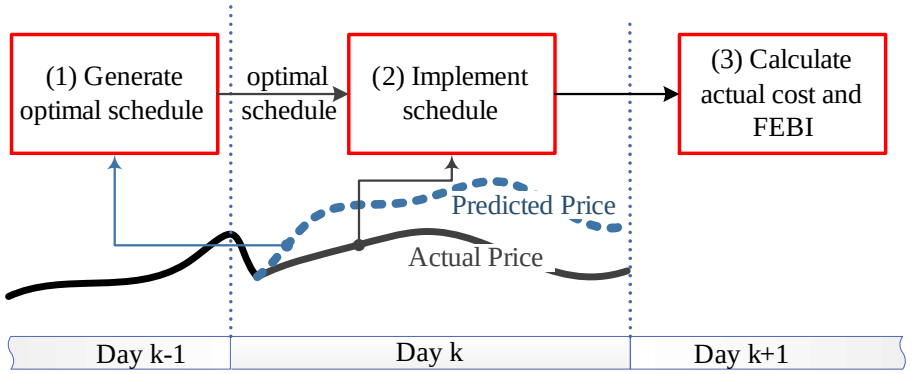

Figure 6.2. Methodology for calculating benefit of a day-ahead forecast.

Step 1: Scheduling for a particular day k begins at the end of day $k-1$, at which time the actual prices (APs) of day k are unknown. The schedule is obtained by solving an optimisation problem given by (6.4).

$$\left\{ \begin{array}{cc} \min & \text{Cost}(\pi_n^{PP}; P(I_n, v_n)) \\ I_n, v_n & \text{s.t. } I_n, v_n \in \Omega, \forall n \in [1, N_t] \end{array} \right\} \tag{6.4}$$

where $\{I_n, v_n\}$, $P(I_n, v_n)$ and π_n^{PP}, denote the scheduling decision variables, power used by the schedule and the predicted day-ahead prices, respectively. Ω denotes all the relevant operational constraints that must be satisfied by the schedule. In the current application, this step is carried out by solving (6.1) and (6.2) with predicted prices for the VSC and OOC plants, respectively. Let $\{I_n^{PP}, v_n^{PP}\}$ and $P_n^{PP} \doteq P(I_n^{PP}, v_n^{PP})$ denote the solution to (6.4) and the corresponding power required by the schedule given the predicted price, respectively.

Step 2: The optimal schedule is then implemented throughout day k during which the actual prices are being revealed.

Step 3: At the end of day k, (6.5) is used to calculate the actual daily cost of the schedule derived from predicted prices, Cost^{PP} , since π_n^{AP} is known.

$$\text{Cost}^{PP} = \Delta t \cdot \sum_{n=1}^{N_t} P_n^{PP} \cdot \pi_n^{AP} \tag{6.5}$$

The FP schedule is then calculated using (6.4), with a FP whose value is the mean of the price during day k. Let the power required by the FP schedule be P_n^{FP}, then the cost, Cost^{FP}, is calculated as shown in (6.6). This is considered as a baseline cost.

$$\text{Cost}^{FP} = \Delta t \cdot \sum_{n=1}^{N} P_n^{FP} \cdot \pi_n^{AP} \tag{6.6}$$

The FEBI for day k can then be calculated using (3). Unlike Cost^{FP}, Cost^{PP} is obtained with information about future prices, which is the predicted price. Therefore Cost^{PP} is normally smaller than Cost^{FP} and FEBI is normally a positive value. A good forecasting methodology should have large positive values of FEBI.

6.3.1 Rank correlation as an indicator of economic benefit

Refs. [24] and [23] criticise the use of MAPE and RMSE for evaluating the economic benefit of forecasts for demand-side applications but do not explore alternative methods of evaluation. They proposed the use of price classification instead. These price classification methods rely on assigning thresholds whose values are said to be dependent on specific applications [23, 93, 94]. Selection of thresholds is straightforward for electrical loads with co-generation since the threshold is simply set to equal the cost of internal generation. However, this is difficult for load-shifting applications such as those considered in this chapter because the schedule depends on the relative difference of the hourly prices and not the absolute values. For example, 40.06 $/MWh can be considered as expensive on 12 October 2012 where it is the maximum price, but cheap on 30 October 2012 where the mean price is 58.62 $/MWh. Thus, setting threshold values is not easy.

Since a good forecast only needs to distinguish between high and low prices, one plausible alternative is to use the correlation between the actual price and the predicted price as an indicator of a forecast method's economic benefit. The most commonly used correlation coefficient is the Pearson product-moment (PPM) coefficient, which measures the linear dependence between two variables. However, since the electricity price series is nonlinear with many spikes, an RC would be the most appropriate to use [21]. The RC measures statistical dependence without the assumption of linearity and it is considered a robust measure of correspondence [95, 96]. The Kendall RC between a predicted (π_n^{PP}) and actual price (π_n^{AP}) series is used in this chapter. The fact that RC is based on ranks, it only measures the ability of a forecast to correctly identify peaks and valleys in the price series and disregards the absolute value of the prices.

The Kendal RC between a predicted (π_n^{PP}) and actual price (π_n^{AP}) series is calculated using (6.7).

$$\mathrm{RC} = \begin{cases} 2\cdot(N_C - N_D)/24(24-1) & \text{(generally, or)} \\ (N_C - N_D)/\sqrt{(N_C + N_D + N_{TA})\cdot(N_C + N_D + N_{TP})} & \text{(when there are ties)} \end{cases} \tag{6.7}$$

where N_C and N_D are the number of concordant and discordant pairs respectively. The pair of observations (π_i^{PP},π_i^{AP}) and (π_j^{PP},π_j^{AP}) are said to be concordant when $rank(\pi_i^{PP}) > rank(\pi_j^{PP})$ and $rank(\pi_i^{AP}) > rank(\pi_j^{AP})$, or $rank(\pi_i^{PP}) < rank(\pi_j^{PP})$ and $rank(\pi_i^{AP}) < rank(\pi_j^{AP})$. N_{TA} and N_{TP} represent the number of rank ties for actual prices, $rank(\pi_i^{AP}) = rank(\pi_j^{AP})$ and predicted prices, $rank(\pi_i^{PP}) = rank(\pi_j^{PP})$, respectively. A tie is considered neither discordant nor concordant. The number 24 used is used in the equation because the daily price series is predicted on hourly basis over 24 hours.

As an example, consider the 4-h long predicted price series {24.5, 25.0, 32.6, 52.1} \$/MWh and corresponding actual prices {26.3, 22.2, 40.7, 28.9} \$/MWh. The ranks of the series are {1,2,3,4} and {2,1,4,3} and the 4 sets of observations are A (1, 2) ≡ (24.5, 26.3), B (2, 1) ≡(25.0, 22.2), C (3, 4) ≡(32.6, 40.7) and D (4, 3)≡(52.1, 28.9). The concordant pairs are (A,C), (A,D), (B,C) and (B,D), while (A,B) and (C,D) are the discordant pairs. Thus, $N_C = 4$, $N_D = 2$ and there are no ties. Using the 4-h long series, the first condition of (6.7) applies, therefore $\mathrm{RC} = 2\cdot(4-2)/4(4-1) = 1/3$.

The Spearman and Kendall correlations are the most commonly used methods of calculating RC, but the Kendall RC is selected because it has been shown to be more robust and simple to compute [95]. One of the more robust proposed methods of calculating RC is the median correlation coefficient [95]. However, our preliminary analysis has indicated that this method is inferior because it treats the price spikes as outliers, thereby, underestimating the correlation coefficient. The limitation of correlation is that a small sample size can only calculate large correlation values with enough confidence level. For example, only values above 0.28 can be calculated with a commonly used standard of 95% confidence level using our 24-h samples of daily prices, for the PPM [97].

6.4 ELECTRICITY PRICE FORECASTING

Forecasting electricity prices is conducted using three methods, namely; seasonal mean prices (MP), least-square support vector machine (LSSVM) and an adaptive neuro-fuzzy inference system (ANFIS). For MP, the hourly average prices of the training data are calculated and used as the day-ahead price prediction. In the cases of both the LSSVM and ANFIS, one-step ahead models are trained and used to recursively predict prices 24 h ahead. The details of this procedure are outlined in [98] using wind speed data. The LSSVM and ANFIS predictors use selected price lags over the past 48 h as model inputs.

LSSVM is a form of SVM that simplifies the formulation of SVM, resulting in a set of linear equations. The advantage of LSSVM is that it requires less training effort than the normal SVM. The LSSVM model employed here uses a Gaussian kernel. The details about training an LSSVM regression model are available in [99, 100]. ANFIS is an adaptive multi-layered network that maps multiple inputs to an output using fuzzy logic constructs. A comprehensive introduction to ANFIS is available in [101]. ANFIS has been used successfully in a number of recent publications [102, 103, 104]. The ANFIS model implemented in this chapter uses the Sugeno-type structure with three triangular windows on the best three price lags.

The maximum average values of MAPE, RMSE and RC are 27.1%, 15.2% and 0.59, for all three forecast methods over the eight-months testing period as shown in Table 6.1. The prediction saves up to 16.6% (for OOC) and 14.6% (for VSC) of the cost when compared to scheduling without any price information (FP schedule). A review of price forecasting mechanisms shows that MAPE accuracy

Table 6.1. The average values of performance indicators.

Forecast	VSC	OCC	Benefit Indicators		
Method	FEBI	FEBI	MAPE	RMSE	RC
MP	14.7	14.6	27.1	15.2	0.58
LSSVM	16.6	13.7	19.3	13.0	0.59
ANFIS	13.4	10.0	20.1	13.6	0.52

reported in many chapters is within the range of 1–36% [19, 23, 21]. The RMSE error on the Spanish market is reported to be in the range of 5–10% [20]. Therefore, the average performances of the considered forecast methods shown in Table 6.1, are good enough because they give comparable ranges of accuracy to those reported in literature. It is also worth noting that prediction accuracy varies with price volatility so prediction performance of the same method may vary with price data [23].

6.5 SIMULATION RESULTS AND DISCUSSIONS

6.5.1 Effect of price volatility on economic benefit

The electricity price modelling, forecasting as well as the simulation of the plants are carried-out in the Matlab environment. A perfect prediction must give the exact value of the actual price. Therefore, ideally when the optimal solutions of (6.4) are reached, the FEBI of the actual price is always equal to or bigger than that of any other forecast method. This means that the FEBI calculated using the actual price represents the upper limit of the economic benefit ($FEBI_{max}$) that can be achieved by any forecast method.

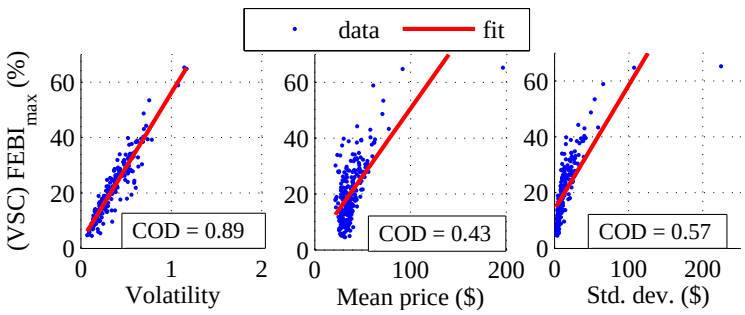

Figure 6.3. Dependence of daily maximum economic benefit on three factors for VSC.

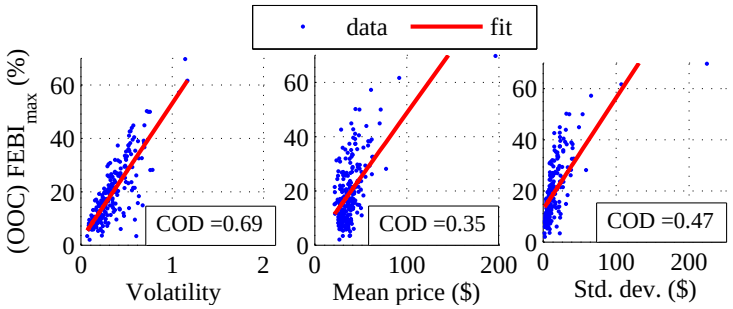

Figure 6.4. Dependence of daily maximum economic benefit on three factors for OOC.

Price volatility (v_j) is defined as the ratio of the standard deviation (Std. dev) to the mean of daily prices [100]. Figs. 6.3 and 6.4 show the dependence of FEBI$_{max}$ on mean price, Std. dev and volatility for each of the 241 days of testing. They also show the coefficient of determination (COD) for a linear fit. The strong linear dependence of volatility on economic benefit is clearly visible. This result is intuitive, since it implies that price forecasting is mostly required when the variability of the hourly prices in a day is high. However, it also means a forecasting method derives varying amounts of benefit on each day even when the forecasting method's accuracy is constant. A comparison between Figs. 6.3 and 6.4 shows a particularly higher number of days with high volatility and low FEBI$_{max}$ values for the OOC plant than the VSC plant. This indicates a distinct difference in the behaviour between the two methods of control. This behaviour is explained in Section 6.5.3. It is worth noting that the prediction of FEBI$_{max}$ by the volatility cannot be perfect because the plants are scheduled not only to reduce the operating cost, but also to minimise mechanical stress in the components.

6.5.2 Indicators of economic benefit

A summary of the performances of economic benefit indicators and forecasting methods for eight seasons is given in Table 6.2. For winter and summer 2012, Table 6.2 shows that the values of MAPE and RMSE for MP are higher than those of ANFIS. This wrongly suggests that ANFIS's predictions are more accurate than those of MP. A comparison of FEBI values clearly shows that MP provides a better forecast method than ANFIS in terms of the economic benefit. On the contrary, the higher values of RC for the MP compared to ANFIS indicate that MP is able to forecast more accurately the relative difference in hourly prices in a day than ANFIS; as a result it gives higher values of FEBI. In fact the comparison of RC values is able to rank the forecast methods in a correct order of average economic benefit for six seasons out of a total of eight. That is, excluding the two autumn seasons. By

Table 6.2. A seasonal summary of forecasting performances.

Season	Forecast method	VSC FEBI	OOC FEBI	MAPE	RMSE	RC
Autumn 2010	MP	10.3	14.4	23.5	11.6	0.46
	LSSVM	12.4	11.5	18.4	10.8	0.48
	ANFIS	10.9	12.7	19.2	11.1	0.45
Winter 2010	MP	17.6	16.9	33.7	19.3	0.50
	LSSVM	14.2	13.2	25.0	18.1	0.43
	ANFIS	11.5	5.7	23.3	12.0	0.32
Spring 2011	MP	22.6	19.8	29.3	24.8	0.62
	LSSVM	20.8	18.6	21.9	22.8	0.60
	ANFIS	16.7	13.5	23.8	24.3	0.55
Summer 2011	MP	22.4	18.3	41.6	22.1	0.77
	LSSVM	21.8	13.2	19.8	14.9	0.76
	ANFIS	18.6	9.2	24.2	17.1	0.69
Autumn 2011	MP	3.9	4.9	28.5	12.2	0.40
	LSSVM	10.7	11.3	16.6	9.1	0.44
	ANFIS	9.7	11.1	18.9	10.2	0.39
Winter 2012	MP	10.2	9.7	17.5	7.9	0.65
	LSSVM	8.6	5.5	13.0	6.3	0.50
	ANFIS	6.9	2.0	12.2	6.2	0.48
Spring 2012	MP	2.3	8.6	21.9	13.9	0.43
	LSSVM	20.3	17.1	20.1	13.0	0.63
	ANFIS	12.0	11.5	22.2	14.0	0.52
Summer 2012	MP	24.4	20.5	24.5	13.2	0.80
	LSSVM	22.8	15.9	19.8	12.0	0.76
	ANFIS	19.9	11.9	21.4	13.1	0.67

comparison MAPE is successful in only two.

The failure of average RC in predicting the right order (ranking) of economic benefit between MP and LSSVM during the autumn of 2011 may be attributed to two possible reasons. The first reason is that the accuracy of correlation coefficients is low because only 24 samples are used per day [97]. Therefore, the average values of RC given by forecast methods during these seasons are too close to distinguish between the methods confidently. Thus, RC performs poorly because correlation values are low. Another reason is the variation in volatility during the season. It has already been established in Section 6.5.1 that high volatility tends to present bigger opportunities for scheduling cost reduction. A forecast may have higher correlations during periods of high volatility even though the average value of RC is low. This would give such a forecast disproportionately high benefits since a forecast is more beneficial during periods of high volatility. To investigate this, correlation values adjusted by volatilities can be used. The total volatility-adjusted RC can be calculated by,

$$\text{Total volatility adjusted RC} = \left(\sum_{j=1}^{N_{days}} \text{RC}_j \cdot \frac{v_j}{v_{max}}\right) \tag{6.8}$$

where N_{days} is the number of days, 30 days in the case of autumn 2011. v_{max} is the maximum volatility value during Autumn 2011. Using (6.8) the Autumn of 2011 gives the values 6.34, 6.99 and 6.45 corresponding to MP, LSSVM and ANFIS, respectively. These values are in agreement with the values of FEBI. Therefore, it is prudent to do a comparison based upon a volatility-adjusted RC whenever the RC values are very close to each other, as is the case with Autumn 2011, in Table 6.2.

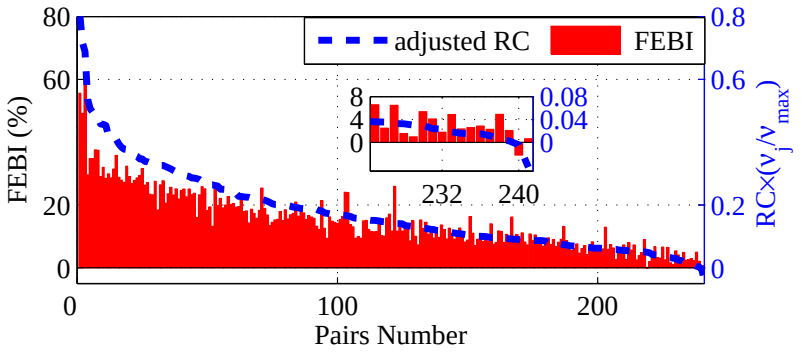

Figure 6.5. Dependence of economic benefit on RC for LSSVM forecasts.

Fig. 6.5 shows the ordered pairs of FEBI and volatility-adjusted RC, for the LSSVM forecasting method. As expected, Fig. 6.5 shows that adjusted RC values are visibly proportional to the FEBI. The

pair with the smallest FEBI and adjusted RC correctly appears towards the end, as pair number 240. However, the volatility adjustment does not improve the performance of MAPE and RMSE. Scatter plots of adjusted values for RC, MAPE and RMSE give linear fits to FEBI with COD values of 0.91, 0.58 and 0.31, respectively. These again show the superiority of RC in indicating the magnitude of economic benefit.

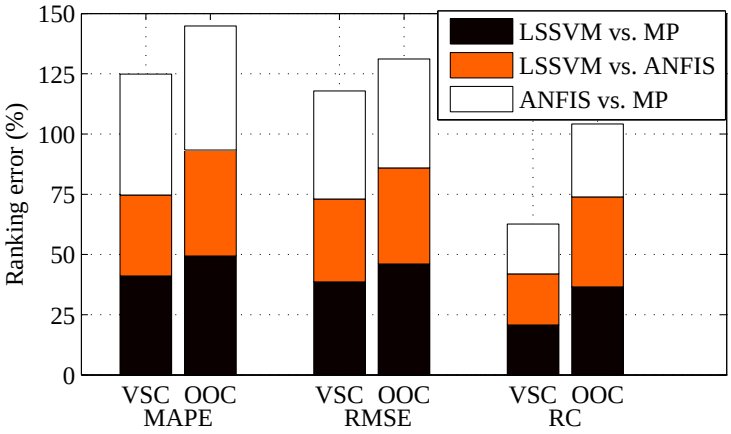

Figure 6.6. Ranking error when comparing the benefit between forecasts.

The three indicators (without adjustment) are further tested on their ability to rank the performance between any two of the three prediction algorithms used. The summary of the ranking errors is shown in Fig. 6.6. The average ranking error for RC is 20.1% and 34.7 % for the VSC and OOC plants, respectively. This indicates that it is harder to predict the economic benefit of an OOC plant than that of a VSC.

6.5.3 Using an artificial forecast

Dependence of economic benefit on RC for LSSVM forecasts method in a load-shifting application, a set of artificial forecasts (AFs) is created using (6.9).

$$\begin{aligned} \pi_n^{\mathrm{AFP}}(c_{\mathrm{mean}}) &= c\pi_n^{\mathrm{AP}} + (1-c)\pi_n^{\mathrm{dist}} \\ \text{where } c &= c_{\mathrm{mean}} + \mathbf{U}[-0.2, +0.2] \end{aligned} \tag{6.9}$$

where π_n^{AFP} and π_n^{AP} denote the AF prices generated and the AP forecast, respectively. π_n^{dist} is a disturbance price that is negatively correlated to AP. The mean of the uniformly distributed parameter c_{mean} is varied between 0 and 1.6 in steps of 0.2 so as to generate multiple forecasts.

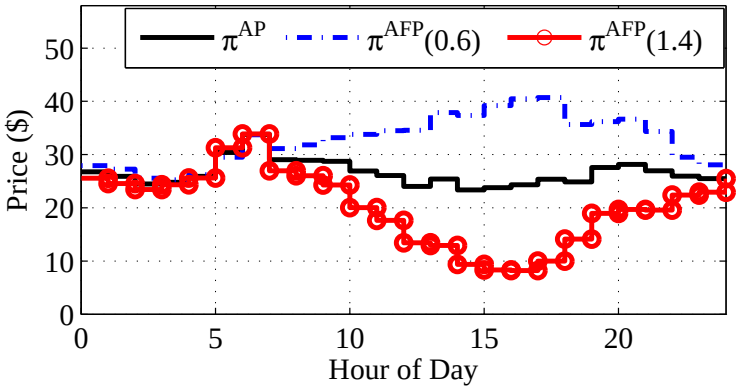

Figure 6.7. Actual price and artificial forecast over a 24-h period.

The AFs become closer to the AP as c_{mean} increases from 0 to 1 and decreases from 1.6 to 1, but from opposite sides, as illustrated by Fig. 6.7. When c_{mean} is 0 the AF is almost equal to π_n^{dist}. Thus, the indicators are at their worst values, as shown in Figs. 6.8 and 6.9. When c_{mean} is 1 the AF is almost equal to the AP. As a result, the MAPE and RC values are close to 0% and 1, respectively

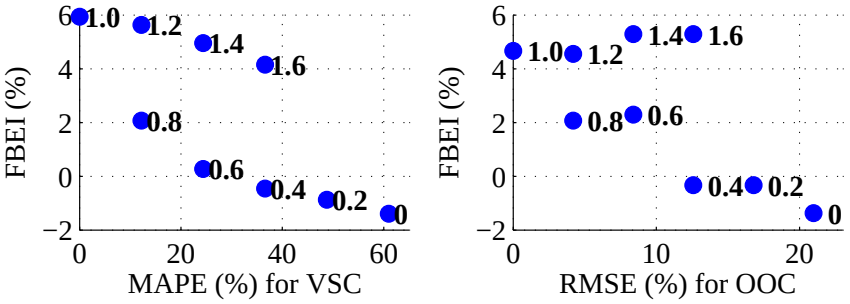

Figure 6.8. Dependence of economic benefit on MAPE and RMSE for the artificial forecast.

Fig. 6.8 shows that the economic benefit of $\pi_n^{\text{AFP}}(1.4)$ is far better than of $\pi_n^{\text{AFP}}(0.6)$ even though their respective MAPE of 25.1% and 23.7% are close. This is because the forecasts are equidistant from the AP, even though they lie on opposite sides, as shown in Fig. 6.7. It is worth noting that the values of RMSE for both forecasts are also close, with values of 9.1 and 8.4, respectively.

The forecast $\pi_n^{\text{AFP}}(1.4)$, which tends to follow the trend of the AP in identifying periods of low prices, is more correlated than $\pi_n^{\text{AFP}}(0.6)$, which opposes the trend. Therefore $\pi_i^{\text{AFP}}(1.4)$ should perform

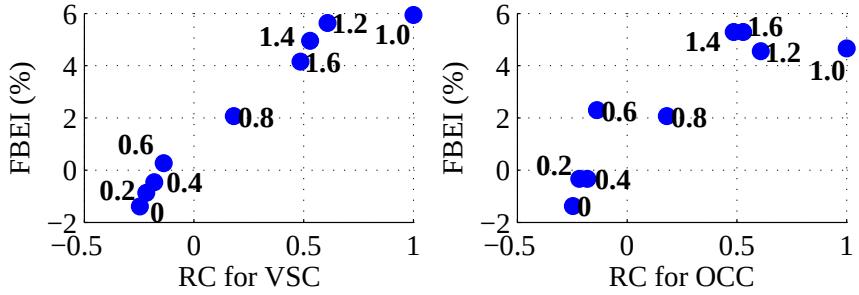

Figure 6.9. Dependence of economic benefit on RC, for the artificial forecast.

better than $\pi_n^{\text{AFP}}(0.6)$, as correctly indicated by RC in Fig. 6.9 This result agrees with the observations made in [24], that the PP trends and not specific values are important when scheduling a load-shifting plant.

Fig. 6.9 shows that the RC performs better for the VSC than the OOC plant. This is because the OOC plant tends to be more insensitive to small changes in RC. For example, $\pi_n^{\text{AFP}}(0.2)$ and$\pi_n^{\text{AFP}}(0.4)$ as well as $\pi_n^{\text{AFP}}(1.2)$ and $\pi_n^{\text{AFP}}(1)$ have almost equal economic benefit. The reason for this behaviour becomes clear when comparing the typical schedules in Fig. 6.1. The power usage of the VSC plant can vary flexibly between 0 and the maximum value, while it is restricted to either full/no power for the OOC plant. Thus the OOC becomes insensitive to small variations in the price forecast's RC.

Another observation for the OOC plant in Fig. 6.9 is that there are cases where AF with a slightly smaller RC result in better economic benefits. This is due to the fact that the scheduling problem defined in (6.2) optimises both energy cost and a mechanical objective. Therefore the very low prices of $\pi_n^{\text{AFP}}(1.4)$ and $\pi_n^{\text{AFP}}(1.6)$ encourage the OOC to have more start-ups, thereby enabling the plant to reduce more cost compared to $\pi_n^{\text{AFP}}(1)$. The number of start-ups in $\pi_n^{\text{AFP}}(1)$, $\pi_n^{\text{AFP}}(1.4)$ and $\pi_n^{\text{AFP}}(1.6)$ are 4, 6 and 6, respectively. This is also the reason why Fig. 6.4 shows a particularly high number of days with high volatility and low values of FEBI_{max} when compared to the VSC plant in Figs. 6.3.

6.5.4 Sensitivity analysis

The preceding discussion implies that the success of RC as an indicator of economic benefit is dependent on the weighting parameter (ω) in (1) and (2). Fig. 6.10 shows the values of COD for

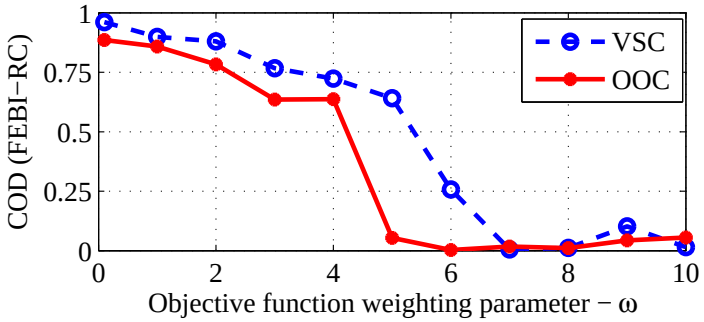

Figure 6.10. Predictability of economic benefit as ω changes.

Table 6.3. Ranking error sensitivity to storage size.

Type	Ranking	storage size (% of 5595 tons)			
	Index	75	100	150	300
VSC	MAPE	41.4	41.6	43.0	43.0
	RMSE	38.5	39.3	42.6	41.5
	RC	23.9	20.9	23.4	24.2
OOC	MAPE	51.7	48.3	43.6	48.7
	RMSE	48.8	43.7	43.7	49.4
	RC	43.4	34.7	33.3	42.3

the plots of the FEBI versus RC for different values of ω. Increasing the value of ω decreases the emphasis of the resulting schedule towards optimising energy cost and increases the impact of the mechanical cost. As expected, the results in Fig. 6.10 show that the usefulness of RC decreases with decreasing emphasis on optimising the energy cost. It is also worth noting that the COD of the OOC plant falls faster than that of the VSC plant as ω increases.

Table 6.3 compares the abilities of RC, MAPE and RMSE in ranking the forecast methods according to their economic benefit for varying amounts of the plant's storage size, as percentage of its original value. The results show that RC remains a better indicator regardless of the storage size. The results for the VSC plant are fairly stable across all storage sizes. However, increasing the storage size in OOC increases the possibility of multiple start-up and this makes the performance of forecasts more unpredictable. This explains the large error values when the storage size is above 200%. Also, the binary problem of the OOC becomes too difficult for the optimiser to solve quickly when the storage

size decreases. As a result many of the solutions become sub-optimal. This is why the ranking error of RC is large when 75% storage size is used.

6.6 CONCLUSIONS

This chapter presents an assessment of the economic impact of price prediction on a load-shifting industrial plant. Rank correlation between forecast and actual prices is found to be a suitable indicator of economic performance of a forecast in day-ahead scheduling of load-shifting applications. The suitability of RC is attributable to its ability to capture the similarity between the trends in the actual and forecast prices. The analysis shows that MAPE and RMSE are not suitable indicators of the economic benefit because they merely measure the absolute error of a prediction. These results are in agreement with current literature, which declares that the prediction of relative price trend and not the actual value, is useful for load-shifting applications [24]. The economic benefit increases with increasing price volatility in the day-ahead scheduling of load-shifting applications. The results show that the economic benefit obtained from price forecasts becomes less predictable when more emphasis is placed on other operational requirements, such as mechanical stress of components, apart from cost reduction. The results also indicate that it is easier to predict the economic performance of a forecast for a plant controlled using variable speed drives than one controlled by an on/off switch.

Future work on needs to consider the creation of a new class of price prediction algorithm that would be more suitable for load-shifting applications. These algorithms have to make accurate predictions on the future price trend and not focus on getting accurate point forecasts.

CHAPTER 7 SUMMARY

This chapter presents a summary of conclusions and possible future work. The summary is sectioned into five themes addressed in this thesis:

- **Conveyor energy model**:

The analysis in Chapter 3 has shown that the most prominent weakness of the current conveyor energy models comes from the fact that they do not model the flow of material on the belt. The error due to this inadequacy is exaggerated in the belts. Thus, the newly proposed model for long conveyors includes a partial differential equation that captures the flow of material on the belt. The newly proposed model is shown to perform better than the currently available steady state models on a case study plant. This proposed model is much simpler than the standard models because it requires the knowledge of only two parameters as opposed to more than three in both the cases of CEMA and ISO model. Simulation results have illustrated that the parameters of the newly proposed model can be easily identified recursively with an online experiment from noisy data with up to 15% magnitude of noise the component. Future work on the model may look at improving the model's accuracy by summing the conveyor resistances on shorter discrete sections of the belt. This approach is likely to improve the calculation of primary and secondary resistance's contribution to the total conveyor energy consumption. However, it may equally likely result in a more complicated model. One prominent challenge with the newly proposed model is that improving the accurate modelling of material on the belt rapidly increases the number of model variables and hence the computational burden. Future work needs to that explore alternative model discretisation techniques that may achieve increased accuracy with lesser increases in the computational burden. Future work on the model must also incorporated the use of multiple drives since they are common in long conveyor applications.

- **Demand-side management of BCS operated in time-based tariffs**:

The scheduling of BCS for optimal energy and operational cost reduction is demonstrated for three different time-base tariffs, namely; time-of-use, critical peak pricing and real time pricing. This analysis is spread within Chapters 3 to 6. Chapters 3 to 5 consider the Time-of-Use tariff. The critical peak pricing tariff is considered in Chapter 5, while Chapter 6 focuses exclusively on real-time pricing. The analysis indicates that it is possible to operate BCS cost effectively and efficiently under all of these tariffs. The results show that given enough storage, the optimiser can reduce belt speed in order to avoid high price periods and increase speed in order to take advantage of low price periods. Future work may consider a more comprehensive comparative study of many known tariff options and attempt to establish which tariffs are more appropriate for what kind of BCS.

The results in Chapter 6 show that accurate pricing information is crucial for the maximisation of energy cost savings obtained from the optimiser. The results show that the best RTP price forecast scheme is the one that accurately predicts the overall daily price trend and not necessarily the price values. The results also indicate that it is easier to predict the economic performance of an RTP price prediction scheme when the conveyors are controlled by varying belt speed continuously as opposed to on/off control. Another interesting possible future work would be to establish a RTP prediction model that is most suitable for application in scheduling of BCS specifically and any load-shifting load, in general.

- **Energy management of BCS with downhill conveyors**:

A case-study application of a BCS with DHC shows that capturing the energy of DHC is an attractive energy saving measure with payback periods of less than 5 years. The availability of tariffs that allow selling energy to the grid further lower the payback period for investing in regenerative drives and make this intervention even more economically attractive. The results show that the resulting optimal operational schedule for such BCS depends on how profitable/useful the energy extracted from DHC is. That is, the optimiser maximises the speed of operation of DHC during peak times when the BCS is able to sell electricity of the grid. However, the optimiser produces moderate speeds that merely captures the energy from DHC for internal use, during other non-peak periods. Further research work is necessary to validate whether the resulting belt speed changes can be practically implemented particularly because these conveyors are downhill.

- **BCS scheduling with uncertanity and the impact of storage size**:

In this work, uncertainty in optimal scheduling of BCS arise in two ways; (1) in uncertain electricity pricing information such as RTP and CPP and (2) in the uncertain demand of bulk material inherited from downstream processes. In Chapter 6 forecasting is used to deal with price uncertainty. The analysis in Chapter 5 shows that an MPC based scheduling algorithm is better than the optimal control based algorithm, for scheduling BCS under the uncertain tariff of CPP. This is because, unlike the OC based algorithm, the MPC based algorithm can perform both intra- and inter-day load-shifting. Thus the MPC base algorithm is able to avoid high electricity prices during critical days. Storage is also useful in mitigating the effects of uncertainty in the demand of bulk material. However, modelling and incorporating uncertainty into a stochastic scheduling algorithm is shown to be a better option of dealing with randomness. That is, the proposed chance-constrained MPC based scheduling algorithm is demonstrated as an effective method of calculating robust BCS schedules. The chance-constraints also provide an intuitive formula for sizing the conveyor system's storage size.

The amount of storage in the BCS limits the amount of load-shifting and so the amount of cost saving possible under a time-based tariff. However, the results in Chapters 4 and 5 show that the storage's ability to lower costs is limited and that increasing the storage size does not always result into more energy savings. Thus, BCS simulations are needed to verify the savings before investing in storage expansion.

REFERENCES

[1] *Belt conveyor for bulk material*, 6th ed., Conveyor Equipment Manufacturers Association (CEMA), Naples, Florida, USA, 2005.

[2] *Rollers and components for bulk handling*, Rumelca Holdings S.p.A, Almè (BG), Italy, 2003, [Online] Available: http://www.rulmecacorp.com/Conveyor_Idler_Roller_catalog/.

[3] S. Zhang and X. Xia, "A new energy calculation model of belt conveyor," in *IEEE AFRICON 2009*. Nairobi, Kenya: IEEE, 23-25 Sep. 2009, pp. 1–6.

[4] *ISO 5048:1989 Continous mechanical handling equipment - Belt conveyor with carrying idlers – Calculation of operating power and tensile forces*, International Organization for Standardization (ISO) Standard, 1989.

[5] *Phoenix Conveyor Belts Design Fundamentals - New DIN 22101*, Phoenix Conveyor Belts Systems GmbH, Hamburg, Germany, 2004, [Online] Available: http://www.phoenix-conveyorbelts.com/.

[6] S. Zhang and X. Xia, "Modeling and energy efficiency optimization of belt conveyors," *Applied Energy*, vol. 88, no. 9, pp. 3061–3071, 2011.

[7] J. Hiltermann, G. Lodewijks, D. L. Schott, J. C. Rijsenbrij, J. A. J. M. Dekkers, and Y. Pang, "A methodology to predict power saving of troughed belt conveyors by speed control," *Particulate Science and Technology*, vol. 29, no. 1, pp. 14–27, 2011.

[8] B. Jeftenić, L. Ristić, M. Bebić, S. Štatkić, I. Mihailović, and D. Jevtić, "Optimal utilization of the bulk material transport system based on speed concontrol drives," in *International Conference on Electrical Machines - ICEM 2010*. Rome, Italia: IEEE, 2010, pp. 1–6.

[9] A. T. de Almeida, F. J. T. E. Ferreira, and D. Both, "Technical and economical considerations in the application of variable-speed drives with electric motor systems," *IEEE Transactions on Industrial Applications*, vol. 41, no. 1, pp. 188–199, Jan. 2005.

[10] L. B. Ristić and B. I. Jeftenić, "Implementation of fuzzy control to improve energy efficiency of variable speed buk materail transportation," *IEEE Transactions on Industrial Electronics*, vol. 59, no. 7, pp. 2959–2968, 2012.

[11] R. Saidur, S. Mekhilef, M. Ali, A. Safari, and H. Mohammed, "Applications of variable speed drive (VSD) in electrical motors energy savings," *Renewable and Sustainable Energy Reviews*, vol. 16, no. 1, pp. 543–550, 2012.

[12] A. Elaiw, X. Xia, and A. M. Shehatac, "Application of model predictive control to optimal dynamic dispatch of generation with emission limitations," *Electric Power Systems Research*, vol. 84, no. 1, pp. 31–44, 2012.

[13] M. H. Albadi and E. F. El-Saadany, "A summary of demand response in electricity markets," *Electric Power Systems Research*, vol. 78, no. 11, pp. 1989–1996, 2008.

[14] "Primer on Demand-Side Management with an emphasis on price-responsive programs," Report prepared by Charles River Associates for The World Bank, Tech. Rep. CRA No. D06090, Feb. 2005. [Online]. Available: http://documents.worldbank.org

[15] A. Faruqui and S. George, "Quantifying customer response to dynamic pricing," *The Electricity Journal*, vol. 18, no. 4, pp. 53–63, May 2005.

[16] Q. Zhang, X. Wang, and M. Fu, "Optimal implementation strategies for critical peak pricing," in *6th International Conference on the European Energy Market (EEM 2009)*. Leuven, Belgium: IEEE, 27-29 May 2009, pp. 1–6.

[17] Z. Wang and F. Li, "Critical peak pricing tariff design for mass consumers in great britain," in *IEEE Power and Energy Society General Meeting*. San Diego, California, USA: IEEE, 24-29 Jul. 2011, pp. 1–6.

[18] *Strategic pricing direction for standard tariffs*, Eskom Holdings SOC Ltd, Sandton, South Africa, 2007, [Online] Available: http://www.eskom.co.za/CustomerCare/TariffsAndCharges/Documents/Stratpricidir2.pdf.

[19] S. K. Aggarwal and L. M. S. A. Kumar, "Electricity price forecasting in deregulated markets: A review and evaluation." *International Journal of Electrical Power & Energy Systems*, vol. 31, no. 1, pp. 13–22, 2009.

[20] L. S. Coelho and A. A. P. Santos, "A RBF neural network model with GARCH errors: Application to electricity price forecasting." *Electric Power Systems Research*, vol. 81, no. 1, pp. 74–83, 2011.

[21] N. Amjady and F. Keynia, "A new prediction strategy for price spike forecasting of day-ahead electricity markets," *Appllied Soft Computing*, vol. 11, pp. 4246–4256, 2011.

[22] Y. Dong, J. Wang, H. Jiang, and J. Wu, "Short-term electricity price forecast based on the improved hybrid model." *Energy Conversion and Management*, vol. 52, no. 8, pp. 2987–2995, 2011.

[23] H. Zareipour, A. Janjani, H. Leung, A. Motamedi, and A. Schellenberg, "Classification of future electricity market prices," *IEEE Transactions on Power Systems*, vol. 26, no. 1, pp. 165–173, Feb. 2011.

[24] H. Zareipour, C. A. Canizares, and K. Bhattacharya, "Economic impact of electricity market price forecasting errors: A demand-side analysis," *IEEE Transactions on Power Systems*, vol. 25, no. 1, pp. 254–262, Feb. 2010.

[25] E. Delarue, P. V. D. Bosch, and W. D'haeseleer, "Effect of the accuracy of price forecasting on profit in a price based unit commitment," *Electric Power Systems Research*, vol. 80, no. 10, pp.

1306–1313, 2010.

[26] B. Mohammadi-Ivatloo, H. Zareipour, M. Ehsan, and N. Amjady, "Economic impact of price forecasting inaccuracies on self-scheduling of generation companies," *Electric Power Systems Research*, vol. 81, pp. 617–24, 2011.

[27] M. Bae, H. Kim, E. Kim, A. Y. Chung, H. Kim, and J. H. Roh, "Toward electricity retail competition: Survey and case study on technical infrastructure for advanced electricity market system," *Applied Energy*, vol. 133, pp. 252–273, Nov. 2014.

[28] Y. Yamamoto, "Pricing electricity from residential photovoltaic systems: A comparison of feed-in tariffs, net metering, and net purchase and sale," *Solar Energy*, vol. 86, no. 9, pp. 2678–2685, 2012.

[29] A. Bakirtzis, Y.-H. Kim, and A. Meliopoulos, "Monte carlo simulation for evaluating retail wheeling effects," *Electric Power Systems Research*, vol. 60, no. 3, pp. 137–144, 2002.

[30] *Eskom submission to NERSA for Genflex tariff and incoporation of the MEC into the NMD rules*, Eskom Holdings SOC Ltd, Sandton, South Africa, 2013, [Online] Available: http://www.nersa.org.za/Admin/Document/Editor/file/Notices/Invitations/Eskom's proposed Genflex Tariff sublished for stakeholder comments 19 July 2013.pdf.

[31] T. Mathaba and X. Xia, "Optimal and energy efficient operation of conveyor-belt systems with downhill conveyors," *Energy Efficiency*, Jul. 2016.

[32] A. Middelberg, J. Zhang, and X. Xia, "An optimal control model for load shifting - with application in the energy management of a colliery," *Applied Energy*, vol. 86, no. 7, pp. 1266–1273, Aug. 2009.

[33] S. Zhang and X. Xia, "Optimal control of operation efficiency of belt conveyor systems," *Applied Energy*, vol. 87, pp. 1929–1937, Jun. 2010.

[34] H. Zhang, X. Xia, and J. Zhang, "Optimal sizing and operation of pumping systems to achieve energy efficiency and load shifting," *Electric Power Systems Research*, vol. 86, pp. 41–50, May 2012.

[35] J. Nocedal and S. J. Wright, *Numerical Optimization*, 1st ed. 233 SpringStreet, New York, NY 10013, USA: Springer Science & Business Media, 2006.

[36] R. L. Haupt and S. L. Haupt, *Practical genetic algorithm*, 2nd ed. Hoboken, New Jersey: John Wiley & Sons, Inc., 2004.

[37] L. N. Trefethen, *Finite Difference and Spectral Methods for Ordinary and Partial Differential Equations*. Cornell University-Department of Computer Science and Center for Applied Mathematics, 1996.

[38] D. He, Y. Pang, and G. Lodewijks, "Determination of acceleration for belt conveyor speed control in transient operation," *IACSIT International Journal of Engineering and Technology*, vol. 8, no. 3, pp. 206–211, 2016.

[39] ——, "Speed control of belt conveyors during transient operation," *Powder Technology*, vol. 301, pp. 622–631, 2016.

[40] T. Mathaba, X. Xia, and J. Zhang, "Analysing the economic benefit of electricity price forecast in industrial load scheduling," *Electric Power Systems Research*, vol. 116, pp. 158–165, Nov. 2014.

[41] B. Moreno, M. T. García-Álvarez, C. Ramos, and E. Fernández-Vázquez, "A general maximum entropy econometric approach to model industrial electricity prices in Spain: A challenge for the competitiveness," *Applied Energy*, vol. 135, pp. 815–824, Dec. 2014.

[42] R. Granell, C. J. Axon, and D. C. H. Wallom, "Predicting winning and losing businesses when changing electricity tariffs," *Applied Energy*, vol. 133, pp. 298–307, Nov. 2014.

[43] T. Mathaba, X. Xia, and J. Zhang, "Optimal scheduling of conveyor belt systems under critical peak pricing," in *International Power and Energy Conference (IPEC) 2012*. Ho Chi Minh City, Vietnam: IEEE, 12-14 Dec. 2012, pp. 315–320.

[44] G. Fedorko, V. Molnar, D. M., A. Grincova, M. Dovica, J. Zivcak, T. Toth, and N. Husakova, "Failure analysis of belt conveyor damage caused by the falling material. Part I: Experimental measurements and regression models," *Engineering Failure Analysis*, vol. 36, pp. 30–38, Jan. 2014.

[45] C. A. Wheeler, A. W. Roberts, and M. G. Jones, "Calculating the flexure resistance of bulk solids transported on belt conveyors," *Particle & Particle Systems Characterization*, vol. 21, no. 4, pp. 340–347, Nov. 2004.

[46] S. Zamorano, "Long distrance conveying - choosing the right option," Bulk solids handling, Mar. 2011, http://www.bulk-solids-handling.com/conveying_transportation/mechanical_coveyor_systems_belt_conveyor_systems/articles/305378/. Last accessed on 23 August 2013.

[47] G. Lodewijks, "The design of high speed belt conveyors," in *Conference on belt conveying - BELTCON 10*. Johannesburg, South Africa: International Materials Handling Conference, 19-21 Oct. 1999, pp. 1–20.

[48] Y. Hou and Q. Meng, "Dynamic characteristics of conveyor belts," *Journal of China University of Mining and Technology*, vol. 18, no. 4, pp. 629–633, Dec. 2008.

[49] I. G. Mulani, "Calculation of artificial friction conveying coefficient f, and a comparision between ISO and CEMA," in *Bulk Material Handling by Conveyor Belt 5*, A. Reicks and M. T. Myers, Eds. Littleton, Colorado, USA: Society for Mining, Metallurgy and Exploration,Inc. (SME), 2004, pp. 55–63.

[50] W. A. Strauss, *Partial differential equations - An Introduction*, 2nd ed., S. Corliss, Ed. Hoboken, New Jeysey, USA: John Wiley & Sons, Inc., 2008, no. 10-11.

[51] T. J. vanDelft, "Modeling and model predictive control of a conveyor-belt dryer - applied to the

drying of fish feed," Master's thesis, Norwegian University of Science and Technology, June 2010.

[52] J. Tessier, C. Duchesne, and G. Bartolacci, "A machine vision approach to on-line estimation of run-of-mine ore composition on conveyor belts," *Minerals Engineering*, vol. 20, no. 12, pp. 1129–1144, Oct. 2007.

[53] T. Ananthan and M. V. Vaidyan, "An FPGA-based parallel architecture for on-line parameter estimation using the RLS identification algorithm," *Microprocessors and Microsystems*, no. 5, pp. 496–508, 2014.

[54] L. Olivier, B. Huang, and I. Craig, "Dual particle filters of state and parameter estimation with application to a run-of-mine ore mill," *Journal of Process Control*, no. 4, pp. 710–717, Apr. 2012.

[55] *Tariff and charges booklet 2013/14*, Eskom Holdings SOC Ltd, Sandton, South Africa, 2013, [Online] Available: http://www.eskom.co.za/CustomerCare/TariffsAndCharges/Documents/ESKOM TC BOOKLET 2013-14.pdf.

[56] T. Mathaba and X. Xia, "A parametric energy and material flow model for long conveyor-belts," *Energies*, vol. 8, no. 12, pp. 13 590–13 608, 2015.

[57] J. Rodríguez, J. Pontt, G. Alzamora, N. Becker, O. Einenkel, and A. Weinstein, "novel 20-MW downhill conveyor system using three-level converters," *IEEE Transactions on Industrial Electronics*, vol. 49, pp. 1093–1100, Oct. 2002.

[58] P. Lűchinger, U. Maier, and R. A. Errath, "Active Front End technology in the application of a down hill conveyor," in *IEEE Cement Industry Technical Conference Record*. Phoenix, Arizona,USA: IEEE, 9-14 Apr. 2006, pp. 175–194.

[59] *Technical guide No. 8 - Electrical bracking*, ABB Ltd., Zurich, Switzerland, 2011, [Online] Available: http://www.abb.com/abblibrary/DownloadCenter/.

[60] A. González-Gil, R. Palacin, and P. Batty, "Sustainable urban rail systems: Strategies and technologies for optimal management of regenerative braking energy," *Energy Conversion and Management*, vol. 75, pp. 374–388, Nov. 2013.

[61] J. Zhang, C. Lv, M. Qiu, Y. Li, and D. Sun, "Braking energy regeneration control of a fuel cell hybrid electric bus," *Energy Conversion and Management*, vol. 76, pp. 1117–1124, Dec. 2013.

[62] V. Musolino, A. Pievatolo, and E. Tironi, "A statistical approach to electrical storage sizing with application to the recovery of braking energy," *Energy*, vol. 36, no. 11, pp. 6697–6704, Nov. 2011.

[63] N. Mitrovic, M. Petronijevic, V. Kostic, and B. Jeftenic, "Electrical drives for crane application," in *Mechanical Engineering*, M. Gokcek, Ed. Rijeka, Croatia: InTech, 2012, pp. 131–156, [Online] Available: http://www.intechopen.com/books/mechanical-engineering/electrical-drives-for-crane-application/.

[64] R. Pelzer, E. Mathews, D. le Roux, and M. Kleingeld, "A new approach to ensure successful implementation of sustainable demand side management (DSM) in south african mines," *Energy*, vol. 33, no. 8, pp. 1254–1263, Aug. 2008.

[65] P. Warren, "A review of demand-side management policy in the UK," *Renewable and Sustainable Energy Reviews*, vol. 29, pp. 941–951, Jan. 2014.

[66] *Active Front End - Options for Altivar 61 and Altivar 71*, Schneider Electric SE, Rueil-Malmaison, France, 2013, [Online] Available: http://www.schneider-electric.com/.

[67] N. Madlool, R. Saidur, N. Rahim, and M. Kamalisarvestani, "An overview of energy savings measures for cement industries," *Renewable and Sustainable Energy Reviews*, vol. 19, pp. 18–29, Mar. 2013.

[68] T. Ma, H. Yang, and L. Lu, "Feasibility study and economic analysis of pumped hydro storage and battery storage for a renewable energy powered island," *Energy Conversion and Management*, vol. 79, pp. 387–397, Mar. 2014.

[69] L. Zhang, X. Xia, and J. Zhang, "Improving energy efficiency of cyclone circuits in coal beneficiation plants by pump-storage systems," *Applied Energy*, vol. 119, pp. 306–313, Apr. 2014.

[70] F. J. T. E. Ferreira, J. A. C. Fong, and A. T. de Almeida, "Ecoanalysis of variable-speed drives for flow regulation in pumping systems," *IEEE Transactions on Industrial Electronics*, vol. 58, no. 6, pp. 2117–2125, Jun. 2011.

[71] J. Ondraczek, N. Komendantova, and A. Patt, "WACC the dog: The effect of financing costs on the levelized cost of solar PV power," *Renewable Energy*, vol. 75, pp. 888–898, Mar. 2015.

[72] A. Roberts, "Chute performance and design for rapid flow conditions," *Chemical Engineering & Technology*, vol. 26, no. 2, pp. 163–170, 2003.

[73] N. Venkatesan, J. Solanki, and S. Solanki, "Market optimization for microgrid with demand response model," in *North American Power Symposium (NAPS)*. Boston, Massachusetts,USA: IEEE, 4-6 Aug. 2011, pp. 1–6.

[74] A. Bego, L. Li, and Z. Sun, "Identification of reservation capacity in critical peak pricing electricity demand response program for sustainable manufacturing systems," *International Journals of Energy Research*, vol. 38, no. 6, pp. 728–736, 2014.

[75] D. Mazurkiewicz, "Analysis of the ageing impact on the strength of the adhesive sealed joints of conveyor belts," *Journal of Materials Processing Technology*, vol. 208, no. 1, pp. 477–485, 2008.

[76] S. Zhang, "Model predictive control of operation efficiency of belt conveyor," in *29th Chinese Control Conference (CCC)*. Beijing, China: IEEE, 29-31 Jul. 2010, pp. 1854–1858.

[77] J. M. Maciejowski, *Predictive Control: With Constraints*, 1st ed. London, UK: Prentice Hall, 2002.

[78] D. Mayne, J. Rawlings, C. Rao, and P. Scokaert, "Constrained model predictive control: Stability and optimality," *Automatica*, vol. 36, no. 6, pp. 789–814, Jun. 2000.

[79] J. Zhang and X. Xia, "A model predictive control approach to the periodic implementation of the solutions of the optimal dynamic resource allocation problem," *Automatica*, vol. 47, no. 2, pp. 358–362, 2011.

[80] A. J. vanStaden, J. Zhang, and X. Xia, "A model predictive control strategy for load shifting in a water pumping scheme with maximum demand charges," *Applied Energy*, vol. 88, no. 12, pp. 4785–4794, Dec 2011.

[81] J. Široký, F. Oldewurtel, J. Cigler, and S. Prívara, "Experimental analysis of model predictive control for an energy efficient building heating system," *Applied Energy*, vol. 88, no. 9, pp. 3079–3087, Sep. 2011.

[82] Y. Ma, A. Kelman, A. Daly, and F. Borrelli, "Predictive control for energy efficient buildings with thermal storage: Modeling, stimulation, and experiments," *IEEE Control Systems Magazine*, vol. 32, no. 1, pp. 44 –64, Feb. 2012.

[83] F. Gavilan, R. Vazquez, and E. F. Camacho, "Chance-constrained model predictive control for spacecraft rendezvous with disturbance estimation," *Control Engineering Practice*, vol. 20, no. 2, pp. 111–122, 2012.

[84] T. G. Hovgaard, L. F. Larsen, K. Edlund, and J. B. Jørgensen, "Model predictive control technologies for efficient and flexible power consumption in refrigeration systems," *Energy*, vol. 44, no. 1, pp. 105–116, Aug. 2012.

[85] U. E. Ekpenyong, J. Zhang, and X. Xia, "An improved robust model for generator maintenance scheduling," *Electric Power Systems Research*, vol. 92, pp. 29–36, Nov. 2012.

[86] A. Schwarm and M. Nikalaou, "Chance-constrained model predictive control," *AIChE Journal*, vol. 45, no. 8, pp. 1743–1752, Aug. 1999.

[87] S. Pappas, L. Ekonomou, D. Karamousantas, G. Chatzarakis, S. Katsikas, and P. Liatsis, "Electricity demand loads modeling using autoregressive moving average (ARMA) models," *Energy*, vol. 33, no. 9, pp. 1353–1360, Sep. 2008.

[88] M. Moazzami, A. Khodabakhshian, and R. Hooshmand, "A new hybrid day-ahead peak load forecasting method for Iran's national grid," *Applied Energy*, vol. 101, pp. 489–501, Jan. 2013.

[89] W. Charytoniuk and J. Niebrzydowski, "Confidence interval construction for load forecast," *Electric Power Systems Research*, vol. 48, no. 2, pp. 97–103, Dec. 1998.

[90] L. Chisci, J. Rossiter, and G. Zappa, "System with persistent disturbances predictive control with restricted constraints," *Automatica*, vol. 37, no. 7, pp. 1019–1028, Jul. 2001.

[91] G. E. duPlessis, L. Liebenberg, and E. H. Mathews, "The use of variable speed drives for cost-effective energy savings in south african mine cooling systems," *Applied Energy*, vol. 111, pp. 16–27, Nov. 2013.

[92] E. M. Wanjiru and X. Xia, "Energy-water optimization model incorporating rooftop water harvesting for lawn irrigation," *Applied Energy*, vol. 160, pp. 521–531, Dec. 2015.

[93] S. Anbazhagan and N. Kumarappan, "A neural network approach to day-ahead deregulated electricity market prices classification," *Electric Power Systems Research*, vol. 86, pp. 140–150, May 2012.

[94] ——, "Day-ahead deregulated electricity market price classification using neural network input featured by DCT," *International Journal of Electrical Power & Energy Systems*, vol. 37, no. 1, pp. 103–109, 2012.

[95] C. Croux and C. Dehon, "Influence functions of the spearman and kendall correlation measures," *Statistical Methods & Applications*, vol. 19, no. 4, pp. 497–515, 2010.

[96] E. B. Niven and C. V. Deutsch, "Calculating a robust correlation coefficient and quantifying its uncertainty," *Computers & Geosciences*, vol. 40, pp. 1–9, Mar. 2012.

[97] W. Trochim, *The Research Methods Knowledge Base*, 2nd ed. Cincinnati: Atomic Dog Publishing, 2000.

[98] T. Mathaba, X. Xia, and J. Zhang, "Short-term wind power prediction using Least-Square Support Vector Machines," in *Power Engineering Society Conference and Exposition in Africa (PowerAfrica), 2012 IEEE*. Johannesburg, South Africa: IEEE, 9-13 Jul. 2012, pp. 1–6.

[99] J. Suykens, T. Gestel, J. Brabanter, B. Moor, and J. Vandewalle, *Least Squares Support Vector Machines.*, 1st ed. 5 Toh Tuck Link, Singapore: World Scientific Publishing Company, 2002.

[100] J. Zhou, J. Shi, and G. Li, "Fine tuning support vector machines for short-term wind speed forecasting," *Energy Conversion and Management*, vol. 52, pp. 1990–8, Apr. 2011.

[101] J. S. R. Jang, "ANFIS: adaptive-network-based fuzzy inference system," *IEEE Transactions on Systems Man and Cybernetics*, vol. 23, no. 3, pp. 665–685, May 1993.

[102] M. Mohandes, S. Rehman, and S. Rahman, "Estimation of wind speed profile using adaptive neuro-fuzzy inference system (ANFIS)," *Applied Energy*, vol. 88, no. 11, pp. 4024–4032, Nov. 2011.

[103] A. Azadeh, S. M. Asadzadeh, M. Saberi, V. Nadimi, A. Tajvidi, and M. Sheikalishahi, "A neuro-fuzzy-stochastic frontier analysis approach for long-term natural gas consumption forecasting and behavior analysis: The cases of Bahrain, Saudi Arabia, Syria, and UAE," *Applied Energy*, vol. 88, no. 11, pp. 3850–3859, Nov. 2011.

[104] H. Pousinho, V. Mendes, and J. Catalão, "Short-term electricity prices forecasting in a competitive market by a hybrid PSO-ANFIS approach," *International Journal of Electrical Power & Energy Systems*, vol. 39, no. 1, pp. 29–35, 2012.